Dissertations, Master's Theses and Master's Reports

2017

STRUCTURAL CHARACTERISTICS AND CORROSION BEHAVIOR OF BIO-DEGRADABLE ZN-LI ALLOYS IN STENT APPLICATION

Shan Zhao
Michigan Technological University, shanzhao@mtu.edu

STRUCTURAL CHARACTERISTICS AND
CORROSION BEHAVIOR OF BIO-DEGRADABLE ZN-LI ALLOYS
IN STENT APPLICATION

By

Shan Zhao

A DISSERTATION

Submitted in partial fulfillment of the requirements for the degree of

DOCTOR OF PHILOSOPHY

In Materials Science and Engineering

MICHIGAN TECHNOLOGICAL UNIVERSITY

2017

This dissertation has been approved in partial fulfillment of the requirements for the

Degree of DOCTOR OF PHILOSOPHY in Materials Science and Engineering.

Department of Materials Science and Engineering

Dissertation Co-Advisor: *Jaroslaw W. Drelich, Ph.D.*

Dissertation Co-Advisor: *Jeremy Goldman, Ph.D.*

Committee Member: *Stephen L. Kampe, Ph.D.*

Committee Member: *Yongmei Jin, Ph.D.*

Committee Member: *Feng Zhao, Ph.D.*

Department Chair: *Stephen L. Kampe, Ph.D.*

Table of Contents

List of Figures

List of Tables

Preface

This doctoral dissertation is based on two technical articles and one review paper in peer-reviewed journals finished in 2016. They are all related to the design of bio-degradable Zn-based metallic stents. The full references for the three articles presented herein are listed below.

In Chapter 3 "Results and Discussions: Structural characteristics and in vitro biodegradation of a novel Zn-Li alloy prepared by induction melting and hot rolling", I performed majority of materials preparation, all materials characterization and all writing under supervision of Professor Jaroslaw W. Drelich and Professor Jeremy Goldman, while Cameron T. McNamara, Nicholas Verhun and Jacob Braykovich contributed to the wire EDM cutting and hot rolling. In Chapter 4 "Results and Discussions: Zn-Li Alloy after Extrusion and Drawing: Structural, Mechanical Characterization, and Biodegradation in Abdominal Aorta of Rat", I performed majority of materials preparation, characterization and writing under supervision of Professor Jaroslaw W. Drelich and Professor Jeremy Goldman, while Dr. Jan-M. Seitz and his team in Germany contributed to the wire extrusion; Roger Guillory and Elisha Earley contributed to the histological analysis, and Professor Jeremy Goldman contributed to the animal surgeries. Professors, staff, graduate and undergraduate students who assisted during the finishing of this dissertation are listed in the Acknowledgements section.

1. **<u>S Zhao</u>**, C T. McNamara, N Verhun, J P. Braykovich, J Goldman, J Drelich. Structural characteristics and in vitro biodegradation of a novel Zn-Li alloy prepared by induction melting and hot rolling (2017 *Metallurgical and Materials Transactions A*, 48(3), 1204-1215)

2. **<u>S Zhao</u>**, J M. Seitz, R Eifler, H J. Maier, R J. Guillory II, E Earley, J Goldman, J Drelich. Zn-Li Alloy Wire after Extrusion and Drawing: Structural, Mechanical Characterization, and Biodegradation in Abdominal Aorta of Rat (2017 *Materials Science and Engineering: C*, 76, 301-312)

3. PK Bowen, ER Shearier, **<u>S Zhao</u>**, RJ Guillory, F Zhao, J Goldman, J Drelich. Bio-degradable metals for cardiovascular stents: From clinical concerns to recent Zn-alloys, 2016 *Advanced Healthcare Materials* 5 (10), 1121-1140

Acknowledgement

I would like to express my highest gratitude to my advisor Professor Jaroslaw Drelich for his guidance, support, patience and encouragement throughout my doctoral study at Michigan Tech. His invaluable suggestions and timely feedback helped me at various stages of my research. His dedication and enthusiasm to work, his friendliness, warm-hearted attitude, confidence, and optimism have been profoundly influential to me.

My sincere gratitude goes to my co-advisor, Professor Jeremy Goldman. I truly appreciate his helpful discussions about issues that came out during the *in vivo* experimentation and his careful and timely review of my drafts. I am also deeply honored to be among the students in his MY4940 Tissue Engineering class, which is one of the best class experience I have ever had at Michigan Tech.

I would like to express my special appreciation and thanks to my dissertation committee members: Professors Stephen L. Kampe, Yongmei Jin, and Feng Zhao for their insightful advices and constant encouragement during my dissertation research.

I would especially like to thank the incredible professors in Materials Science and Engineering Department at Michigan Tech: Professor Stephen L. Kampe for providing me the opportunity to attend the DMMM2 conference and connect with many successful and influential women engineers, Professor Stephen Hackney for discussions on microstructures, Professor Larry Sutter for assisting with ESEM whenever I have a question, Professor Paul Sanders for providing me with invaluable feedback of my department seminar presentation, Professor Jean Kampe for helping with networking with

11

Completing this work would have been all the more difficult were it not for the support and friendship provided by fellow graduate students and scholars at Michigan Tech: Dr. Patrick Bowen, Dr. Jan.-M Seitz, Dr. Cam McNamara, Dr. Helen Ranck, Roger Guillory, Jeff Brookins, Nicholas Verhun, Jacob Braykovich, Sara Schellbach, Adam Drelich, Elisha Earley, Matt Tianen, Catherine Galligan, Dr. Yuan Liu, Mingxiao Ye, Dr. Hualan Jin, Zhiyong Yin, Avishan Arab Shomali, Dr. Jie Zhou, Dr. Liwei Geng, Dr. Chenlong Zhang, Dr. Jephias Gwamuri, Li Chen, Dr. Kyle Deane, Huaguang Wang, Dr. Onur Guven, Dilek Senol Arslan, Karl Warsinski, Mick Small, Felicia Nip.

A special thanks to my family. Words cannot express how grateful I am to my mother Mrs. Kuiying Han, my father Mr. Xiucai Zhao, and my sister Dan Zhao for their constant unconditional support - both emotionally and financially, and all of the sacrifices that they have made for me. Their love for me inspired me to strive towards my goal and sustained me thus far.

I particularly thank my best friend and fiancé, Professor Tao Yang, not only for his insightful research suggestions and life philosophy but also for his incredible patience to tolerate my idiosyncrasies and listen whenever I needed. There were times when I was in doubt and it was his determination and constant encouragement that ultimately made it possible for me to see this project through.

List of Abbreviations

Abbreviation	Full name
AMS	Absorbable Metal Stent
XRD	X-ray Diffraction
SEM	Scanning Electron Microscopy
BEI	Backscattered Electron Image
ICP-OES	Inductively Coupled Plasma Optical Emission Spectrometry
ESEM	Environmental Scanning Electron Microscopy
FT-IR	Fourier transform infrared
CR	Corrosion Rate
SBF	Simulated Body Fluid
IACUC	Institutional Animal Care and Use Committee
YM	Young's Modulus
YS	Yield Strength
UTS	Ultimate Tensile Strength
EDM	Electro Discharge Machining
HV	Vickers microhardness
FRA	Frequency Response Analyzer
EDS	Energy Dispersive Spectrometer
RD	Rolling Direction

TD	Transverse Direction
EW	Equivalent Weight
RT	Room Temperature
CSA	Cross Sectional Area
H&E	Hematoxylin and Eosin

Abstract

Zinc has begun to be studied as a bio-degradable material in recent years due to its excellent corrosion rate and optimal biocompatibility. Unfortunately, pure Zn's intrinsic ultimate tensile strength (UTS; below 120 MPa) is lower than the benchmark (about 300 MPa) for cardiovascular stent materials, raising concerns about sufficient strength to support the blood vessel. Thus, modifying pure Zn to improve its mechanical properties is an important research topic.

In this dissertation project, a new Zn-Li alloy has been developed to retain the outstanding corrosion behavior from Zn while improving the mechanical characteristics and uniform biodegradation once it is implanted into the artery of Sprague-Dawley rats.

The completed work includes:

- Manufactured Zn-Li alloy ingots and sheets via induction vacuum casting, melt spinning, hot rolling deformation, and wire electro discharge machining (wire EDM) technique; processed alloy samples using cross sectioning, mounting, etching and polishing technique;

- Characterized alloy ingots, sheets and wires using hardness and tensile test, XRD, BEI imaging, SEM, ESEM, FTIR, ICP-OES and electrochemical test; then selected the optimum composition for *in vitro* and *in vivo* experiments;

- Mimicked the degradation behavior of the Zn-Li alloy *in vitro* using simulated body fluid (SBF) and explored the relations between corrosion rate, corrosion products and surface morphology with changing compositions;

- Explanted the Zn-Li alloy wire in abdominal aorta of rat over 12 months and studied its degradation mechanism, rate of bioabsorption, cytotoxicity and corrosion product migration from histological analysis.

Introduction

Bio-degradable stents are envisaged to support the arterial wall during remodeling and to degrade thereafter. Therefore, it may eliminate the potential chronic inflammation [1] and thrombosis risks [2] of permanent stents and alleviate the repeating procedures for stenting at the same site in the event of restenosis [3]. Over the past several years, Mg-based and Fe-based materials have been widely investigated for coronary stent applications with very limited success [4-6]. These previous reports demonstrated that neither iron nor magnesium is ideal as a stent material due to either incomplete degradation of iron corrosion products [7] or premature degradation of magnesium [8]. Consequently, new bio-degradable materials are needed.

Zinc is one of the most abundant nutritionally essential elements in the human body [9]. Zinc has begun to be studied as a bio-degradable material in recent years [10]. It is metallically bio-degradable and exhibits both an excellent corrosion rate and optimal biocompatibility. Unfortunately, pure Zn's intrinsic ultimate tensile strength (UTS; below 120 MPa) is lower than the benchmark (about 300 MPa) for cardiovascular stent materials, raising concerns about sufficient strength to support the blood vessel. Thus, modifying pure Zn to improve its mechanical properties is an important research topic.

Li is one of the few elements with significant solubility in zinc, and Zn-Li is therefore among a few potentially age-hardenable systems. The idea of adding lithium into zinc to improve the strength largely comes from the positive effects observed for magnesium alloys such as LAE442, which has 4 wt.% lithium, 4 wt.% aluminium and 2 wt.% rare-

earth elements. LAE442 has been shown to be non-allergenic [11], bio-degradable, and to degrade at a lower rate than the pure material without the formation of radiographic gas [12, 13] and with a more uniform degradation behavior [13]. It is now widely considered as the most promising implant for orthopedic use [14]. The toxic potential of a zinc-lithium stent should therefore be negligible in terms of the released elements and their quantities. Indeed, based upon the projected rate of stent corrosion, the quantity of released elements will never exceed the level that can be safely assimilated by the body and its organs. With regard to local toxic effects, rapid transport of ions in vascular tissue [15] should prevent elemental enrichment, cytotoxicity, or necrosis in the implant's vicinity.

However, a review of the available literature suggests most of the previous studies in this binary Li-Zn system focused on its thermodynamic properties, preliminary charge-discharge, polarization characteristics [16], and the reactivity of lithium-ion batteries [17]. Currently, no research has been conducted on Zn-Li alloys as a bio-degradable implant material.

This dissertation research creatively addresses this challenge by alloying Li with Zn to improve its mechanical properties through manipulation of metal micro-/nano-structure. Chapter 1 provides an extensive review of the current status on the stenting technique and conventional metallic and polymeric Absorbable Metal Stent (AMS). Chapter 2 validates the proposed Zn-Li alloy in stent application and provides the detailed research diagram and hypotheses. Chapter 3 shows the structural characteristics of Zn-xLi alloy (with x=2, 4, 6 at.%) and the in vitro biodegradation results, suggesting that addition of Li for further in vivo test should be less than 4 at.%. Chapter 4 lists the characteristics and preliminary

in vivo degradation results of Zn-Li wire obtained from implantation in rat abdominal arteries. Chapter 5 summarizes the results and demonstrates the promise of this Zn-Li alloy in bio-degradable coronary stent.

Chapter 1 Literature Review

1.1 Medical Problem and Stenting Technique

In 1977, Andreas Grüntzig performed the first balloon coronary angioplasty [18], which advanced the technology of coronary stents. Stenting, clinically known as percutaneous coronary intervention (PCI), has become a proven procedure for the treatment of arterial occlusions. During stenting, one or more stent is delivered and placed into a narrowed coronary artery by using a catheter system that is inserted into artery through a small incision in the arm or groin. This approach reduces the early recoil and late vascular remodeling that plagued balloon angioplasty treatment alone. Permanent metallic implants presently consist of high-strength corrosion-resistant alloys such as stainless steel (316L) and cobalt-chromium L605 (CoCr).

The drug-eluting stent (DES) approach was invented to mainly decrease the high rates of restenosis and repeat revascularizations [19, 20]. It pioneered a new area for stents by restoring blood flow via mechanical scaffolding and simultaneously releasing a pharmaceutical agent that alleviates the restenosis response to the foreign stent material. The reduction in restenosis of 60-80% across the board has driven its widespread acceptance [21, 22]. However, further reports precluded the practices of DES on complex subsets of patients and lesions, such as in tortuous vessels, small vessels, or long diffuse calcified lesions; major adverse cardiac events were also found more frequent in the DES group than in the bare-metal stent group (3.7% vs 1.0%) [23]. Moreover, concerns have been raised over the long-term safety of first-generation DESs, which is remarkably

associated with an increased rate of adverse clinical events, particularly late-stage stent thrombosis [24].

1.2 Absorbable Metal Stent (AMS)

1.2.1 The concept of AMS

Followed by decades of developing strategies to minimize the corrosion of metallic biomaterials, there is now an increasing trend to use corrodible metals in medical applications [25]. The AMS concept has been breaking this paradigm recently, with several materials emerging as potential alternatives for vascular scaffolding that circumvent the long term risks of permanent stents. Since the major effect of stent implantation is provided by its scaffolding, it is required to be retained for 6-12 months during which arterial remodeling and healing is completed [26]. After this period, the stent is preferred to be broken down and excreted by the body. In pediatric interventions, which involves arteries that have not completed their growth cycle, the disappearance of the stent will enable natural vessel growth and will avoid the need for recatheterization and serial stent balloon dilatation until adulthood. In the case of a fully absorbable stent, the problems of late stent thrombosis and prolonged anti-platelet therapy are avoided. Thus, the development of bio-degradable stents, which can fulfill the mission and step away, is the next logical progression for the industry [3-5, 27].

Implantation of metallic stents is always accompanied by damage to the endothelial lining and stretching of the vessel wall [28].
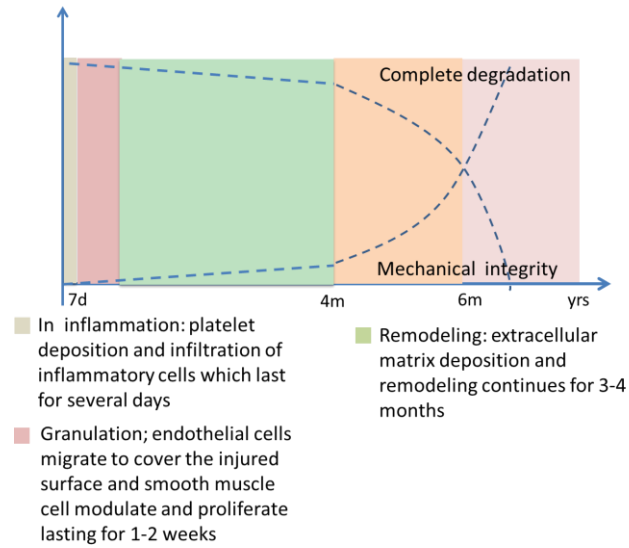
Fig. 1.1. The schematic diagram of degradation behavior and the change of mechanical integrity of AMSs during the vascular healing process.

As shown in Fig. 1.1, the injured vessels exhibit a wound healing response that can be described in three overlapping phases: inflammation, granulation and remodeling [29]. For zinc, an ideal middle ground between degradation and mechanical integrity during in vivo implantations was observed [10]. Zinc corrosion begins at a very low degradation rate, which is beneficial for this application as a zinc-based stent would maintain mechanical integrity during arterial vessel remodeling. Thereafter, the degradation progresses while the mechanical integrity decreases. Stent degradation ideally occurs at a sufficient rate that will not cause an intolerable accumulation of degradation product around the implantation site. A uniform corrosion mechanism is superior to localized corrosion in that the corrosion begins from the surface to the bulk to maintain uniform mechanical integrity [30]. Localized corrosion such as pitting should be avoided since this could lead to the stent's cracking or fragmenting, ultimately ending with blood vessel injuries [30].

To date, no ideal bio-degradable stent has been invented. Depending on the lesion to be treated, there is often a compromise of one or more of the above factors. For example, stents with low surface area may not be very radio-opaque, while lesions requiring total coverage may require stents having high surface area. In contrast to balloon angioplasty where restenosis has been shown to be due to the combination of intimal hyperplasia, vascular remodeling, and elastic recoil, restenosis after stenting is due solely to intimal hyperplasia [31, 32]. The intimal hyperplasia relates to an exaggerated wound healing response: smooth muscle cell migration, proliferation and extracellular matrix elaboration mediated by the endothelial cell injury [33]. Because clinically used stents are permanent implants, their presence may be a stimulus for prolonged inflammatory and foreign body responses, which could potentially interfere with the wound healing response [28]. In humans, the vessel wall healing process is usually complete between 3 to 6 months post stenting. However, a foreign body response has been observed as late as 320 days post implantation [34]. Studies aimed at improving current stent performance focused mainly on drug-eluting stents.

1.2.2 The design of an ideal AMS

Theoretically, if all aspects of stent implantation are considered, the ideal stent should have the following characteristics [28]:

- Flexible - have the capacity to negotiate curved and tortuous coronary segments;
- Radio-opaque - easily visible during angiography;
- Low unexpanded profile - facilitates the passing and positioning of the stent in the artery without predication with a balloon catheter;
- Low roughness - minimize surface area for potential thrombogenic interactions;

- Scaffolding effect - capacity to hold open the artery against the vessel wall's constrictive tendencies (minimize recoil) and hold the stent at its selected implantation site, for example, the tensile strength should be over 300 MPa, elongation to failure should be over 15-18% and elastic recoil on expansion should be less than 4%;

- Show both blood and tissue compatibility;

- Not induce an excessive inflammatory or neointimal response;

- Intermediate corrosion rate - it should degrade with an appropriate rate so that the loosing of the mechanical strength from the dissolution matches the supporting function from tissue regeneration; and to make sure that the amount of the releasing elements are tolerable to the human body [25]. It is believed that at least 6 months' integrity is required. Complete degradation should occur after the vessel remodeling process has finished.

1.2.3 Conventional metallic and polymeric AMS*

1.2.3.1 Current status

Bio-degradable stents are envisaged to support the arterial wall during the remodeling and to degrade thereafter. Pure Fe was the first metal tested, although the majority of research was done on Mg and its alloys. Over the past decade, Mg-based and Fe-based materials have been well accepted and widely investigated for coronary stent applications.

_____

*The material contained in this section was previously published in Advanced Healthcare Materials by PK Bowen, ER Shearier, S Zhao, RJ Guillory, F Zhao, J Goldman, and J Drelich, and is reproduced here with permission.

Tremendous work has been focused on: (1) pure Mg and pure Fe and their alloying with essential elements (Ca, Sr, Zn, Co, C and Si) or low toxic elements (Mn, Sn and Zr), and the rare earth elements (Y and Gd) [35-41]; (2) novel structured bio-degradable metals (porous, ultrafine, nanocrystalline and glassy structures) [42-44]; (3) surface modifications by mechanical, chemical and electrochemical treatment [45, 46]; (4) animal testing and clinical trial of AE21, WE43, Mg-based AMS and pure Fe stent/wires [5, 6, 14, 47-49]. All those previous studies demonstrated that neither iron nor magnesium is ideal for stents. Iron is considered as having a relatively low in vivo degradation rate. However, its ferromagnetic nature constitutes a problem as an implantable device and it has also been shown to produce a large volume of potentially hazardous iron oxide, which may not degrade easily in the human body [49].

As for magnesium, it is less harmful but it degrades too fast (only 1-2 months) [10] and also its ductility is very limited. Many attempts have been conducted to improve the performance of Mg by alloying [64] and advanced processing techniques [63, 65]. For example, it was demonstrated that alloying Mg with Li can change the crystal structure from hexagonal to body-centered cubic (bcc), producing an increase in ductility, but in exchange the UTS dropped to 132 MPa [50], much too low a value for a cardiovascular stent.

The first implantation of Fe stents in the descending aorta of New Zealand white rabbits demonstrated no significant inflammatory response, neointimal proliferation or systemic toxicity [51]. Subsequent implantations of Fe stents in minipigs [52] and juvenile domestic pigs [6] confirmed that Fe degrades without excess inflammation, local toxicity or

thrombosis. Additionally, the high radial strength of Fe could make its stent struts thinner, while a high ductility makes it easy to deliver via catheter-based systems [26]. However, reports on Fe stents have indicated that it cannot corrode completely during the follow up period [51]. In order to increase the degradation rate for Fe, tremendous work has been focused either on the development of alloys or modification of the microstructure by heat [53], mechanical [54] or solution treatment [41]. Another limitation for Fe stents comes from the large volume of potentially hazardous iron oxide products, which may not degrade easily in the human body [49]. Stainless steel 316 L (SS 316L) is included as the gold standard metal for clinical stent applications. Alloying with manganese (Mn) [55] or electro casting [56] was shown to increase the strength and degradation rate of pure Fe [55]. Fe-Mn alloys [40, 41, 55, 57-59] exhibited similar mechanical properties to those of SS 316L. The as-formed austenitic phase decreased the magnetic susceptibility which enhanced compatibility with the magnetic resonance imaging (MRI). From biological facts, the presence of Mn is more appropriate than nickel (used for the SS 316L), which is more toxic and carcinogenic [60]. Electron casting and annealing at 550°C produced a fine grain structure with an average grain size of 4 μm, resulting in a superior ductility and ultimate tensile strength (UTS) [56].

Mg has been considered to be another attractive base-metal candidate because of its good biocompatibility and low thrombogenicity [38, 61-63]. Mg alloys have a large range of UTS and elongation, from 86 to 280 MPa and from 3% to 20%, respectively. However, pure Mg usually corrodes too fast in aggressive chloride environments including body fluid [63]. This fast degradation could not only make a Mg stent lose mechanical integrity in a

short time, but also overload the tissue with degradation products that may lead to neointimal formation [26].

Bio-degradable polymers have been tested for cardiovascular stent applications since the late 1980s. Bio-degradable metals, although considered for implants much earlier (in XVII century for Fe [77] and at the turn of the XIX century for Mg [78]), practically attracted interest for cardiovascular applications at the beginning of XXI century. Pure Fe was the first metal tested, although the majority of research was done on Mg and its alloys. As of today only Mg-based and PLLA-based stents went beyond animal testing and were tested clinically in humans (Tables 1.1 and 1.2).

To date, fully bio-degradable polymeric stent technology has progressed considerably further relative to their more desirable metallic counterparts, [79] as summarized by data in Table 1.2, with several devices having already obtained market approval in Europe or in clinical trials.

Table 1.1. Examples of pre-clinical and clinical tests on bio-degradable polymers and metals

Implant	Implant Site and Time	Major Test Results
PLLA Igaki-Tamai stent (with ST638 or ST494) **[66]**	Porcine coronary arteries, 21d	Neointimal formation and geometric remodeling were significantly less at the ST638-loaded stent site than at the ST494 site.
Igaki-Tamai stent [67, 68]	Human patient artery, 6 months to 10 years	No stent thrombosis and no major cardiac event occurred within 30 days. No major cardiac event, except for repeat angioplasty, developed within 6 months. Long-term (>10 years) clinical outcomes showed acceptable major adverse cardiac events and scaffold thrombosis rates without stent recoil and vessel remodeling.
PLLA stent[69]	Porcine Coronary Artery, 16 weeks	Histological examination revealed no inflammation and minimal neointimal hyperplasia
Copolymeric polylactide stent[70]	Rabbit aorta, 34 months	No inflammatory reaction observed after 6 months and it was completely degraded by 24 months.
Paclitaxel-eluting PDLLA[71]	Porcine coronary arteries, 3 months	The histomorphometric analysis at 3 weeks demonstrated inhibition of neointimal formation by 53% with the paclitaxel-loaded PDLLA when compared to the PDLLA stent, and by 44% when compared to metal stents.
Pure Fe stent [51]	Rabbits (descending aorta), 6-18 months	No thrombogenicity, no significant neointimal proliferation and systemic toxicity, faster degradation at junctions of the stent
Pure Fe stent [52]	Porcine (descending aorta), 360 d	Degradation product adjacent to the stent struts and within adventitia accompanied by macrophages; no sign of toxicity
Pure Fe stent [6]	Pig coronary artery, 28d	Fe stent is very safe
Pure Fe wire [72]	Rat (artery lumen or artery matrix), 1-9 months	Fe wire experienced substantial corrosion within artery matrix, whereas it experienced minimal biocorrosion in blood-contacting environment
AE21[73] (Mg alloy)	Pig (coronary artery), 56d	Mg alloy is satisfactory; 40% loss of perfused lumen diameter due to neointima formation; degradation time needs to be extended
WE43 [74] (Mg alloy)	Minipig (coronary artery), 56d	Mg alloy stents are safe and reliable; the struts are covered by neointima after 6 d; higher minimal lumen diameter on week 4 and 12 than the 316L stent group
WE 43 [8]	Domestic (28d) or minipigs Pig (coronary artery, 3 months)	Degradation after 28 d post-surgery; less neointima compare to 316L stent; stenosis increased from 28 d to 3 months; decreased lumen area
WE43 [75]	Domestic pig coronary artery,28d	Reduced endothelial proliferation, presence of gas pockets
Mg stent [76]	Left pulmonary artery of a preterm baby patient, 5 months	Complete degradation occurred during 5 months; no in-stent obstruction or neointimal hypertrophy was observed; the degradation level was tolerated and the stent secured reperfusion of the previously occluded left pulmonary artery.

Table 1.2. Bio-degradable stents developed or under development (as per Iqbal et al. [80] and Boland et al. [81]): a – with obtained market approval in Europe, b – used in pre-clinical trials, c – in clinical trials, d – discontinued

Stent	Material	Coating	Drug	Strut thickness [μm]	Absorption time [month]
Polymeric					
[a]Igaki-Tamai	PLLA	None	None	170	24
[d]ABSORB BVS	PLLA	PDLLA	Everolimus	156	18-24
1.0	PLLA	PDLLA	Everolimus	156	18-24
[a]ABSORB BVS	PLLA	None	Everolimus	156	18-24
1.1	PLLA	None	Myolimus	150	12-24
[a]ABSORB GT1	PLLA	Salicylate	Sirolimus	200	6-9
[a]DeSolve	SA/AA	Salicylate	Sirolimus	175	12
[d]Ideal BTI	PTD-PC	None	None	200	24
[pc]Ideal BioStent	PTD-PC	None	Sirolimus	200	4-6
[d]REVA	PTD-PC	None	NA	114-228	24
[c]ReZolve	PDLLA	None	None	170	3-6
[c]Fantom	PLLA	None	None	150-200	3-6
[a]ART 18AZ	PLLA	NA	Sirolimus	160	NA
[c]Fortitude	PLLA,	NA	EPC,	150	NA
[pc]Xinsorb	PLDA-		sirolimus		
[pc]Acute BRS	ECL				
Metallic					
[d]AMS 1.0	Mg alloy	None	None	165	<4
[d]DREAMS-1	Mg alloy	None	Paclitaxel	120	9
[c]DREAMS-2	Mg alloy	PLLA	Sirolimus	125	9

This may be due to the pre-existence of numerous well-characterized Food and Drug Administration (FDA) approved polymeric materials from which to manufacture a fully bio-degradable polymeric stent, with the most frequently used polymer being PLLA [82, 83]. However, the recent ABSORB II trial [84]—which evaluated the performance of a polymeric scaffold relative to a conventional metallic drug-eluting device—found poor post-intervention luminal gains when polymeric devices were employed. This was due, in part, to the reluctance of participating physicians to fully expand the brittle polymeric material [85]. Furthermore, a 10-year follow-up with patients that had received an Igaki-Tamai PLLA coronary stent found poor tissue remodeling through histological analysis

[86]. The area previously occupied by PLLA appeared to be filled with proteoglycan, a component of extracellular matrix, but was acellular.

Bio-degradable polymeric materials have the developmental advantage of degrading predominantly by a simple hydrolysis reaction, producing predictable degradation products, and degrading through similar mechanisms whether evaluated *in vitro* or *in vivo* [87]. In contrast, the development of a suitable metallic material for stenting applications, though promising [73], has been elusive. This may be due to the lack of suitable pre-existing materials, as well as the high cost and complexity of developing new materials. Metallic materials often corrode via complex mechanisms that produce a wide range of products, and the rates and products of corrosion can differ fundamentally between *in vitro* and *in vivo* conditions [88-91]. This has made it difficult to translate success at the bench top into a successful stent. Consequently, the scientific and industrial community has engaged in more than a decade-long focus on Mg and Fe [92] that has failed to realize the promise of acceptable fully bio-degradable metallic alternative to the emerging fully bio-degradable polymeric stents.

1.2.3.2 Mechanical facts

Bio-degradable stents are designed to provide mechanical support for the arterial wall during the remodeling period and to degrade with the progression of tissue regeneration [30]. Ideally, in order to achieve the appropriate scaffolding, the mechanical properties of the candidate materials should be close to those of 316L stainless steel, which has been traditionally considered the gold standard material for stent constructs [93]. The stent

material itself and its degradation products should also be non-toxic and compatible in the cardiovascular environment [26].

The mechanical properties and degradation rates for polymers and metals tested for cardiovascular stent applications are compiled in Tables 1.3 and 1.4. The mechanical properties reported in these tables include elastic (Young's) modulus (YM), yield strength (YS), ultimate tensile strength (UTS) and elongation. These mechanical properties are indicators of stent radial strength, acute and chronic recoil, axial and radial flexibility, deliverability, profile and lifetime integrity [94]. The YM provides a measure of how well the stent material resists deformation. Stents are typically delivered through a balloon catheter and then expanded upon proper positioning in the artery. The stent material needs to sustain deformations without cracking or fragmenting during delivery. The critical value for the YM of materials used for stents is not well defined but it is preferable to have a high value to reduce stent recoil.

Materials with a high UTS (>300 MPa) and low YS (~200 MPa) value are preferred for the design of stents. A high UTS, combined with high YM, is needed to increase the stent's radial strength. A low YS is desirable for ease of crimping the stent onto a balloon tipped catheter and then expanding the stent at low balloon pressures during deployment. A YS that is too high can trigger acute recoil during or after balloon deflation. Unfortunately, most of the materials with high UTS also have a high YS. Many polymers do not exhibit a proportional limit in tension and so YS is often not reported. As shown in Tables 1.3 and 1.4, the UTS values for metals are superior to those of polymers.

Table 1.3. Mechanical and degradation properties of polymers tested for cardiovascular stent applications [68, 95] (The values heavily depend on the molecular weight and should be treated as approximate values only.)

Polymer	Melting Point [°C]	Young Modulus [GPa]	Ultimate Tensile Strength [MPa]	Elongation [%]	Degradation Time [month]
PLLA	170-180	2.8-4.0	50	5-10	>24 [68]
PGA	225-230	>7.0	55	15-20	6-12
PDLLA	amorphous	1.4-2.7	-	3-10	12-16
PCL	55-65	0.2-0.3	10	300-500	>24
TD-PCP [96]	290-320	-	10-30	10-13	7

Additionally, the YM value should be as high as possible to prevent acute recoil, and elastic recoil of stent on expansion should be below 4%. Poncin and Proft additionally suggest using the YS/YM ratio in characterizing the elastic range of materials, which provides an indication of the expected recoil upon deflation of the balloon [110]. This value is between 0.16 and 0.32 for stainless steel and cobalt alloys used in manufacturing of permanent stents. Bio-degradable stent materials should probably have similar YS/YM values. Both UTS and elongation to failure influence fatigue resistance and fracture toughness of the stents. An elongation of 30% or higher is typically preferred in materials used for stent design, although the acceptable criterion often reported is >15-18%.

Table 1.4. Mechanical and degradation properties of Fe and Mg and their alloys tested for cardiovascular stent applications

Material	Metallurgy	Grain size [μm]	YM [GPa]	YS [MPa]	UTS [MPa]	Elongation [%]	DR [mm/year]
Iron and Iron Alloys							
SS316L [97]	annealed	12-30	193	190	490	40	-
Armco Fe [98]	annealed	40	200	150	200	40	0.20
Fe-35Mn [55]	annealed	<100		230	430	30	0.44
Fe-10Mn-1Pd [58]	heat-treated	-	60	850-950	1450-1550	2-8	-
Fe-21Mn-0.7C-1Pd [99, 100]	heat-treated	-	50-100	690-1095	1020-1320	24-48	0.21
Fe [56]	electrocasted annealed at 550ºC	2-8	54	270	290	18	0.46-1.22
Alloyed Fe with (Mn, Co, Al, W, Sn, B, C and S) [40]	as rolled	100-400	-	390-450	520-860	5-10	0.09-0.19
Nanocrystalline Fe [54]	Equal channel angular processing	0.08-0.20	-	-	250-450	-	0.09-0.2
Magnesium and Magnesium Alloys							
Pure Mg [53]	as cast	-	41	20	86	13	407
WE43 alloy [101]	extruded T5	10	44	195	280	2	1.35
AM60B-F [53, 101, 102]	die cast	25	45	-	220	6-8	8.97
AZ91D [88, 101]	die cast	-	-	150	230	3	2.80
AZ31 [101, 103]	extruded	-	45	125-135	235	7	1.17*
ZW21 [26, 104, 105]	extruded	4	-	200	270	17	-
WZ21 [26, 104, 105]	extruded	7	-	140	250	20	-
Mg-Zn [61, 106]	extruded	-	42	170	280	19	0.16
Mg-Zn-Mn [101, 107]	extruded	-	-	247	280	22	0.92*
Mg-Ca [101, 108, 109]	extruded	-	-	136	240	11	1.71

 *the degradation rate for AZ31 and Mg-Zn-Mn is from *in vivo* test, others are calculated from potentiodynamic polarization test.

The minimum lifetime before failure of permanent stents made of 316L stainless steel is 10 years, which translates to ~400 million cycles. The same criteria do not apply to absorbable stents; at present, there is no standard defined for this new generation of cardiovascular stents. Since a bio-degradable stent needs to retain its mechanical integrity for 3 to 6 months, the stent material should be acceptable if it is able to sustain ~10 to 20 million cycles before failure occurs.

Despite the increased challenges faced in their development, metallic materials hold several important advantages over polymeric materials. Metallic stents are considered to be superior to polymeric devices in terms of mechanical performance (i.e. ultimate tensile strength elastic range [94]) and ease of translation to a clinical environment. Their greater mechanical strength and better elastic properties are more similar to traditional metallic stents and permit a greater flexibility in stent designs and a wider range of expandable diameters during deployment. The reduced radial strength and ductility of polymeric stents have necessitated substantially larger struts (which have the side effect of increasing vascular injury and blood flow disruptions) and the introduction of a locking mechanism to maintain luminal cross sectional area following deployment [111]. The larger polymer stents require a larger catheter for delivery relative to metal stents, which may exclude pediatric populations [112]. The larger stent struts may also increase susceptibility to early and midterm thrombosis [113]. The locking mechanism further constrains stent design flexibility and the freedom to control the final stent diameter during deployment. It may also be a concern from a device safety standpoint, as this complex feature may increase the risks of device failure. Even in a successful deployment, lower material ductility may also affect the clinician's willingness to expand a polymer stent sufficiently to completely

overcome recoil and achieve full deployment. This effect was hypothesized to have led to significantly lower post-procedure luminal gains with a polymeric stent relative to a metallic stent in the Absorb II clinical trial [114, 115].

As compared to polymers, Fe- and Mg-based metallic absorbable scaffolds:

- exhibit similar radial force to stainless steel [53] and cobalt chromium stents [6];
- display the superior profile of metallic scaffolds, which makes them more deliverable [116]; and
- can bioabsorb at comparable rates with arterial remodeling and wound healing [53].

1.2.3.3 Biocompatibility and corrosion facts

Mechanical strength similarity to conventional stents allows clinicians to have reasonable deployment expectations when using a bio-degradable metallic stent. The potentially beneficial bioactivity of corrosion products [117] raises the exciting prospect that pathogenic cell responses to stent implantation may be modulated as the stent corrodes. Therefore, the ability to control corrosion rates and behavior by conventional metallurgical and alloying approaches may allow for corrosion product-mediated reprogramming of host responses near the host-implant interface. As of today, only stents made of Mg alloys have been reported to go through clinical trials.[79] The first design of Mg-based stents from Biotronik (AMS-1.0), composed of about 93 wt.% of Mg and 7 wt.% of rare earth elements, degraded in electrolyte solutions in about 60 days [80]. Although the degradation rate was too high, pre-clinical studies indicated a rapid endotheliazation [118]. Clinical studies on 63 patients confirmed the stent's safety, with no cardiac death, myocardial infarction, or thrombosis, although the target lesion revascularization was ~24% and ~27% at 4 and 12

months, respectively [119]. Improved metallic stents from Biotronik (DREAMS-1 and DREAMS-2) utilize the Mg-alloy exhibiting a slower degradation rate and improved radial strength than what was used for AMS-1.0. DREAMS-1 additionally incorporated anti-proliferative drugs to reduce neointimal hyperplasia and prevent restenosis. DREAMS-2 is an improved version of DREAMS-1 that instead of incorporateing drug into a porous structure of metal, is additionally covered with a drug-eluting PLLA thin coating. Immunosuppressive and antiproliferative drug prevents restenosis, whereas PLLA reduces the stent's degradation rate at the early stage.

Biocompatibility and corrosion facts of degradable alloys and polymers are listed in Table 1.5. For bio-degradable metals, the released metallic ions may induce local and systemic toxicity to host cells. Therefore, the overall amount of the element used to design a final device and the local release rate for each ion during degradation should be carefully examined. The degradation mode for polymers seems less harmful, but its *in vivo* long term overdose effects should not be neglected. A possible cause for concern for polymers is a recent report that a degraded Igaki-Tamai polymer stent was replaced with proteoglycans [86]. This may indicate poor extracellular matrix regeneration within the footprint of a PLLA stent. Poor matrix regeneration may be a consequence of the mode of polymer degradation vs. that of metals, which proceeds by a bulk degradation that may produce voids inside the material vs. surface corrosion taking place directly at the tissue-metal interface, which allows for an expansion of the tissue front directly into the degrading implant footprint.

Table 1.5. Key properties and aspects of potential bio-degradable metals and polymers for cardiovascular stent applications [120]

	Fe-alloys	Mg-alloys	Polymers
Essential trace element	Yes	Yes	No
Recommended daily intake	6-20 mg	375-500 mg	-
Blood serum level	5.0-17.6 g/l	0.73-1.06 mM	-
***In vivo* long term overdose effects**	Damage of lipid membranes, proteins and DNA; Stimulus for inflammations; Increase of free radicals.	Excessive Mg leads to nausea; Reduction of the excitability of neuromuscular, smooth muscular and cardiac regions.	Adverse tissue reactions; Inflammatory tissue reactions, necrosis and aneurysms.
Effect on local pH during degradation	Alkalescent	Alkalescent	Acidic
Corrosion mode	Localized corrosion	Mostly localized and pitting	Hydrolytic (volume) or enzymatic (surface)
Expected gaseous corrosion products	None	Hydrogen	None
Expected solid corrosion products	$Fe(OH)_2$, $\alpha\text{-FeO}(OH)$, Fe_3O_4	$Mg(OH)_2$, MgO, $MgCl_2$, $(Ca_{1-x}Mg_x)_{10}(PO_4)_6OH_2$	Water soluble and non-soluble oligomers

1.3 Zn-based stent: An innovative solution for bio-degradable stent

With the purpose of searching for suitable alloying elements, Song [64] explored *in vitro* corrosion rates of several magnesium alloys in 2007, pointing out that Ca, Mn and Zn could be appropriate candidates. Zinc, as one of the most abundant nutritionally essential elements in the human body [9], began to be studied as an alloying element or bio-degradable material. Zhang [61] studied the binary Mg-6Zn magnesium alloy which showed reduced corrosion rate, good biocompatibility *in vivo* and suitable mechanical properties. In 2011, Vojtech D et al. [121] prepared binary Zn-Mg alloys containing Mg content up to 3 wt.%, and found that the addition of 1 wt.% Mg significantly improved the

mechanical properties of pure Zn from 30 MPa (UTS) to 110 MPa (UTS). They also indicated that pure Zn and binary Zn-Mg alloys exhibited close corrosion rates (~0.018-0.145 mm/yr), which were significantly lower than those of Mg and AZ91HP alloys. Recently Bowen et al. [10] examined the *in vivo* corrosion behavior of pure zinc for the first time and concluded that unlike iron, the corrosion of pure zinc does not produce a potentially hazardous product. Zinc also corrodes much slower than magnesium (4-6 months), indicating the best aspect of zinc in AMS field [10]. One major concern for a pure zinc stent is the low tensile strength (only 120 MPa) and zinc might not be strong enough to hold open human arteries. Material used for the stent needs to have the tensile strength >200 MPa, preferentially close to 300 MPa [122]. Improvements in mechanical properties of zinc can be approached through either manipulation of metal micro-/nano-structure [123, 124] or alloying [121].

References

[1] Farb A. Morphological Predictors of Restenosis After Coronary Stenting in Humans. Circulation 2002;105:2974-80.

[2] Cook S, Wenaweser P, Togni M, Billinger M, Morger C, Seiler C, et al. Incomplete stent apposition and very late stent thrombosis after drug-eluting stent implantation. Circulation 2007;115:2426-34.

[3] Colombo A, Karvouni E. Bio-degradable stents : "fulfilling the mission and stepping away". Circulation 2000;102:371-3.

[4] Erne P, Schier M, Resink TJ. The road to bio-degradable stents: reaching clinical reality? Cadiovasc Intervent Radiol 2006;29:11-6.

[5] Peuster M, Wohlsein P, Brugmann M, Ehlerding M, Seidler K, Fink C, et al. A novel approach to temporary stenting: degradable cardiovascular stents produced from corrodible metal-results 6-18 months after implantation into New Zealand white rabbits. Heart 2001;86:563-9.

[6] Waksman R, Pakala R, Baffour R, Seabron R, Hellinga D, Tio FO. Short-term effects of biocorrodible iron stents in porcine coronary arteries. J Interv Cardiol 2008;21:15-20.

[7] Yang L, Zhang E. Biocorrosion behavior of magnesium alloy in different simulated fluids for biomedical application. Mater Sci Eng C 2009;29:1691-6.

[8] Waksman R, Pakala R, Kuchulakanti PK, Baffour R, Hellinga D, Seabron R, et al. Safety and efficacy of bio-degradable magnesium alloy stents in porcine coronary arteries. Catheter Cardiovasc Interv 2006;68:607-17.

[9] Tapiero H, Tew KD. Trace elements in human physiology and pathology: zinc and metallothioneins. Biomed Pharmacother 2003;57:399-411.

[10] Bowen PK, Drelich J, Goldman J. Zinc exhibits ideal physiological corrosion behavior for bio-degradable stents. Adv Mater 2013;25:2577-82.

[11] Witte F, Abeln I, Switzer E, Kaese V, Meyer-Lindenberg A, Windhagen H. Evaluation of the skin sensitizing potential of bio-degradable magnesium alloys. J Biomed Mater Res, Part A 2008;86:1041-7.

[12] Thomann M, Krause C, Bormann D, von der Höh N, Windhagen H, Meyer-Lindenberg A. Comparison of the resorbable magnesium . alloys LAE442 und MgCa0.8 concerning their mechanical properties, their progress of degradation and the bone-implant-contact after 12 months implantation duration in a rabbit model. Mat-wiss u Werkstofftech 2009;40:82-7.

[13] Witte F, Fischer J, Nellesen J, Vogt C, Vogt J, Donath T, et al. In vivo corrosion and corrosion protection of magnesium alloy LAE442. Acta Biomater 2010;6:1792-9.

[14] Krause A, Von der Höh N, Bormann D, Krause C, Bach FM, Windhagen H, et al. Degradation behaviour and mechanical properties of magnesium implants in rabbit tibiae. J Mater Sci 2010;45:624-32.

[15] Xu LP, Yu GN, Zhang E, Pan F, Yang K. In vivo corrosion behavior of Mg-Mn-Zn alloy for bone implant application. J Biomed Mater Res, Part A 2007;83A:703-11.

[16] Wang JQ, King P, Huggins RA. Investigations of binary lithium-zinc, lithium-cadmium and lithium-lead alloys as negative electrodes in organic solvent-based electrolyte. Solid State Ionics 1986;20:185-9.

[17] Bichat MP, Pascal JL, Gillot F, Favier F. Electrochemical Lithium Insertion in Zn3P2 Zinc Phosphide. Chem Mater 2005;17:6761-71.

[18] Grüntzig A. Transluminal dilatation of coronary artery stenosis The Lancet 1978;311:263.

[19] Holmes JD, Hirshfeld JJ, Faxon D, Vlietstra R, Jacobs A, King IIIS, et al. ACC expert consensus document on coronary artery stentsDocument of the American College of Cardiology1. J Am Coll Cardiol 1998;32:1471-82.

[20] Caixeta A, Leon MB, Lansky AJ, Nikolsky E, Aoki J, Moses JW, et al. 5-Year Clinical Outcomes After Sirolimus-Eluting Stent ImplantationInsights From a Patient-Level Pooled Analysis of 4 Randomized Trials Comparing Sirolimus-Eluting Stents With Bare-Metal Stents. J Am Coll Cardiol 2009;54:894-902.

[21] Serruys PW, Ong AT, Morice MC, De Bruyne B, Colombo A, Macaya C, et al. Arterial Revascularisation Therapies Study Part II - Sirolimus-eluting stents for the treatment of patients with multivessel de novo coronary artery lesions. EuroIntervention : journal of EuroPCR in collaboration with the Working Group on Interventional Cardiology of the European Society of Cardiology 2005;1:147-56.

[22] Daemen J, Ong AT, Stefanini GG, Tsuchida K, Spindler H, Sianos G, et al. Three-year clinical follow-up of the unrestricted use of sirolimus-eluting stents as part of the Rapamycin-Eluting Stent Evaluated at Rotterdam Cardiology Hospital (RESEARCH) registry. Am J Cardiol 2006;98:895-901.

[23] Waksman R, Pakala R. Drug-Eluting Balloon: The Comeback Kid? Circulation: Cardiovascular Interventions 2009;2:352-8.

[24] Maisel WH. Unanswered questions--drug-eluting stents and the risk of late thrombosis. N Engl J Med 2007;356:981-4.

[25] Zheng YF, Gu XN, Witte F. Bio-degradable metals. Mater Sci Eng Reports 2014;77:1-34.

[26] Moravej M, Mantovani D. Bio-degradable metals for cardiovascular stent application: interests and new opportunities. International journal of molecular sciences 2011;12:4250-70.

[27] Saito S. New horizon of bio-degradable stent. Catheter Cardiovasc Interv 2005;66:595-6.

[28] Proefschrift. Stents and Vascular Woundhealing [PhD dissertation]. D. M. Whelan 1999: Erasmus University Rotterdam; 1999.

[29] Forrester JS, Fishbein M, Helfant R, Fagin J. A paradigm for restenosis based on cell biology: Clues for the development of new preventive therapies. J Am Coll Cardiol 1991;17:758-69.

[30] Hermawan H. Bio-degradable Metals: From Concept to Applications: Springer Science & Business Media; 2012.

[31] Kornowski R, Mintz GS, Kent KM, Pichard AD, Satler LF, Bucher TA, et al. Increased Restenosis in Diabetes Mellitus After Coronary Interventions Is Due to Exaggerated Intimal Hyperplasia: A Serial Intravascular Ultrasound Study. Circulation 1997;95:1366-9.

[32] Kornowski R, Hong MK, Tio FO, Bramwell O, Wu H, Leon MB. In-Stent Restenosis: Contributions of Inflammatory Responses and Arterial Injury to Neointimal Hyperplasia. J Am Coll Cardiol 1998;31:224-30.

[33] Louis SF, Zahradka P. Vascular smooth muscle cell motility: From migration to invasion. Exp Clin Cardiol 2010;15:e75-e85.

[34] Van Beusekom HMM, Van der Giessen WJ, Van Suylen RJ, Bos E, Bosman F, Serruys PW. Histology after stenting of human saphenous vein bypass grafts: OBEIrvations from surgically excised grafts 3 to 320 days after stent implantation. J Am Coll Cardiol 1993;21:45-54.

[35] Kirkland NT, Lespagnol J, Birbilis N, Staiger MP. A survey of bio-corrosion rates of magnesium alloys. Corros Sci 2010;52:287-91.

[36] Mueller WD, Lucia Nascimento M Fau - Lorenzo de Mele MF, Lorenzo de Mele MF. Critical discussion of the results from different corrosion studies of Mg and Mg alloys for biomaterial applications. Acta Biomater 2010;6:1749-55.

[37] Zhang E, Yang L. Microstructure, mechanical properties and bio-corrosion properties of Mg–Zn–Mn–Ca alloy for biomedical application. Mater Sci Eng A 2008;497:111-8.

[38] Hort N, Huang Y, Fechner D, Störmer M, Blawert C, Witte F, et al. Magnesium alloys as implant materials – Principles of property design for Mg–RE alloys. Acta Biomater 2010;6:1714-25.

[39] Peng Q, Huang Y, Zhou L, Hort N, Kainer KU. Preparation and properties of high purity Mg–Y biomaterials. Biomaterials 2010;31:398-403.

[40] Liu B, Zheng YF. Effects of alloying elements (Mn, Co, Al, W, Sn, B, C and S) on biodegradability and in vitro biocompatibility of pure iron. Acta Biomater 2011;7:1407-20.

[41] Liu B, Zheng YF, Ruan LQ. In vitro investigation of $Fe_{30}Mn_6Si$ shape memory alloy as potential bio-degradable metallic material. Mater Lett 2011;65:540-3.

[42] Yusop AH, Bakir AA, Shaharom NA, Abdul Kadir MR, Hermawan H. Porous bio-degradable metals for hard tissue scaffolds: a review. International journal of biomaterials 2012;2012:1-10.

[43] Ge Q, Dellasega D Fau - Demir AG, Demir Ag Fau - Vedani M, Vedani M. The processing of ultrafine-grained Mg tubes for bio-degradable stents. Acta Biomater 2013;9.

[44] Li H, Zheng Y, Qin L. Progress of bio-degradable metals. Progress in Natural Science: Materials International 2014;24:414-22.

[45] Narayanan TSNS, Park I-S, Lee M-H. 2-Surface modification of magnesium and its alloys for biomedical applications: Opportunities and challenges. Surface Modification of Magnesium and its Alloys for Biomedical Applications. Oxford: Woodhead Publishing; 2015. p. 29-87.

[46] Chu PK, Wu GS. 3-Surface design of bio-degradable magnesium alloys for biomedical applications. Surface Modification of Magnesium and its Alloys for Biomedical Applications. Oxford: Woodhead Publishing; 2015. p. 89-119.

[47] Erdmann N, Angrisani N, Reifenrath J, Lucas A, Thorey F, Bormann D, et al. Biomechanical testing and degradation analysis of MgCa0.8 alloy screws: A comparative in vivo study in rabbits. Acta Biomater 2011;7:1421-8.

[48] Zhang E, Xu L, Yu G, Pan F, Yang K. In vivo evaluation of bio-degradable magnesium alloy bone implant in the first 6 months implantation. J Biomed Mater Res A 2009;90A:882-93.

[49] Pierson D, Edick J, Tauscher A, Pokorney E, Bowen P, Gelbaugh J, et al. A simplified in vivo approach for evaluating the bio-degradable behavior of candidate stent materials. J Biomed Mater Res B 2012;100B:58-67.

[50] Sanschagrin A, Tremblay R, Angers R, Dubé D. Mechanical properties and microstructure of new magnesium-lithium base alloys. Mater Sci Eng A 1996;220:69-77.

[51] Peuster M, Wohlsein P, Brugmann M, Ehlerding M, Seidler K, Fink C, et al. A novel approach to temporary stenting: degradable cardiovascular stents produced from corrodible metal - results 6-18 months after implantation into New Zealand white rabbits. Heart 2001;86:563-9.

[52] Peuster M, Hesse C, Schloo T, Fink C, Beerbaum P, Schnakenburg C. Long-term biocompatibility of a corrodible peripheral iron stent in the porcine descending aorta. Biomaterials 2006;27:4955-62.

[53] Hermawan H, Moravej M, Dubé D, Fiset M, Mantovani D. Degradation Behaviour of Metallic Biomaterials for Degradable Stents. Adv Mater Res 2006;15-17:113-8.

[54] Nie FL ZY, Wei SC, Hu C, Yang G. In vitro corrosion, cytotoxicity and hemocompatibility of bulk nanocrystalline pure iron. Biomed Mater 2010;5.

[55] Hermawan H, Dube D, Mantovani D. Development of Degradable Fe-35Mn Alloy for Biomedical Application. Adv Mater Res 2007;15.

[56] Moravej M, Prima F, Fiset M, Mantovani D. Electroformed iron as new biomaterial for degradable stents: Development process and structure–properties relationship. Acta Biomater 2010;6:1726-35.

[57] Hermawan H, Dube D, Mantovani D. Degradable metallic biomaterials: design and development of Fe-Mn alloys for stents. J Biomed Mater Res A 2010;93:1-11.

[58] Schinhammer M, Hänzi AC, Löffler JF, Uggowitzer PJ. Design strategy for bio-degradable Fe-based alloys for medical applications. Acta Biomater 2010;6:1705-13.

[59] Hermawan H, Alamdari H, Mantovani D, Dube D. Iron-manganese: new class of metallic degradable biomaterials prepared by powder metallurgy. Powder Metall 2008;51:38-45.

[60] McGregor DB, Baan Ra Fau - Partensky C, Partensky C Fau - Rice JM, Rice Jm Fau - Wilbourn JD, Wilbourn JD. Evaluation of the carcinogenic risks to humans associated with surgical implants and other foreign bodies - a report of an IARC Monographs Programme Meeting. International Agency for Research on Cancer. Eur J Cancer 2000;36:307-13.

[61] Zhang S, Zhang X, Zhao C, Li J, Song Y, Xie C, et al. Research on an Mg-Zn alloy as a degradable biomaterial. Acta Biomater 2010;6:626-40.

[62] Aghion E, Levy G, Ovadia S. In vivo behavior of bio-degradable Mg-Nd-Y-Zr-Ca alloy. Journal of materials science Materials in medicine 2012;23:805-12.

[63] Li L, Gao J, Wang Y. Evaluation of cyto-toxicity and corrosion behavior of alkali-heat-treated magnesium in simulated body fluid. Surf Coat Technol 2004;185:92-8.

[64] Song G. Control of biodegradation of biocompatable magnesium alloys. Corros Sci 2007;49:1696-701.

[65] Wang Y, Wei M, Gao J. Improve corrosion resistance of magnesium in simulated body fluid by dicalcium phosphate dihydrate coating. Mater Sci Eng C 2009;29:1311-6.

[66] Yamawaki T, Shimokawa H, Kozai T, Miyata K, Higo T, Tanaka E, et al. Intramural delivery of a specific tyrosine kinase inhibitor with bio-degradable stent suppresses the restenotic changes of the coronary artery in pigs in vivo. Journal of the American College of Cardiology 1998;32:780-6.

[67] Tamai H, Igaki K Fau - Kyo E, Kyo E Fau - Kosuga K, Kosuga K Fau - Kawashima A, Kawashima A Fau - Matsui S, Matsui S Fau - Komori H, et al. Initial and 6-month results of bio-degradable poly-l-lactic acid coronary stents in humans. Circulation 2000;25:399-404.

[68] Nishio S, Kosuga K, Igaki K, Okada M, Kyo E, Tsuji T, et al. Long-Term (>10 Years) clinical outcomes of first-in-human bio-degradable poly-l-lactic acid coronary stents: Igaki-Tamai stents. Circulation 2012;125:2343-53.

[69] Tamai H, Igaki K, Tsuji T, Kyo E, Kosuga K, Kawashima A, et al. A Bio-degradable Poly-l-lactic Acid Coronary Stent in the Porcine Coronary Artery. Journal of Interventional Cardiology 1999;12:443-50.

[70] Hietala EM, Salminen Us Fau - Stahls A, Stahls A Fau - Valimaa T, Valimaa T Fau - Maasilta P, Maasilta P Fau - Tormala P, Tormala P Fau - Nieminen MS, et al. Biodegradation of the copolymeric polylactide stent. Long-term follow-up in a rabbit aorta model. J Vasc Res 2001;38:361-9.

[71] Vogt F, Stein A, Rettemeier G, Krott N, Hoffmann R, Dahl Jv, et al. Long-term assessment of a novel bio-degradable paclitaxel-eluting coronary polylactide stent. European Heart Journal 2004;25:1330-40.

[72] Pierson D, Edick J, Tauscher A, Pokorney E, Bowen PK, Gelbaugh J, et al. A simplified in vivo approach for evaluating the bio-degradable behavior of candidate stent materials. J Biomed Mater Res B 2012;100B:58-67.

[73] Heublein B, Rohde R, Kaese V, Niemeyer M, Hartung W, Haverich A. Biocorrosion of magnesium alloys: a new principle in cardiovascular implant technology? Heart 2003;89:651-6.

[74] Di Mario C, Griffiths H Fau - Goktekin O, Goktekin O Fau - Peeters N, Peeters N Fau - Verbist J, Verbist J Fau - Bosiers M, Bosiers M Fau - Deloose K, et al. Drug-eluting bio-degradable magnesium stent. J Interv Cardiol 2004;17:391-5.

[75] Waksman R, Pakala R Fau - Okabe T, Okabe T Fau - Hellinga D, Hellinga D Fau - Chan R, Chan R Fau - Tio MO, Tio Mo Fau - Wittchow E, et al. Efficacy and safety of absorbable

metallic stents with adjunct intracoronary beta radiation in porcine coronary arteries. J Interv Cardiol 2007;20:367-72.

[76] Zartner P, Cesnjevar R Fau - Singer H, Singer H Fau - Weyand M, Weyand M. First successful implantation of a bio-degradable metal stent into the left pulmonary artery of a preterm baby. Catheter Cardiovasc Interv 2005;66:590-4.

[77] Seitz J-M, Durisin M, Goldman J, Drelich J. Recent advances in bio-degradable metals for medical sutures: a critical review. Advanced Healthcare Materials 2015:in press.

[78] Witte F. The history of bio-degradable magnesium implants: A review. Acta Biomater 2010;6:1680-92.

[79] Caiazzo G, Kilic ID, Fabris E, Serdoz R, Mattesini A, Foin N, et al. Absorb bio-degradable vascular scaffold: what have we learned after 5 years of clinical experience? Cardiology 2015:in press.

[80] Iqbal J, Gunn J, Serruys PW. Coronary stents: historical development, current status and future directions. Br Med Bull 2013;106:193-211.

[81] Boland EL, Shine R, Kelly N, Sweeney CA, McHugh PE. A review of material degradation modelling for the analysis and design of bio-degradable stents. Annals of biomedical engineering 2015;online DOI: 10.1007/s10439-015-1413-5.

[82] Grube E, Sonoda S, Ikeno F, Honda Y, Kar S, Chan C, et al. Six- and twelve-month results from first human experience using everolimus-eluting stents with bio-degradable polymer. Circulation 2004;109:2168-71.

[83] Tamai H, Igaki K, Kyo E, Kosuga K, Kawashima A, Matsui S, et al. Initial and 6-month results of bio-degradable poly-l-lactic acid coronary stents in humans. Circulation 2000;102:399-404.

[84] Serruys PW, Chevalier B, Dudek D, Cequier A, Carrie D, Iniguez A, et al. A bio-degradable everolimus-eluting scaffold versus a metallic everolimus-eluting stent for ischaemic heart disease caused by de-novo native coronary artery lesions (ABSORB II): an interim 1-year analysis of clinical and procedural secondary outcomes from a randomised controlled trial. Lancet 2015;384:43-54.

[85] Di Mario C, Caiazzo G. Bio-degradable stents: the golden future of angioplasty? Lancet 2015;384:10-2.

[86] Nishio S, Kosuga K, Igaki K, Okada M, Kyo E, Tsuji T, et al. Long-term (> 10 years) clinical outcomes of first-in-human bio-degradable poly-l-lactic acid coronary stents Igaki-Tamai stents. Circulation 2012;125:2343-52.

[87] Onuma Y, Serruys PW. Bio-degradable scaffold: the advent of a new era in percutaneous coronary and peripheral revascularization? Circulation 2011;123:779-97.

[88] Witte F, Fischer J, Nellesen J, Crostack HA, Kaese V, Pisch A, et al. In vitro and in vivo corrosion measurements of magnesium alloys. Biomaterials 2006;27:1013-8.

[89] Willumeit R, Fischer J, Feyerabend F, Hort N, Bismayer U, Heidrich S, et al. Chemical surface alteration of bio-degradable magnesium exposed to corrosion media. Acta Biomater 2011;7:2704-15.

[90] Bowen PK, Drelich J, Goldman J. Magnesium in the murine artery: probing the products of corrosion. Acta Biomater 2014;10:1475-83.

[91] Bowen PK, Drelich A, Drelich J, Goldman J. Rates of in vivo (arterial) and in vitro biocorrosion for pure magnesium. J Biomed Mater Res A 2014.

[92] Zheng YF, Gu XN, Witte F. Bio-degradable metals. Mater Sci Eng R-Rep 2014;77:1-34.

[93] Balcon R, Beyar R, Chierchia S, Scheerder I, Hugenholtz P, Kiemeneij F, et al. Recommendations on stent manufacture, implantation and utilization. Eur Heart J 1997;18:1536-47.

[94] Poncin P, Proft J. Stent tubing: understanding the desired attributes. In: Shrivastava S, editor. Medical Device Materials: Proceedings of the Materials & Processes for Medical Devices Conference. Materials Park, Ohio: ASM International; 2004. p. 253-9.

[95] Damien Kenny ZMH. Bio-degradable stents for pediatric practice: where are we now? Interventional Cardiology 2015;7:245-55.

[96] Lewitus D, Vogelstein Rj Fau - Zhen G, Zhen G Fau - Choi Y-S, Choi Ys Fau - Kohn J, Kohn J Fau - Harshbarger S, Harshbarger S Fau - Jia X, et al. Designing tyrosine-derived polycarbonate polymers for bio-degradable regenerative type neural interface capable of neural recording. Trans Neural Syst Rehabil Eng 2015;19:204-12.

[97] International A. ASTM F138-08, Standard Specification for Wrought 18 Chromium-14 Nickel-2.5 Molybdenum Stainless Steel Bar and Wire for Surgical Implants. West Conshohocken, PA, USA, 2008.

[98] Mani G, Feldman MD, Patel D, Agrawal CM. Coronary stents: A materials perspective. Biomaterials 2007;28:1689-710.

[99] Schinhammer M, Pecnik CM, Rechberger F, Hänzi AC, Löffler JF, Uggowitzer PJ. Recrystallization behavior, microstructure evolution and mechanical properties of bio-degradable Fe–Mn–C(–Pd) TWIP alloys. Acta Materialia 2012;60:2746-56.

[100] Schinhammer M, Steiger P, Moszner F, Löffler JF, Uggowitzer PJ. Degradation performance of bio-degradable FeMnC(Pd) alloys. Materials Science and Engineering: C 2013;33:1882-93.

[101] Gu X-N, Zheng Y-F. A review on magnesium alloys as bio-degradable materials. Frontiers of Materials Science in China 2010;4:111-5.

[102] Lévesque J, Hermawan H, Dubé D, Mantovani D. Design of a pseudo-physiological test bench specific to the development of bio-degradable metallic biomaterials. Acta Biomaterialia 2008;4:284-95.

[103] Rong-chang Z, Jun C, Dietzel W, Hort N, Kainer K. Electrochemical behavior of magnesium alloys in simulated body fluids. Trans Nonferrous Met Soc China 2007;17:166-70.

[104] Hänzi AC, Gerber I, Schinhammer M, Löffler JF, Uggowitzer PJ. On the in vitro and in vivo degradation performance and biological response of new bio-degradable Mg–Y–Zn alloys. Acta Biomaterialia 2010;6:1824-33.

[105] Hanzi ACS, A.S.; Uggowitzer, P.J. Design strategy for microalloyed ultra-ductile magnesium alloys for medical applications. Mater Sci Forum 2009:618-9.

[106] Kubasek J, Vojtech D. Structural characteristics and corrosion behavior of bio-degradable Mg-Zn, Mg-Zn-Gd alloys. Journal of materials science Materials in medicine 2013;24:1615-26.

[107] Zhang E, Yin D, Xu L, Yang L, Yang K. Microstructure, mechanical and corrosion properties and biocompatibility of Mg–Zn–Mn alloys for biomedical application. Materials Science and Engineering: C 2009;29:987-93.

[108] Kannan MB, Raman RKS. In vitro degradation and mechanical integrity of calcium-containing magnesium alloys in modified-simulated body fluid. Biomaterials 2008;29:2306-14.

[109] Li Z, Gu X, Lou S, Zheng Y. The development of binary Mg–Ca alloys for use as bio-degradable materials within bone. Biomaterials 2008;29:1329-44.

[110] Poncin P, Profit J. Stent tubing: understanding the desired attributes. In: Shrivastava S, editor. Materials & Processes for Medical Devices. Materials Park, OH: ASM International; 2004. p. 253-9.

[111] Onuma Y, Ormiston J, Serruys PW. Bio-degradable scaffold technologies. Circ J 2011;75:509-20.

[112] Alexy RD, Levi DS. Materials and manufacturing technologies available for production of a pediatric bio-degradable stent. Biomed Res Int 2013;2013:137985.

[113] Capodanno D, Gori T, Nef H, Latib A, Mehilli J, Lesiak M, et al. Percutaneous coronary intervention with everolimus-eluting bio-degradable vascular scaffolds in routine clinical practice: early and midterm outcomes from the European multicentre GHOST-EU registry. EuroIntervention 2014.

[114] Serruys PW, Chevalier B, Dudek D, Cequier A, Carrie D, Iniguez A, et al. A bio-degradable everolimus-eluting scaffold versus a metallic everolimus-eluting stent for ischaemic heart disease caused by de-novo native coronary artery lesions (ABSORB II): an interim 1-year analysis of clinical and procedural secondary outcomes from a randomised controlled trial. Lancet 2014.

[115] Di Mario C, Caiazzo G. Bio-degradable stents: the golden future of angioplasty? Lancet 2014.

[116] Mani G, Feldman M, Patel D, Agrawal C. Coronary stents: a materials perspective. Biomaterials 2007;28:1689-710.

[117] Bowen PK, Guillory II R, Shearier ER, Seitz JM, Drelich J, Bocks ML, et al. Metallic zinc exhibits optimal biocompatibilitiy for bio-degradable endovascular stents. Mater Sci Eng C 2015.

[118] Waksman R, Pakala R, Kuchulakanti PK, Baffour R, Hellinga D, Seabron R, et al. Safety and efficacy of bio-degradable magnesium alloy stents in porcine coronary arteries. Catheter Cardiovasc Interv 2006;68:607-17.

[119] Garg S, Serruys PW. Coronary Stents Looking Forward. J Am Coll Cardiol 2010;56:S43-S78.

[120] Seitz JM, Durisin M, Goldman J, Drelich JW. Recent Advances in Bio-degradable Metals for Medical Sutures: A Critical Review. Adv Healthc Mater 2015.

[121] Vojtech D, Kubasek J, Serak J, Novak P. Mechanical and corrosion properties of newly developed bio-degradable Zn-based alloys for bone fixation. Acta Biomater 2011;7:3515-22.

[122] Werkhoven RJ, Sillekens WH, van Lieshout JBJM. Processing Aspects of Magnesium Alloy Stent Tube. Magnesium Technology: John Wiley & Sons, Inc.; 2011. p. 419-24.

[123] Zhang X, Yuan G, Wang Z. Mechanical properties and biocorrosion resistance of Mg-Nd-Zn-Zr alloy improved by cyclic extrusion and compression Mater Lett 2012;74:128-31

[124] Kang F, Liu JQ, Wang JT, Zhao X. Equal Channel Angular Pressing of a Mg–3Al–1Zn Alloy with Back Pressure. Adv Eng Mater 2010;12:730-4.

[125] E.M. Savitskii IANS, OTN. Metallurgiya i Toplivo 1960;5:52.

[126] Z.A. Sviderskaya TAB, et al. In the collection: Investigation of Alloys of Nonferrous Metals. Izd AN SSSR 1962;3.

[127] M.V. Zakharov ZAS, et al. Izv. vuzov. Tsvetnaya Metallurgiya 1961;4.

[128] I.N. Fridlyander VFS, and N. V. Shiryaeva. Metally 1965;2.

[129] Drits ME, Kadaner ES, Kuz'mina VI. Effect of lithium on the aging and mechanical properties of Al−Zn−Mg alloys. Metal Science and Heat Treatment 1967;9:920-2.

[130] Schrauzer GN. Lithium: occurrence, dietary intakes, nutritional essentiality. J Am Coll Nutr 2002;21:14-21.

[131] Halford B. Limits Of Lithium. Chemical and Engineering News 2013; 91:15-20.

[132] Micronutrients IoMUPo. Dietary Reference Intakes for Vitamin A, Vitamin K, Arsenic, Boron, Chromium, Copper, Iodine, Iron, Manganese, Molybdenum, Nickel, Silicon, Vanadium, and Zinc. Dietary Reference Intakes for Vitamin A, Vitamin K, Arsenic, Boron, Chromium, Copper, Iodine, Iron, Manganese, Molybdenum, Nickel, Silicon, Vanadium, and Zinc. Washington (DC): National Academy Press; 2001. p. 480-81.

[133] Bowen PK, Guillory Ii RJ, Shearier ER, Seitz J-M, Drelich J, Bocks M, et al. Metallic zinc exhibits optimal biocompatibility for bio-degradable endovascular stents. Materials Science and Engineering: C 2015;56:467-72.

[134] Bowen PK, Shearier ER, Zhao S, Guillory Ii RJ, Zhao F, Goldman J, et al. Bio-degradable Metals for Cardiovascular Stents: from Clinical Concerns to recent Zn-Alloys. Adv Healthc Mater 2016;03 1-20.

[135] H. Hermawan MM, D. Dubé, M. Fiset, D. Mantovani. Degradation Behaviour of Metallic Biomaterials for Degradable Stents. Adv Mater Res 2006;15-17:113-8.

[136] Bowen PK, Shearier ER, Zhao S, Guillory RJ, Zhao F, Goldman J, et al. Bio-degradable Metals for Cardiovascular Stents: from Clinical Concerns to Recent Zn-Alloys. Adv Healthc Mater 2016.

[137] Pelton AD. The Li-Zn (Lithium-Zinc) phase diagram. J Phase Equilib 1991;12:42-5.

[138] Pavlyuk V, Chumak I, Akselrud L, Lidin S, Ehrenberg H. LiZn(4-x) (x=0.825) as a (3+1)-dimensional modulated derivative of hexagonal close packing. Acta Crystallogr B Struct Sci Cryst Eng Mater 2014;70(Pt 2):212-7.

[139] Zintl E, Schneider A. Metals and alloys. XV. X-ray analysis of lithium-zinc alloys. Z Elektrochem Angew Phys Chem 1935;41:764-7

[140] Schönemann H, Schuster H-U. Rev Chim Miner 1976;13:32-40.

[141] Pavlyuk V, Chumak I, Ehrenberg H. Polymorphism of Li2Zn3. Acta Crystallogr Sect B 2012;68:34-9.

[142] Kokubo T, Kushitani H, Sakka S, Kitsugi T, Yamamuro T. Solutions able to reproduce in vivo surface-structure changes in bioactive glass-ceramic A-W. J Biomed Mater Res 1990;24:721-34.

[143] ASTM G31-72 SPfLICToM. West Conshohocken, PA: ASTM International; 2004.

[144] Wang Q, Tan LL, Xu WL, Zhang BC, Yang K. Dynamic behaviors of a Ca-P coated AZ31B magnesium alloy during in vitro and in vivo degradations. Mater Sci Eng B 2011;176:1718-26.

[145] Yang L, Zhang EL. Biocorrosion behavior of magnesium alloy in different simulated fluids for biomedical application. Mater Sci Eng C 2009;29:1691-6.

[146] Helson JA, Breme HJ. Metals as Biomaterials. 4th ed. ed: New York Wiley; 1998. p. 101-51.

[147] Khan MA, Williams RL, Williams DF. The corrosion behaviour of Ti-6Al-4V, Ti-6Al-7Nb and Ti-13Nb-13Zr in protein solutions. Biomaterials 1999;20:631-7.

[148] Jones DA. Principles and prevention of corrosion, 2nd ed. New York, NY: Macmillan Publishing Co.; 1996. p. 142-7.

[149] Bowen PK, Drelich J, Goldman J. Magnesium in the murine artery: probing the products of corrosion. Acta Biomater 2014;10:1475-83.

[150] Hascoët S, Baruteau A, Jalal Z, Mauri L, Acar P, Elbaz M, et al. Stents in paediatric and adult congenital interventional cardiac catheterization. Archives of Cardiovascular Diseases 2014;107:462-75.

[151] Saris NE, Mervaala E Fau - Karppanen H, Karppanen H Fau - Khawaja JA, Khawaja Ja Fau - Lewenstam A, Lewenstam A. Magnesium. An update on physiological, clinical and analytical aspects. Clin Chim Acta 2000;294:1-26.

[152] Cheng J, Zheng YF. In vitro study on newly designed bio-degradable Fe-X composites (X = W, CNT) prepared by spark plasma sintering. Journal of biomedical materials research Part B, Applied biomaterials 2013;101:485-97.

[153] Seitz J-M, Lucas A, Kirschner M. Magnesium-Based Compression Screws: A Novelty in the Clinical Use of Implants. JOM 2016;68:1177-82.

[154] A. Atrens ML, N. I. Zainal Abidin, G.-L. Song. Corrosion of magnesium alloys. Corrosion of magnesium (Mg) alloys and metallurgical influence. Philadelphia, PA, USA: Woodhead; 2011. p. 153.

[155] Zhao S, McNamara CT, Bowen PK, Verhun N, Braykovich JP, Goldman J, et al. Structural characteristics and in vitro biodegradation of a novel Zn-Li alloy prepared by induction melting and hot rolling Metallurgical and Materials Transactions A 2016;Under review.

[156] Abramoff MD, Magalhaes PJ, Ram SJ. Image Processing with ImageJ. Biophotonics International 2004;11:36-42.

[157] Bowen PK, Drelich J, Goldman J. Magnesium in the murine artery: Probing the products of corrosion. Acta Biomaterialia 2014;10:1475-83.

[158] Frost RL, Martens W, Williams PA, Kloprogge JT. Raman and infrared spectroscopic study of the vivianite-group phosphates vivianite, baricite and bobierrite. Mineralogical Magazine 2002;66:1063-73.

[159] Holt C, van Kemenade MJJM, Harries JE, Nelson LS, Bailey RT, Hukins DWL, et al. Preparation of amorphous calcium-magnesium phosphates at pH 7 and characterization by x-ray absorption and fourier transform infrared spectroscopy. Journal of Crystal Growth 1988;92:239-52.

[160] Gibson IR, Bonfield W. Preparation and characterization of magnesium/carbonate co-substituted hydroxyapatites. Journal of materials science Materials in medicine 2002;13:685-97.

[161] Meejoo S, Maneeprakorn W, Winotai P. Phase and thermal stability of nanocrystalline hydroxyapatite prepared via microwave heating. Thermochimica Acta 2006;447:115-20.

[162] Zberg B, Uggowitzer PJ, Loffler JF. MgZnCa glasses without clinically oBEIrvable hydrogen evolution for bio-degradable implants. Nat Mater 2009;8:887-91.

[163] Białobrzeski A, Saja K, Żmudzińska M. Corrosion behaviour of binary Mg-Li alloys for plastic forming. Archives of Foundry Engineering 2011.

[164] Drelich AJ, Bowen PK, LaLonde L, Goldman J, Drelich J. Importance of oxide film in endovascular bio-degradable zinc stents. Surface Innovations 2016;0:1-.

[165] Kokubo T, Takadama H. How useful is SBF in predicting in vivo bone bioactivity? Biomaterials 2006;27:2907-15.

[166] Cui FZ, Feng QL. Biomaterials Science (Chinese Edition): Tsinghua University Press; 2004.

[167] Ding Y, Wen C, Hodgson P, Li Y. Effects of alloying elements on the corrosion behavior and biocompatibility of bio-degradable magnesium alloys: a review. Journal of Materials Chemistry B 2014;2:1912-33.

Chapter 2 Objectives and Hypotheses

2.1 The proposed Zn-Li alloy in stent application

The early use of lithium was as a hardener in aluminum-alloy bearing materials in the 1960s [1-3]. The aging and mechanical properties in ternary and more complex alloy systems were extensively studied at the beginning, due to the great desire of high-strength alloys for operation at room and elevated temperatures in the Soviet Union and abroad. Zakharov and Fridlyander showed the favorable effect of lithium on the mechanical properties of aluminum alloys [3, 4]. Later Drits noted that alloying of Al-Zn-Mg alloys with small amounts of lithium (less than 0.75%) could not only increase the strength properties but also reduce the softening of the alloy on aging at high temperatures and long times [5].

The illumination of adding lithium into zinc to improve the stent largely comes from the positive sides of magnesium alloy LAE442 that has 4 wt.% of lithium, 4 wt.% of aluminium and 2 wt.% of rare-earth elements. LAE442 has been tested as non-allergic [6], bio-degradable, which exhibits slow and regular degradation without the formation of radiographic gas [7, 8], and is widely considered as the most promising bio-degradable implant for orthopedic use [7, 9].

Previous reports on small additions of lithium to bio-degradable alloys include LAE 442, which contains 4 wt.% of lithium and demonstrated good biocompatibility when implanted to the New Zealand rabbit [7]. After three months, it degraded very regularly (4.7 ± 0.1 mm^2) with volume loss of ~46%. No clinical intolerances were found during the 12 month

implantation [7]. It can also be estimated that Li-Zn alloys could slow down the corrosion rate, which means the Zn-Li alloys could probably remain intact *in vivo* for more than 4 months as compared to the pure zinc.

In terms of clinical feasibility, lithium was detected in human organs and fetal tissues already in the late 19th century, leading to early suggestions of possible specific functions in the organism [10]. Animal studies have demonstrated that Li plays a role in the expansion of the pluripotential stem cell pool to more mature progenitor cells and blood elements [10, 11]. In lithium deficient rats, behavioral abnormalities and a significant negative effect on litter size and litter weight at birth were observed [10]. In lithium deficient goats the conception rate was reduced, gravid lithium deficient goats experienced a higher incidence of spontaneous abortions [10]. In humans, the fact that lithium can calm the highs of mania and lift the lows of depression has been known for more than 60 years [11]. It is the only medication that reduces the risk of suicide in bipolar patients and it is inexpensive. However, there are the side effects such as tremors, frequent urination, thyroid problems, weight gain, or even kidney failure if overdosed because the toxic dose of lithium is only about two to three times higher than its therapeutic dose [11].

The toxic potential of a zinc-lithium stent should be negligible. A cut, polished alloy stent may comprise, to a first approximation, ~50 mg of the pure metal. Assuming complete degradation within one year, the expected daily dose of elements are estimated here (shown in Table 2.1), which are far below the daily body consumption allowance [10].

Table 2.1. Released amount of elements from the stent should be below a daily body consumption allowance

Intake	Daily Allowance for Adult males	*Estimated release from Zn-Li alloy
Zn	10 mg [12]	$<140\,\mu g$
Li	0.6 mg [10]	$< 1\,\mu g$

(*The daily amount of release can be obtained by dividing the mass of Zn and Li into 365 days. For alloy Zn-14 at.% Li, if assuming the stent is 50 mg, then the total mass of Li is 0.38 mg so the daily release of Li into biological system is $1\,\mu g$).

2.2 Objectives

The objectives of this Ph.D. research include (Fig.2.1):

- to produce a new Zn-Li alloy system with superior mechanical properties and to understand its phase constitutions, microstructure evolutions and mechanical properties with changing composition; then select for the optimum compositions for *in vitro* and *in vivo* experiments;

- to simulate the degradation behavior of the Zn-Li alloy *in vitro* and explore the relations between corrosion rate, corrosion products and surface morphology with changing compositions;

- to show the potential of the Zn-Li alloy in stent application by investigating the degradation mechanism, the rate of bioabsorption, biocompatibility, cytotoxicity and corrosion product migration *in vivo* using a rat model.
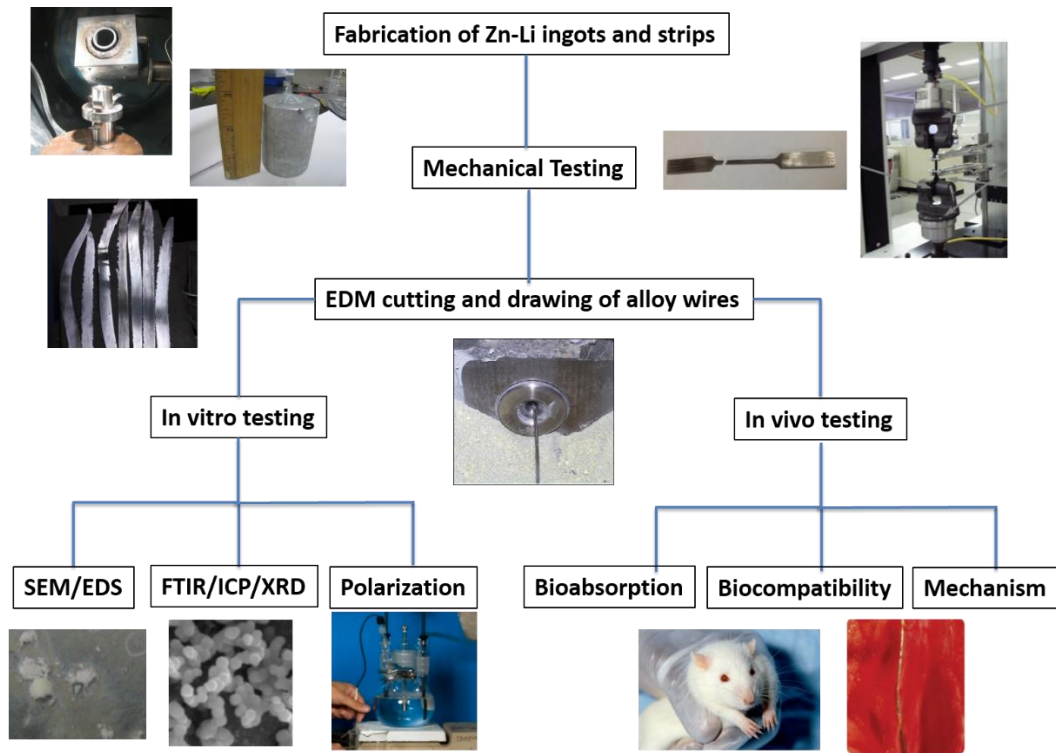
Fig. 2.1. Research flowchart for the Zn-Li system in this proposal

2.3 Hypotheses

Hypothesis I: *The increase of Li from 2% to 6 at.% would increase the mechanical strength of the Zn alloy while retaining suitable ductility due to the intermetallic precipitation hardening.*
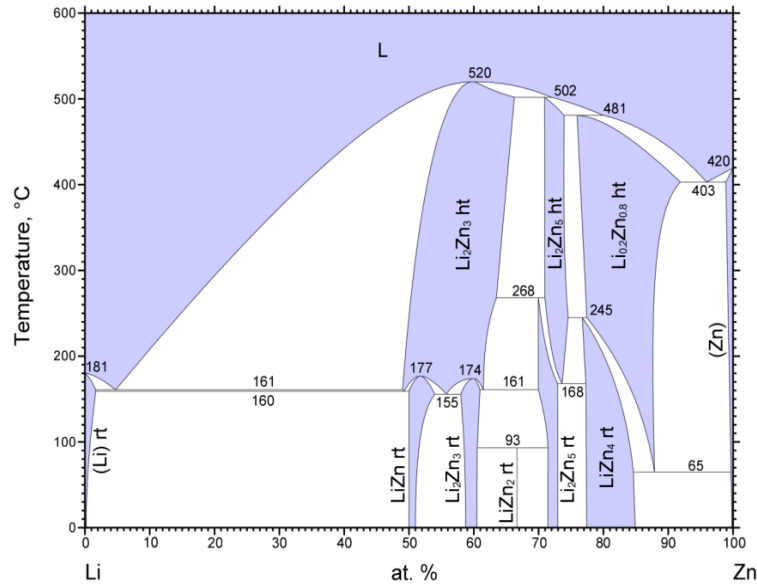
Fig. 2.2. Phase diagram of Zn-Li (Retrieved from the ASM Phase Diagram database)

Based on the binary phase diagram (Fig.2.2) and the compositions we chose, the final product could be a Zn-rich solid solution and the $LiZn_4$ intermetallic. In solid solutions, lithium solute atoms can either sit in substitutional or interstitial positions. The solute atoms cause lattice distortions that impede dislocation motion, increasing the yield stress of the Zn-Li alloys [13]. Increasing the concentration of the lithium atoms will increase the yield strength of zinc while retaining its ductility due to the intermetallic precipitation hardening [14]. However, there could be a limit to the amount of solute that can be added before a second phase is created [13]. Once above this limit concentration, adding more lithium will cause the formation of a second phase. The Zn-Li alloys that compose the second phase precipitates act as pinning points in a similar manner to solutes. If the precipitated atoms are small, the dislocations would cut through them. As a result, new surfaces of the particle

53

would get exposed to the matrix and the particle-matrix interfacial energy would increase; for larger precipitate particles with further additions, looping or bowing of the dislocations would occur which result in longer dislocations [15]. The interaction of precipitated intermetallics with the dislocations could hinder the propagation of dislocations and result in the increase of strength [15]. We hope to establish some relations between the volume fractions of the intermetallics and the mechanical strength.

Another possible strengthening mechanism here is the texture strengthening. In that case, randomly oriented grains would slip on their appropriate glide systems and rotate from their initial conditions, and a strong preferred orientation develops so that certain slip planes tend to align in the direction of rolling [16]. This texture phenomenon depends heavily on the compositions and it happens only when 8 at.% or more lithium is added into the Zn system.

The study of lattice parameters of solid solutions, evolution of microstructures, the volumetric fractions of intermetallics and the texture transformations at different compositions could help us understand the physiochemical characteristics of this alloy system. This could give us direction on if or how the alloying of lithium strengthens zinc, providing a basis for selecting the optimum alloy compositions needed for the *in vitro* and *in vivo* corrosion testing.

Hypothesis II: *The Zn-Li alloy will exhibit near ideal corrosion behavior like pure Zn, and the corrosion rate of Zn-Li alloy will increase a bit with addition of Li according to the relationship: $Corrosion\ Rate = f(i_{corr})$.*

With uniform distribution of anodic/cathodic reactants, corrosion reactions would proceed in a uniform manner which would result in the uniform loss of dimension. As mentioned in *Hypothesis II*, micro-galvanic corrosion could be one of the leading corrosions. Therefore, if small and finely dispersed intermetallic phases are distributed uniformly in the metal matrix, micro-galvanic corrosion would happen everywhere and macroscopically uniform corrosion can be achieved. It should be noted that corrosion also depends on the biological environment. *In vitro* testing fluid consisting of inorganic ions contributes to the formation of mineral-like corrosion layers; while the *in vivo* environment carries organic components such as proteins and cells which might lead to a high nitrogen level in the corrosion layer [17].

In relation to the corrosion rate of most implant materials, electrochemical techniques are used in view of their sensitivity. The most common method of corrosion rate determination for slowly corroding materials is based on the determination of the polarization resistance Rp (ASTM G59).

$$Rp = \frac{\partial \Delta E}{\partial i} \qquad\qquad \text{Eq. 2.1}$$

$$i_{corr} = 10^6 \times \frac{B}{Rp} \qquad\qquad \text{Eq. 2.2}$$

$$B = \frac{b_a b_c}{2.303(b_a + b_c)} \qquad\qquad \text{Eq. 2.3}$$

$$Corrosion\ Rate = 3.27 \times 10^{-3} \frac{i_{corr} EW}{\rho} \qquad\qquad \text{Eq. 2.4}$$

(where i_{corr} defined as corrosion current density, mμA/cm^2; b_a and b_c are Tafel constants obtained from the anodic and cathodic polarization measurement, V; EW the equivalent mass of corroding species, g; ρ is the density of corroding material, g/cm^3).

The corrosion rate of Zn-Li alloys could increase with increasing lithium content: 1) as the lithium is very active, so increasing addition of lithium may increase the activity of the zinc alloys and shift the corrosion potential to more negative values; 2) as we observed from XRD, more lithium would increase the amount of $LiZn_4$ intermetallics. The intermetallic phases would act as a cathode and the Zn matrix act as the anode, which could generate micro-galvanic corrosion. The increased presence of intermetallic phases may lead to the formation of more galvanic cells so that the galvanic corrosion could be enhanced and more severe corrosion would occur; 3) however the increased incorporation of lithium into solid solutions or redundant lithium around solid solutions may reduce the corrosion rate-as they can also decrease the potential differences at the interfaces of phases and matrix. The study of solubility of lithium could help understand this effect.

Hypothesis III: *Zn-Li alloys will exhibit desirable biocompatibility and a benign/stable cellular response in vivo.*

Previous studies with Zn wires within the abdominal aorta demonstrated excellent biocompatibility [18]. At 2.5 months the Zn wire was completely neo-endothelialized with a thin layer of endothelial cells. There was no significant inflammatory response, intimal hyperplasia, or localized necrosis over 6.5 months. These findings indicate that Zn may suppress localized cellular activity that contributes to the thickening of the neo-intimal.

To explore the biocompatibility of alloy wires, both 4N Zn and Zn-Li alloy wire samples with diameter of 0.25 mm and length of 2 cm were punched into the abdominal aorta and then directed into the lumen for 10 mm before exteriorization. In this case, wires were immersed in the flowing blood to mimic the environment of a stent strut. After 2-12

months, rats were euthanized and rat aortas containing the wire implants were harvested. The wires had not become dislocated from their implant location at the time of collection. To preserve the corrosion layer, explanted wires were preserved in 200 proof ethanol.

The leftover wires with aortas were snap-frozen in liquid nitrogen and cryo-sectioned for histological analysis [19]. Before staining, samples were preserved in a -80 ºC freezer. Cross sections were ethanol fixed and then stained with hematoxylin and eosin (H&E), mounted in Permount solution and imaged using an Olympus BX51, DP70 bright-field microscope.

The neointimal tissue with smooth muscle cells and inflammatory cells were inspected around the implants; variations of cell densities in the artery wall, lumen interface and biocorrosion area were measured.

The *in vivo* biocompatibility study of this system would help show the promise of Zn-Li alloy as a cardiovascular stent.

References

[1] E.M. Savitskii IANS, OTN. Metallurgiya i Toplivo 1960;5:52.

[2] Z.A. Sviderskaya TAB, et al. In the collection: Investigation of Alloys of Nonferrous Metals. Izd AN SSSR 1962;3.

[3] M.V. Zakharov ZAS, et al. Izv. vuzov. Tsvetnaya Metallurgiya 1961;4.

[4] I.N. Fridlyander VFS, and N. V. Shiryaeva. Metally 1965;2.

[5] Drits ME, Kadaner ES, Kuz'mina VI. Effect of lithium on the aging and mechanical properties of Al−Zn−Mg alloys. Metal Science and Heat Treatment 1967;9:920-2.

[6] Witte F, Abeln I, Switzer E, Kaese V, Meyer-Lindenberg A, Windhagen H. Evaluation of the skin sensitizing potential of bio-degradable magnesium alloys. J Biomed Mater Res, Part A 2008;86:1041-7.

[7] Thomann M, Krause C, Bormann D, von der Höh N, Windhagen H, Meyer-Lindenberg A. Comparison of the resorbable magnesium . alloys LAE442 und MgCa0.8 concerning their mechanical properties, their progress of degradation and the bone-implant-contact after 12 months implantation duration in a rabbit model. Mat-wiss u Werkstofftech 2009;40:82-7.

[8] Witte F, Fischer J, Nellesen J, Vogt C, Vogt J, Donath T, et al. In vivo corrosion and corrosion protection of magnesium alloy LAE442. Acta Biomater 2010;6:1792-9.

[9] Krause A, Von der Höh N, Bormann D, Krause C, Bach FM, Windhagen H, et al. Degradation behaviour and mechanical properties of magnesium implants in rabbit tibiae. J Mater Sci 2010;45:624-32.

[10] Schrauzer GN. Lithium: occurrence, dietary intakes, nutritional essentiality. J Am Coll Nutr 2002;21:14-21.

[11] Halford B. Limits Of Lithium. Chemical and Engineering News 2013; 91:15-20.

[12] Micronutrients IoMUPo. Dietary Reference Intakes for Vitamin A, Vitamin K, Arsenic, Boron, Chromium, Copper, Iodine, Iron, Manganese, Molybdenum, Nickel, Silicon, Vanadium, and Zinc. Dietary Reference Intakes for Vitamin A, Vitamin K, Arsenic, Boron, Chromium, Copper, Iodine, Iron, Manganese, Molybdenum, Nickel, Silicon, Vanadium, and Zinc. Washington (DC): National Academy Press; 2001. p. 480-81.

[13] Callister WD, Rethwisch DG. Fundamentals of Materials Science and Engineering: An Integrated Approach. Hoboken, NJ: John Wiley & Sons, Inc.; 2008.

[14] Wang SC, Starink MJ. Precipitates and intermetallic phases in precipitation hardening Al–Cu–Mg–(Li) based alloys. International Materials Reviews 2005;50:193-215.

[15] Prawoto Y. Integration of mechanics into materials science research. 1st ed: Lulu enterprise; 2013.

[16] Lowden MAW, Hutchinson WB. Texture strengthening and strength differential in titanium-6Al-4V. Metallurgical Transactions A 1975;6:441.

[17] Zhang S, Zhang X, Zhao C, Li J, Song Y, Xie C, et al. Research on an Mg-Zn alloy as a degradable biomaterial. Acta Biomater 2010;6:626-40.

[18] Bowen PK, Guillory Ii RJ, Shearier ER, Seitz J-M, Drelich J, Bocks M, et al. Metallic zinc exhibits optimal biocompatibility for bio-degradable endovascular stents. Materials Science and Engineering: C 2015;56:467-72.

[19] Pierson D, Edick J, Tauscher A, Pokorney E, Bowen P, Gelbaugh J, et al. A simplified in vivo approach for evaluating the bio-degradable behavior of candidate stent materials. J Biomed Mater Res B 2012;100B:58-67.

Chapter 3 Results and Discussions: Structural characteristics and *in vitro* biodegradation of a novel Zn-Li alloy prepared by induction melting and hot rolling*

Abstract

Zinc shows great promise as a bio-degradable metal, however, the low tensile strength of pure zinc limits its application for endovascular stent purposes. In this study, a new Zn-xLi alloy (with x=2, 4, 6 at.%) was prepared by induction melting in an argon atmosphere and processed through hot rolling. Structures of the formulated binary alloys were characterized by x-ray diffraction and optical microscopy. Mechanical testing showed that the incorporation of Li into Zn increased ultimate tensile strength from <120 MPa (pure Zn) to >560 MPa (x=6 at.%). *In vitro* corrosion behavior was evaluated by immersion tests in simulated body fluid. The Zn-2Li and Zn-4Li corrosion study demonstrated that corrosion rates and products resemble those observed for pure Zn *in vivo*, and in addition, the Zn-4Li alloy exhibits higher resistance to corrosion as compared to Zn-2Li. The findings herein encourage further exploration of Zn-Li systems for structural use in biomedical vascular support applications with the ultimate goal of simplifying stent procedures thereby reducing stent related complications.

Keywords: Zn-Li; microstructure; strength; elongation; *in vitro* biodegradation

---

3.1 Introduction

Bio-degradable stents are envisaged to support the arterial wall during remodeling after stent deployment and to degrade harmlessly thereafter. This new generation of endovascular stents may eliminate the potential for chronic inflammation [1] and thrombosis risks [2] of permanent stents. They could also alleviate the repetition of invasive procedures when stenting at the same site in the event of restenosis [3]. Over the past decade, polymeric and metallic materials have been widely investigated for endovascular stent applications with very limited success [4-7]. The previous reports demonstrated that neither polymers nor metallic candidates such as iron and magnesium are ideal for bio-degradable stenting applications due to either poor mechanical properties [7-10], incomplete bioabsorption of corrosion products [11], or premature degradation [12]. Consequently, the search for new bio-degradable materials continues [7].

Zinc is one of the most abundant nutritionally essential elements in the human body [13] and studies have been initiated examining zinc as a bio-degradable material in recent years [14]. One major concern regarding the use of a pure zinc stent is the material's low intrinsic ultimate tensile strength (UTS) of about 120 MPa or less, where the cardiovascular stent application requires a material with UTS closer to 300 MPa [15]. Improvements in mechanical properties of zinc can be approached through alloying [16, 17] and manipulation of metal micro-/nano-structure [18, 19]. Lithium is one of the few elements with significant solubility in zinc, and Zn-Li is therefore among a few potentially age-hardenable systems.
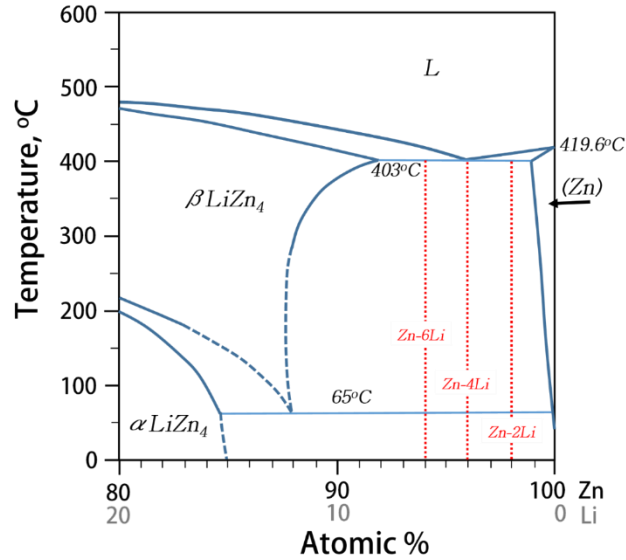
Fig. 3.1. Zinc-lithium phase diagram (prepared based on Ref.[20])

Hypoeutectic 2 at.% Li (0.2 wt.%), eutectic 4 at.% Li (0.4 wt.%) and hypereutectic 6 at.% Li (0.7 wt.%) compositions were chosen for this study based on the phase diagram produced by Pelton [20] (Fig.3.1). The eutectic reaction under the casting conditions used herein is expected to result in prolific lamellar formation during cooling, so that much of the available Li is consumed and the only Li available for post-solidification strengthening is what is left in supersaturation upon cooling below the eutectic temperature in (Zn)Li regions. Therefore, precipitation hardening is expected to play a major role in the 2%, a minor role in the 4%, and a negligible role in the 6% alloy. However, the LiZn$_4$ formed as part of the lamellar structure does have an impact on yield and ultimate strength as the shear moduli between this and the Zn(Li) phase is different, and the strength increment is proportional to $1/\lambda^{1/2}$, where λ is the lamellar spacing, according to a Hall-Petch relation. This effect is expected to play a major role in the 6% alloy, a minor role in the 4%, and a negligible role in the 2% alloy. Strengthening from further grain size refinement is also

61

possible since the recrystallization from hot rolling may produce a finer structure than the as-cast material in all three alloys, although grain size is not explicitly measured here. Work hardening is not anticipated to play a role in these tensile or hardness tests as the alloys here are annealed directly following the hot-rolling process, which is intended to reduce stored dislocation energy while precipitating as much $LiZn_4$ as possible. If crystalline slip becomes too difficult because of the aforementioned obstacles to dislocation motion during loading of an HCP crystal, deformation via twinning mechanisms may be activated which allow deformation through much larger scale atomic rearrangements.

An endovascular metallic stent weighs approximately 50 mg [14]. If it degrades completely within one year, the expected daily dose of Zn and Li would be below 140 and 1 µg, respectively, for an alloy containing 14 at.% Li (Table 3.1). These values are roughly two orders of magnitude below the daily bodily consumption allowances [21, 22] and thus the toxic potential of a zinc-lithium stent is anticipated to be negligible in terms of the overall quantities of the elements released.

Table 3.1. Estimated daily release of Zn and Li from a 50 mg stent compared to daily bodily consumption allowances

Intake	Daily Allowance for Adult males	*Estimated release from Zn-Li alloy
Zn	10 mg [22]	140 µg
Li	0.6 mg [21]	1 µg

(*The daily amount of release can be obtained by dividing the mass of Zn and Li assuming a full degradation timeframe of 365 days. For an alloy of Zn-14 at.% Li and a stent mass of 50 mg, the total mass of Li is 0.38 mg so the daily release of Li into biological system is 1 µg).

With regard to local toxic effects, rapid transport of ions in vascular tissue [23] would prevent elemental enrichment and cytotoxicity in the implant's vicinity [10]. Lithium has

been successfully used in bio-degradable Mg alloy LAE442 which has 4 wt.% of lithium, 4 wt.% of aluminm, and 2 wt.% of rare-earth elements. LAE442 has been shown to be non-allergenic [24], bio-degradable, and to degrade more slowly than pure magnesium without the formation of radiographically oBEIrvable gas [25, 26] and with a more uniform degradation behavior [26]. It has been considered as the most promising implant material for orthopedic use [27].

Based on this evidence, alloying zinc with lithium is expected to produce a stent material with favorable biocompatibility and reasonable strength. To our knowledge, no systematic research has been reported on the Zn-Li alloy as a bio-degradable implant material. Most of the existing studies in the binary Li-Zn system focus on thermodynamic properties [20], the crystal structures of $LiZn_x$ compounds [28], preliminary charge-discharge characteristics [29], and the reactivity of lithium-ion batteries [30]. In the rechargeable Li-ion battery area, the Li-Zn alloys have been considered as an alternative to graphite-based anode materials [28]. As for the five binary Li-Zn intermetallic phases, LiZn was considered to be crystalize in the NaTi structure type [31], and $LiZn_4$ was proposed to have a Mg-type structure with a random distribution of Li and Zn [32]. Crystal structures of Li_2Zn_3 at low and high temperature modifications were determined by single-crystal X-ray diffraction techniques in 2012 [33]. The structures of Li_2Zn_5 and $LiZn_2$ phases remain unexplored.

This new series of bio-degradable Zn-Li alloys is formulated, cast, and processed through hot rolling in this study to simulate commercial processes such as extrusion. The alloys are

characterized regarding their as-processed tensile properties and degradation in simulated body fluid.

3.2 Materials and methods

3.2.1 Alloy preparation

Pure Zn (99.99 wt.%, Alfa Aesar company, Ward Hill, MA) and pure Li foil (99.9 wt.%, Alfa Aesar company, Ward Hill, MA) were loaded into a graphite crucible in an inert-atmosphere glove box to avoid atmospheric oxidation of lithium.
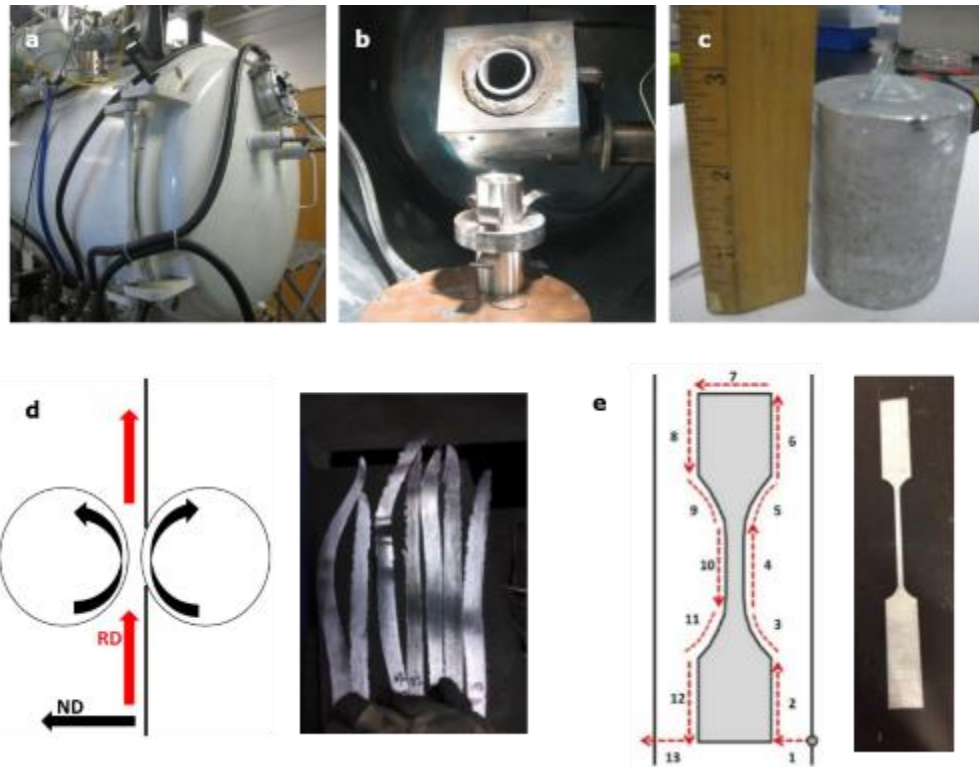
Fig. 3.2. Fabrication of Zn-Li ingots, strips, and dogbone tensile bars; a-c. vacuum induction melting set-up for alloy ingots; d. uniaxial rolling process for reduce ingots from 1.8mm to ~300µm; e. layout of Japax wire EDM g-code for precision cutting of dogbone tensile bars.

A custom vacuum induction melting setup at Michigan Tech (Fig.3.2a-c) was used to fabricate the Zn-Li alloys. They were cast by induction melting with a power of ~3 kW

under a 0.9 atm argon atmosphere. The ultimate vacuum level was 2×10^{-4} torr. A stepper motor controlled by a custom LabView (National Instruments, Austin, TX) script tilt-poured the melt into a 50 mm diameter stainless steel mold. These ingots were squared and sectioned to a size of $35 \times 35 \times 60$ mm and underwent deformation processing via hot rolling to simulate the extrusion process used in conventional stent tube forming. Before rolling, alloys were placed in a box furnace at 662°F (350°C) for several minutes until reaching the furnace temperature. The rolling process was performed on a Fenn (Newington, CT) 2-high mill equipped with 133 mm rolls at 42 rpm (Fig.3.2d).

After three passes through the rolling mill, the sample thickness was recorded and the sample was returned to the furnace for 3 mins. The final sheet was reduced from 35 mm to approximately 300 μm in thickness for a total reduction of cross-sectional area of 99%. From these sheets, dogbone tensile bars were cut for standard tests per ASTM E8/E8M-11 using wire electro discharge machining (wire EDM) on a PC-controlled Japax Lux-3 (McWilliams EDM, Brighton, MI) (Fig.3.2e).

3.2.2 Alloy characterization

Inductively Coupled Plasma Optical Emission Spectrometry (ICP-OES) (PerkinElmer Optima 7000DV, Waltham, MA) was utilized in detecting the compositions of Zn alloy sheets after hot rolling. To produce a solution suitable for ICP-OES analysis, 250 mg of each alloy was dissolved in 40 ml of 6M HCl, which was diluted for analysis.

Microscopy samples of both as-cast and hot-rolled material were mounted in epoxy and polished with 600-grit, 800-grit, and 1200-grit silicon carbide. Final polishing steps were performed using 6 μm, 1 μm and 0.1 μm diamond cloth and 0.05 μm alumina slurry on

microfiber. Microstructure of alloys were recorded using a Leica EC3 (Leica Microsystems; Buffalo Grove, Illinois) digital camera on an Olympus PMG-3 metallograph (Olympus, Shinjuku, Tokyo, Japan).

X-ray diffraction (XRD) was performed on an XDS2000 θ/θ X-ray diffractometer (Scintag Inc., Cupertino, CA) with CuKα radiation (k = 1.540562 Å). The scans were performed continuously from 20° to 100° in 2θ at a speed of 0.6°/min with a step size of 0.02°.

Uniaxial tensile tests were performed using an Instron 5984 electro-mechanical testing machine equipped with a 150 kN load cell (Instron, Norwood, MA). All tests were performed at an initial strain rate of 10^{-3} s^{-1}.

Vickers microhardness (HV) was measured using an M-400-G1 digital hardness tester (LECO, St Joseph, MI) at a load of 200g for 5 s and a minimum of 10 indentations per sample.

Electrochemical measurements were made with a PARSTAT 4000, teamed with the Versa Studio software package (AMETEK/Princeton Applied Research, Berwin, PA). The PARSTAT 4000 is a potentiostat/galvanostat combined with a frequency response analyzer (FRA) contained in a single unit. A three-electrode set-up was employed: the working electrode (Zn-Li coupons, immersed area of 1 cm^2) with Ag/AgCl (SSE) and graphite as the reference and counter electrodes, respectively. The test medium was simulated body fluid in a 98.6°F (37°C) incubator with 5% CO_2 supply, the composition of which is discussed below and also given in Table 3.2.

Table 3.2. Ion concentrations of human blood plasma and the experimental simulated body fluid (SBF)

Ion	Blood plasma	Simulated Body Fluid [34]	Revised Simulated Body Fluid
Na^+	142.0	142.0	160.0
K^+	5.0	5.0	4.0
Mg^{2+}	1.5	1.5	1.0
Ca^{2+}	2.5	2.5	2.5
Cl^-	103.0	148.8	142.0
HCO_3^-	27.0	4.2	26.0
HPO_4^{2-}	1.0	1.0	1.0
SO_4^{2-}	0.5	0.5	0.5
pH	7.2-7.4	7.4	7.4

3.2.3 *In vitro* immersion test and characterization of corrosion product

In vitro corrosion tests were carried out in modified simulated body fluid (SBF). In contrast with the classic tris-buffered (trishydroxymethyl-aminomethane) SBF solution, the content of bicarbonate was elevated to the level found in blood plasma; conveniently, the buffering function of tris was accomplished by the additional bicarbonate. The adoption of this bicarbonate buffering system was important, as it resembles the *in vivo* environment of the acid-base homeostasis of a living host, including the human body. Ion concentrations of the modified SBF used here, traditional SBF [34], and human blood plasma are listed in Table 3.2.

The rolled alloy sheets of 300 μm thickness were cut into 1×1 cm squares. Pure Zn was also used here as control. *In vitro* submersion took place in 50 ml centrifuge tubes, where the coupons were covered with 40 ml of SBF medium and placed in an incubator at 98.6°F

(37°C) and 5% CO_2 atmosphere for 4, 7, and 14 days. The ratio of solution volume to specimen area (V/S) was ~20 ml/cm^2, which was suggested by the ASTM G31-72 to ensure the volume is large enough to avoid medium changes during corrosion [35]. The pH was measured at 7.2-7.4 throughout the experiment.

Although ISO 10993-15:2000 recommended a V/S ratio of less than 1 ml/cm^2, various V/S ratios ranging from 0.33 ml/cm^2 [36] to 7375 ml/cm^2 [37] have been chosen by researchers. It is difficult to specify a standard V/S for all immersion tests since the ratio should be based on the implantation environment the researchers intend to mimic [38]. Therefore, even for the same alloy from different research groups, the *in vitro* corrosion results are not compared [38]. It is known that *in vitro* methods are quick and relatively inexpensive, but it's also apparent that predicting *in vivo* behavior from *in vitro* testing can be misleading [37]. Local pH, impurities, processing, the concentration of the pitting anion [39] and proteins [40] can all play a role in metallic corrosion.

Surface morphological and elemental analyses were carried out on the samples following *in vitro* corrosion using a JSM 6400 scanning electron microscope (SEM) (JEOL, Peabody, MA) equipped with an energy dispersive spectrometer (EDS). The accelerating voltage and working distance used for all samples was 20 kV and 39 mm, respectively. Fourier Transform Infrared Spectroscopy (FTIR) was conducted in diffuse reflectance mode with a Genesis II FTIR spectrophotometer (SUNY Genesso, Genesso, NY). A series of 1024 scans was performed at 1 cm^{-1} resolution from 400 to 4000 cm^{-1}.

3.3 Results and Discussion

3.3.1 Elemental analysis

Experimental compositions of the alloys are given in Table 3.3. For all three Zn-Li alloys, the experimental compositions from ICP-OES were slightly lower than the nominal compositions. Ni and Fe were detected as trace impurities from Zn; Ni remained below the detection limit for the three alloys and Fe concentration was also very low.

Table 3.3. ICP-OES compositional analysis of rolled Zn alloys

Sample ID	Li/at.% Nominal	Li/at.% Experimental	Fe/at.%	Ni /at.%	Zn/at.%
Zn	<0.01	<0.01	<0.01	<0.10	Bal.
Zn-2Li	2.00	1.10	0.03	<0.10	Bal.
Zn-4 Li	4.00	3.20	0.01	<0.10	Bal.
Zn-6 Li	6.00	5.50	0.01	<0.10	Bal.

3.3.2 XRD analysis
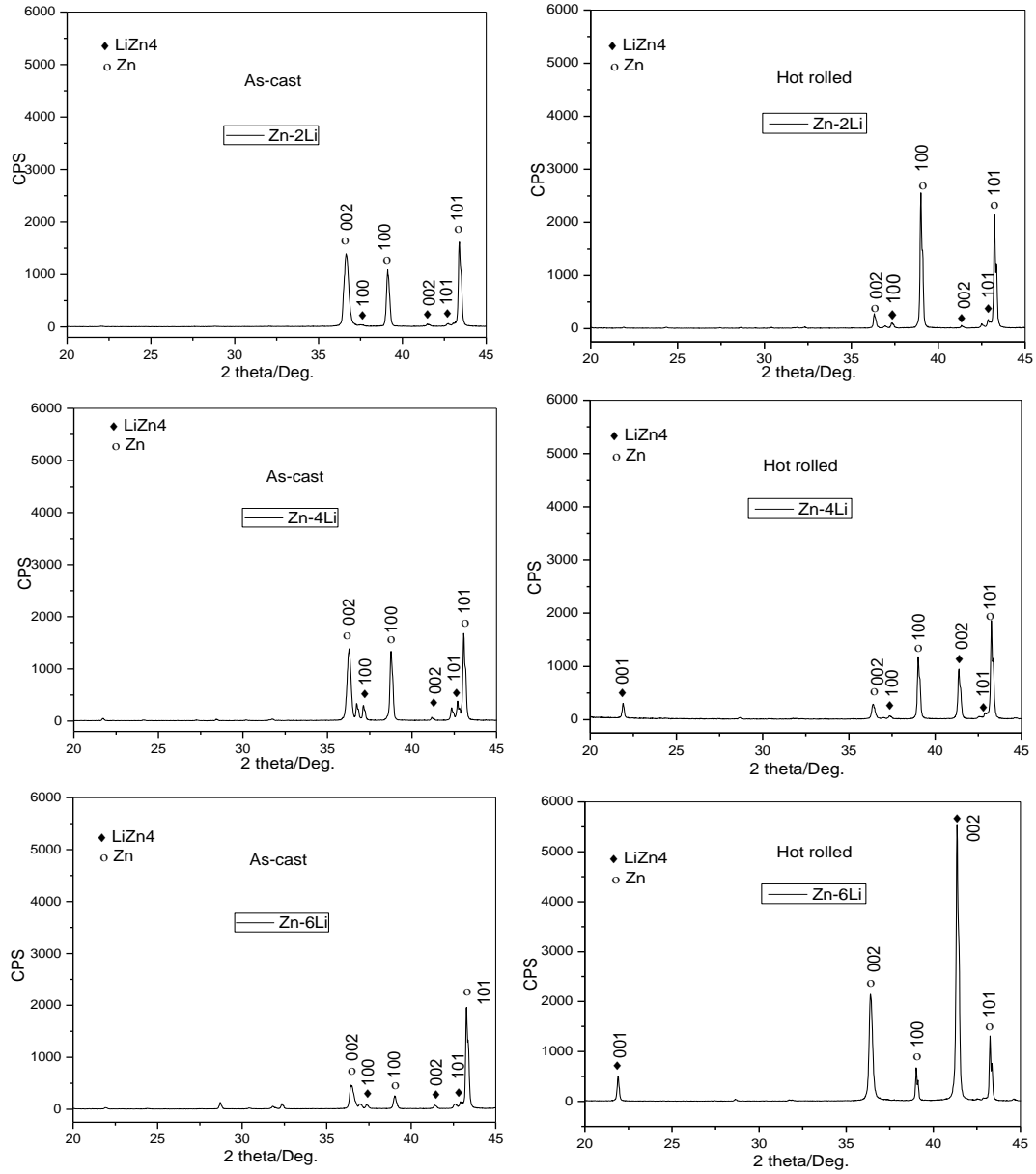
Fig. 3.3. XRD patterns of as-cast and hot rolled alloys with different compositions

XRD patterns for Zn-xLi (x=2, 4, 6 at.%) before and after hot rolling are shown in Fig.3.3. All the investigated samples exhibit dual-phasic character with the main phase of zinc and minor phase of $LiZn_4$. Patterns were collected at room temperature, and the $LiZn_4$ phase present in all as-cast and as-processed material is assumed to be of the low-temperature α-

variety as all cooling was done slowly in air to allow the eutectoid relaxation to occur. For the as-cast samples, peaks corresponding to Zn are high and narrow, indicating relatively large grain sizes and very little lattice deformation. Peaks corresponding to the intermetallic phase $LiZn_4$ in as-cast samples have the highest relative intensities in the Zn-4Li alloy with peaks from sets of (101), (002), and (100) planes, indicating prolific nucleation and growth of $LiZn_4$ during solidification at this composition.

After hot rolling, the rolling direction-transverse direction (RD-TD) cross sections are examined and the preferential orientation of $LiZn_4$ and the Zn lattice change as observed by the increased intensities of the (002) and (001) peaks relative to the (101) peak for the same phase in both cases (Fig.3.3).
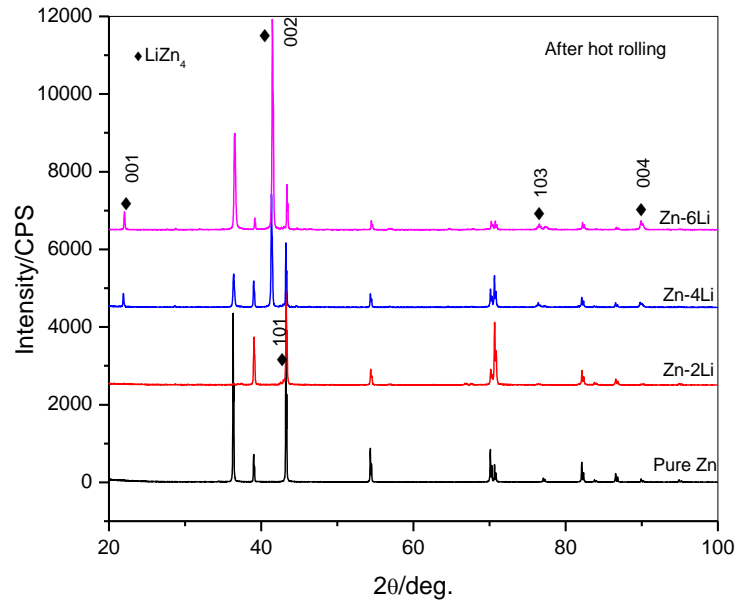
Fig. 3.4. Full scan range XRD patterns of hot rolled alloys with different compositions. $LiZn_4$ peaks are identified.

Peaks corresponding to LiZn4 also increase in intensity relative to those for the Zn lattice with the increase of Li due to larger volume fractions of LiZn4 available in the more concentrated alloys (Fig.3.4). Minor peaks at $2\theta=21.7^{o}$ and 89.9^{o} are observed which do not correspond to known reflections in the JCPDS-ICDD database. In order to determine if these peaks originate from the Zn+LiZn4 mixture, an estimation of the structure factor (F) using these two phases was carried out using Equations 1-3 with results displayed in Table 3.4.

Table 3.4. Structure factors for ordered and disordered states of Zn(Li)+LiZn4

h	k	l	2θ	Sin/λ	f_{Li}	f_{Zn}	$|F|^2$ (disordered)	$|F|^2$ (ordered)
0	0	1	22	0.24	1.65	20.5	0	1076
0	0	2	42	0.43	1.20	15.5	2556	615
0	0	3	64	0.58	0.82	12.5	0	399
0	0	4	89	0.65	0.70	11.5	1396	349
1	0	1	43	0.44	1.15	15.0	448	571
1	0	0	37	0.39	1.30	15.8	166	639

1) If disordered (i.e. solid solution):

$$F = 2 \times f_{ave}\left[\left(e^{i2\pi\left(\frac{1}{3}h+\frac{2}{3}k+\frac{1}{4}l\right)} + e^{i2\pi\left(\frac{2}{3}h+\frac{1}{3}k+\frac{3}{4}l\right)}\right)\right] \qquad \text{Eq. 3.1}$$

$$f_{ave} = \frac{4}{5} \times f_{Zn} + \frac{1}{5} \times f_{Li} \qquad \text{Eq. 3.2}$$

2) If ordered (i.e. dual-phasic):

$$F = 2 \times \frac{1}{5} f_{Li} e^{i2\pi\left(\frac{1}{3}h + \frac{2}{3}k + \frac{1}{4}l\right)} + 2 \times \frac{4}{5} f_{Zn} e^{i2\pi\left(\frac{2}{3}h + \frac{1}{3}k + \frac{3}{4}l\right)} \quad \text{Eq. 3.3}$$

The theoretical values of 2θ at (00l) planes (Table 3.5) are then obtained from:

$$sin^2 \theta = \frac{\lambda^2}{4a^2}\left(h^2 + k^2 + l^2 \frac{a^2}{c^2}\right) \quad\quad\quad \text{Eq. 3.4}$$

where LiZn$_4$ has the structure P6$_3$/mmc (no. 194, HCP) with a = 0.27702(8) and c = 0.43785(9) nm.

Table 3.5. Theoretical and experimental values of 2θ for h=k=0 and l=1, 2, 3, or 4

(hkl)	2 θ (Theoretical)	2 θ (Experimental)
001	21.80	21.70
002	41.46	41.40
003	63.71	×
004	89.94	89.95

The matching of the theoretical 2θ values from structure factor calculations with experimentally observed diffraction peaks indicates that the two unidentified peaks do originate from the Zn+LiZn$_4$ structure but are not tabulated in the current database. In a previous study on α-LiZn$_4$ powder [30], a structural model was determined in which both Zn and Li were seated in the (1/3, 2/3, 1/4) 2c site with a Li/Zn ratio equal to 0.28 (experimental value). This phase was isostructural with elemental HCP Zn, consistent with the findings of the current study. It is concluded that hot rolling both promotes precipitation of the ordered LiZn$_4$ phase and produces texture in which the matrix and the LiZn$_4$ phase both have preferred orientations with the c-axis normal to the RD-TD plane. Interestingly,

no occurrence of the (003) reflection was observed in Ref. [28] or the present study, though this is an allowable reflection based on the structure factor equations above for the dual-phasic approximation. This could suggest a different arrangement of Zn and Li atoms in the $LiZn_4$ phase, or the peak intensity could simply be below the resolution limit of the XRD and filtered out of the spectrum.

3.3.3 Microstructural features
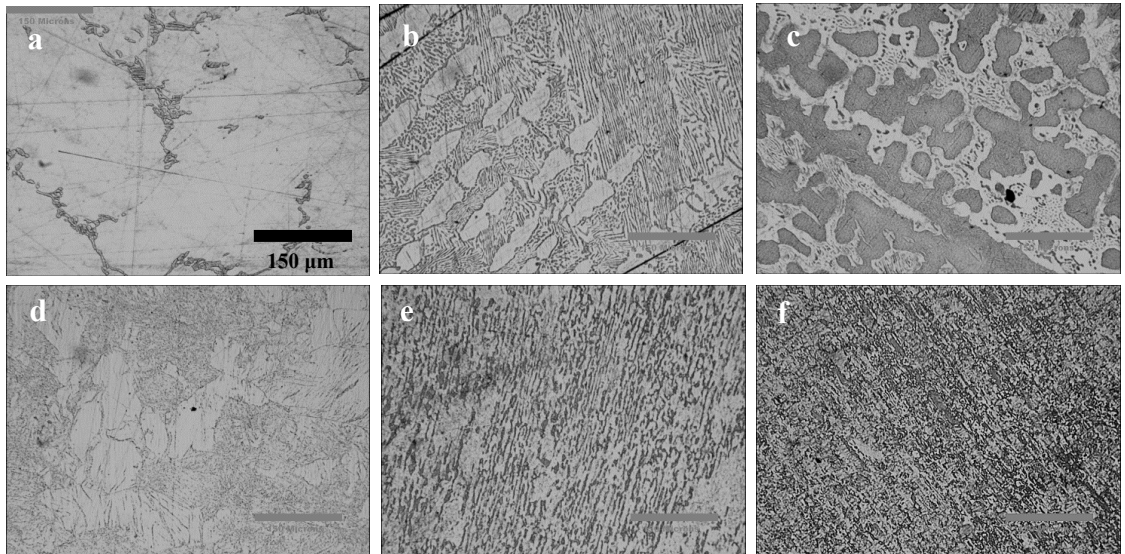
Fig. 3.5. Optical micrographs of as-cast (a-c) and hot-rolled (d-f) Zn-Li alloys with Li content increasing from 2 to 4 to 6 at.% from left to right. The scale bar in panel a. applies to all 6 micrographs.

Optical micrographs from RD-TD cross sections of alloy sheets before and after hot rolling are shown in Fig.3.5. Microstructures are consistent with Scheil/Scheil-Gulliver nonequilibrium solidification conditions. For Zn-2Li, small amounts of $Zn+LiZn_4$ are present in the α-Zn matrix. With Zn-4Li, a mixture of lamellar $Zn+LiZn_4$ grains and α-Zn grains is observed. The lamellae are observed in grains with apparently random orientation. For Zn-6Li, dendritic arms and trunks are observed consisting of $Zn+LiZn_4$ which have a

74

very tight lamellar spacing with interdendritic channels of Zn(Li). The random arrangement of grains observed in the hypoeutectic alloy tended towards directional solidification with increasing Li content. The fact that pro-eutectic grains of α-Zn are observed for Zn-4 at.% Li in Fig.3.5 points to a slightly lower experimental composition than 4 at.% Li in this cross-section. This is confirmed by ICP-OES results, shown in Table 3.3.

After the hot rolling and annealing process, the Zn-4Li and Zn-6Li samples exhibit severe rolling texture and no occurrence of equiaxed grains; dendrite arms and trunks are refined and the grain width decreases from ~50 μm to ~10 μm. In contrast, the hypoeutectic alloy exhibits equiaxed grains almost exclusively. This oBEIrvation points to dynamic recrystallization occurring during the hot rolling process or static recrystallization afterwards for this alloy but not for the higher Li alloys. However, the texture that develops during rolling is retained: the XRD scans in Fig.3.3 show an increase in the intensity of the (100) peak relative to the (101) for all three alloys.

For all alloys here, the high-temperature intermetallic phase β-LiZn$_4$, present in both lamellar structures and as precipitated particles, relaxes to the room-temperature α-LiZn$_4$ phase at the eutectoid temperature of 65 °C [20]. Evidence of this reaction was not observed metallographically, and it is assumed that all β-LiZn$_4$ converts to α-LiZn$_4$ with ease.

3.3.4 Mechanical testing
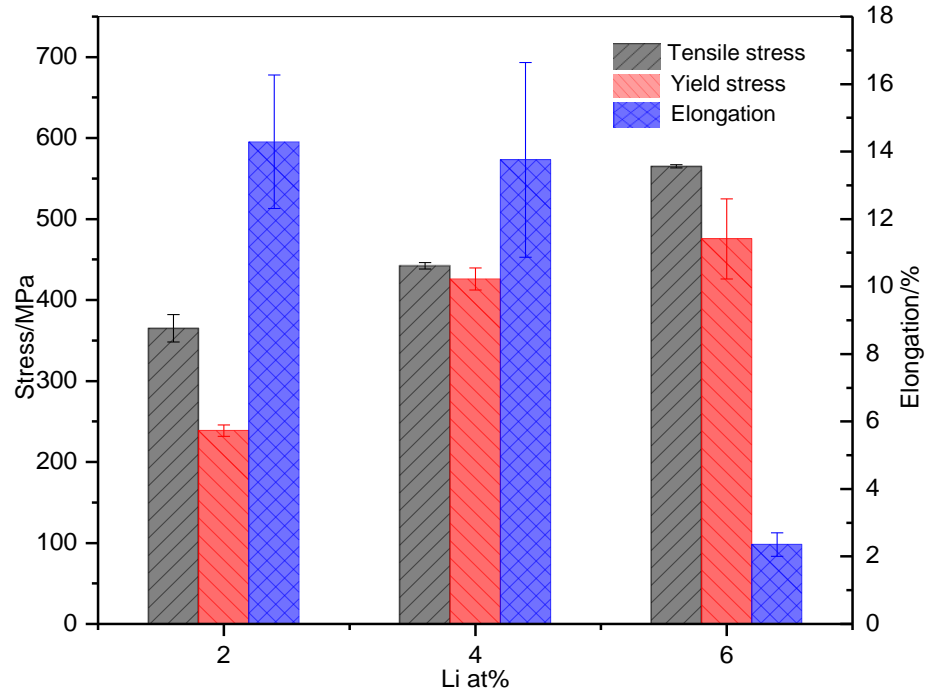
Fig. 3.6. Ultimate tensile strength (UTS), yield strength, and elongation to failure of Zn-2Li, Zn-4Li, and Zn-6Li with error bars representing standard deviation in measurement

Yield strength, UTS, and ductility values for all tested alloys are shown in Fig.3.6. The 300 MPa UTS and 200 MPa yield strength benchmarks for bio-degradable stent materials [14] are exceeded at all alloying levels. Higher contents of Li give higher tensile strengths due to the larger volume fractions of the $LiZn_4$ phase. Ductility of the Zn-2Li and Zn-4Li alloys are favorable compared to very limited ductility of Zn-6Li in view of benchmark values of 15-18% elongation to failure for bio-degradable stent materials [14]. While these are excellent properties for a stent material, further study is needed to delineate the exact strengthening mechanisms operating in each alloy. Based on these empirical strength and ductility values, alloys with lower content of Li (2 and 4 at.%, nominally) were selected for *in vitro* corrosion testing.
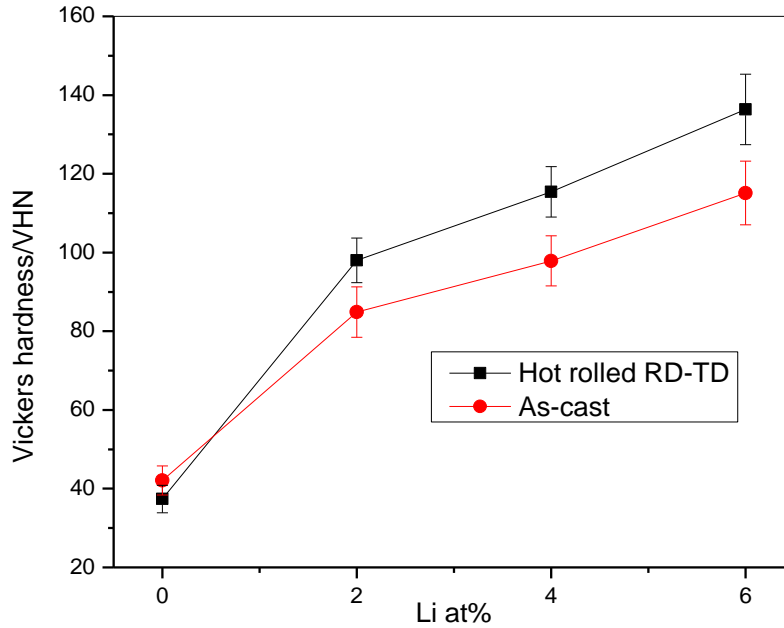
Fig. 3.7. Vickers microhardness of hot rolled and as-cast alloys with different compositions.

As shown in Fig.3.7, the hardness of Zn-2Li increases from 85±6 to 98±6 after hot rolling, and Zn-4Li and Zn-6Li increase from 98±6 to 115±6 and 115±8 to 136±9, respectively. This is a 15% percent increase in hardness for Zn-2Li and 18% for Zn-6 at.%. This can attribute to precipitation strengthening through the formation of $LiZn_4$, evidenced by XRD, and boundary strengthening by the highly refined grain structure (Fig.3.5). Zn-6 at.% has the finest grains (only a few microns in width) and the highest volume fraction of $LiZn_4$; this combination gives the highest hardness and the strengthening effect from hot-rolling is more evident. An increase in dislocation density is highly probably following a 99% reduction in area, but much of the hardening effect is likely lost during the post-deformation recovery anneal. Texture effects might also play a role in this system as some preferential orientation of $LiZn_4$ was detected in Fig.3.3, which may lead to anisotropy in

mechanical properties as a consequence of the limited number of slip systems available in Zn.

3.3.5 Corrosion rate in SBF
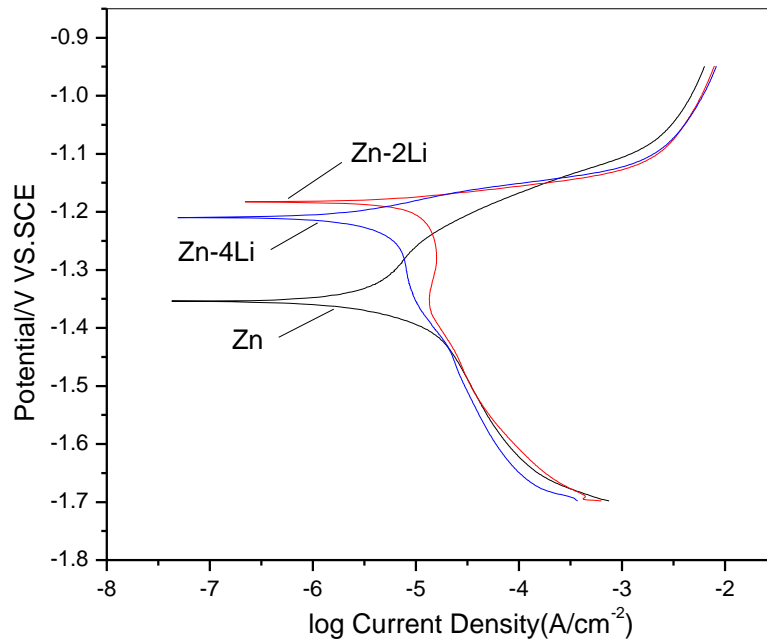
Fig. 3.8. Potentiodynamic curves of different alloys after immediate immersion in SBF medium

For the investigated Zn-Li alloys and pure Zn, the approximate values of corrosion potential and corrosion current were determined from Tafel slopes [41]. In order to estimate the corrosion current values, the anodic curve was extrapolated until it intersected with the level of corrosion potentials as shown in Fig.3.8 and Table 3.6. A high current density (current on the surface) at the corresponding potential indicates a high corrosion rate of the alloy. Comparison between the Zn-Li alloy curves with pure Zn shows that the alloys with

2 and 4 at.% Li have similar curves. The corrosion rates of the various tested materials are estimated (Table 3.6, column 3) through Tafel extrapolation.

Table 3.6. Corrosion potentials, corrosion current densities and corrosion rates, obtained from the polarization curves, for Zn, Zn-2Li, and Zn-4Li

Sample	E_{corr} / V *vs.* SCE	i_{corr} / (μA/cm^{-2})	Corrosion Rate /(μm/year)
Zn	-1.35	0.88	13
Zn-2Li	-1.18	3.43	50
Zn-4Li	-1.21	0.73	10

The Zn-4 at.% Li alloy exhibits the lowest current density (0.73 μA/cm^2) and therefore the highest resistance to corrosion compared to the other two samples. The corrosion resistance could due to the formation of a protective passive layer, typically the surface-product surface film (Fig.3.8). The thicker the passive layer and better attachment to the surface, the higher the corrosion resistance of alloy.

Corrosion rates were estimated in terms of penetration rate (CR) using the Faraday's law:

$$CR = K_1 \frac{i_{corr}}{\rho} EW \qquad \text{Eq. 3.5}$$

$$EW = \frac{1}{\Sigma \frac{n_i f_i}{w_i}} \qquad \text{Eq. 3.6}$$

where: CR is in mm/yr, i_{corr} in μA/cm^2, K_1=3.27×10^{-3} mm·g/μA·cm·yr, ρ =density in g/cm^3, EW is the equivalent weight of the alloy, f_i =the mass fraction of the ith element in the alloy, w_i= the atomic weight of the ith element in the alloy, and n_i= the valence of the ith element of the alloy.

According to the calculation results summarized in Table 3.6, penetration rates for Zn-Li alloys in SBF are 50-60 μm·yr^{-1}, and are comparable to Zn studied in plasma (10 μm·yr^{-1}) [26], whole blood (50 μm·yr^{-1}) [26], and *in vivo* (20-50 μm·yr^{-1}) [10].

3.3.6 Morphology and EDS of corrosion products
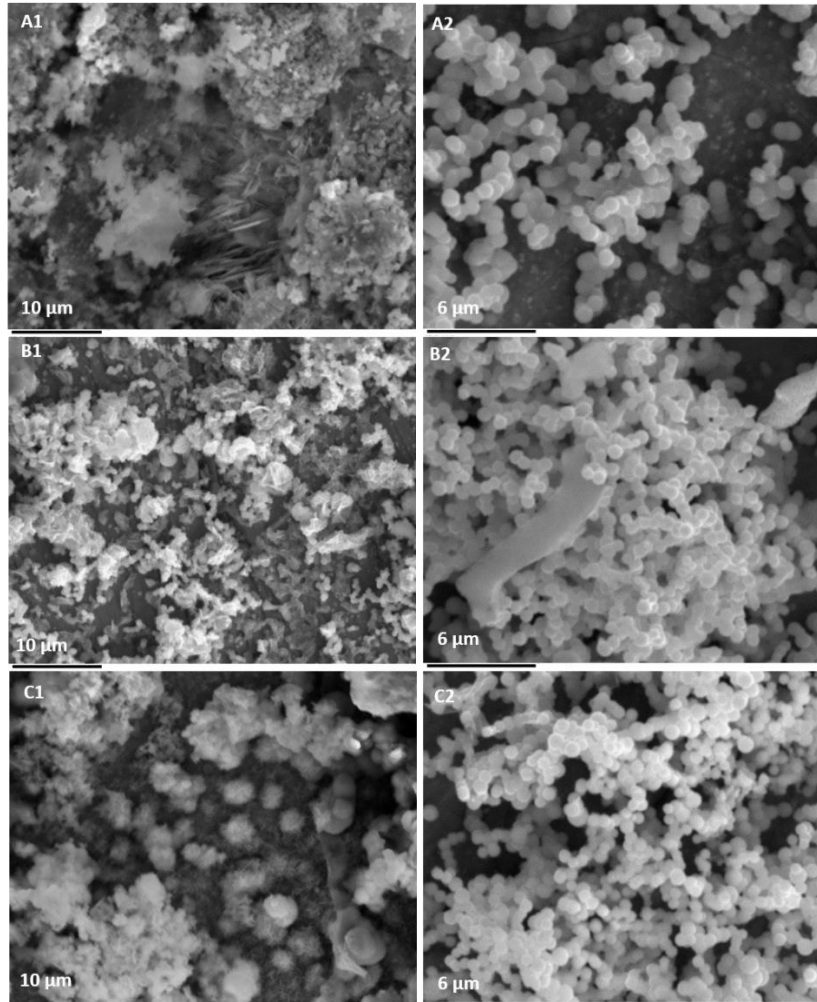
Fig. 3.9. SEM micrographs of Zn-Li surfaces after immersion in SBF. From row A to C, Li increases from 0 to 2 to 4 at.%; from column 1 to 2, immersion period increases from 4 to 14 days.

Images of corroded surfaces are shown in Fig.3.9 for Zn, Zn-2Li and Zn-4Li after immersion in SBF for 4 and 14 days. At the 4 day time point, Zn and the two alloys exhibit morphologically different surface deposits. The initial products formed on the Zn substrate comprised sharp elongated crystals, and flower-like and porous aggregates (Fig.3.9-A1). The Zn-2Li substrate displays a finer initial crystal network and is decorated with agglomerated clusters on top in light contrast (Fig.3.9-B1). The Zn-4Li substrate is covered with sponge-like structures embedded with regular spheres and irregular aggregates (Fig.3.9-C1). After 14 days immersion, the three samples appear very similar with each substrate coated in a regular and well-defined population of spherical particles with average diameter of roughly 1 μm in all cases (Fig.3.9-A2, B2, C2).
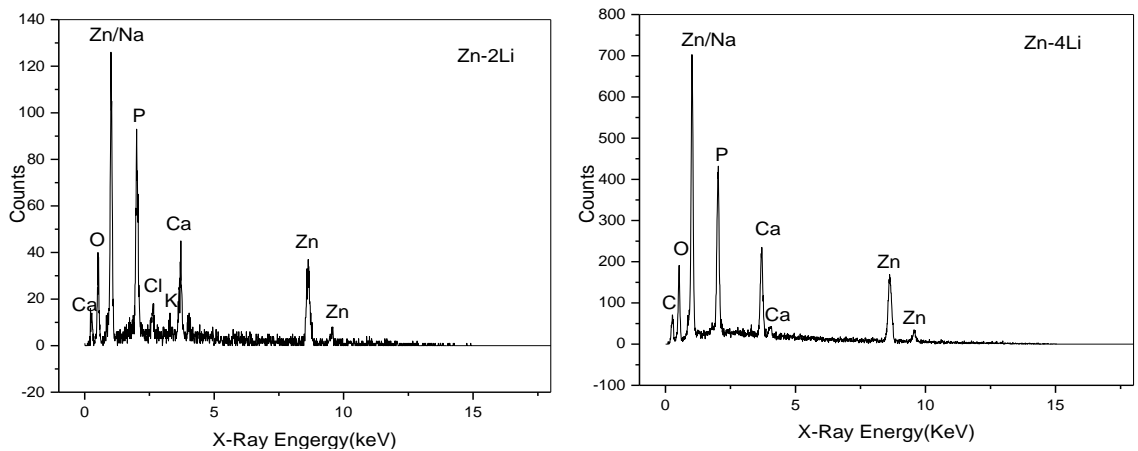
Fig. 3.10. EDS spectra of Zn-Li alloy surface products after immersion in SBF for 14 days

To gain a first approximation of the elemental compositions of the particles formed on the sample surfaces during the immersion testing, EDS analysis of some of the sample surfaces (Fig.3.10) was performed. These scans confirmed the presence of Ca, P, and O, suggesting that the particles could be mainly composed of calcium phosphate, similar to what was

found in a previous study on Mg *in vivo* [42], although with a much different morphology here.
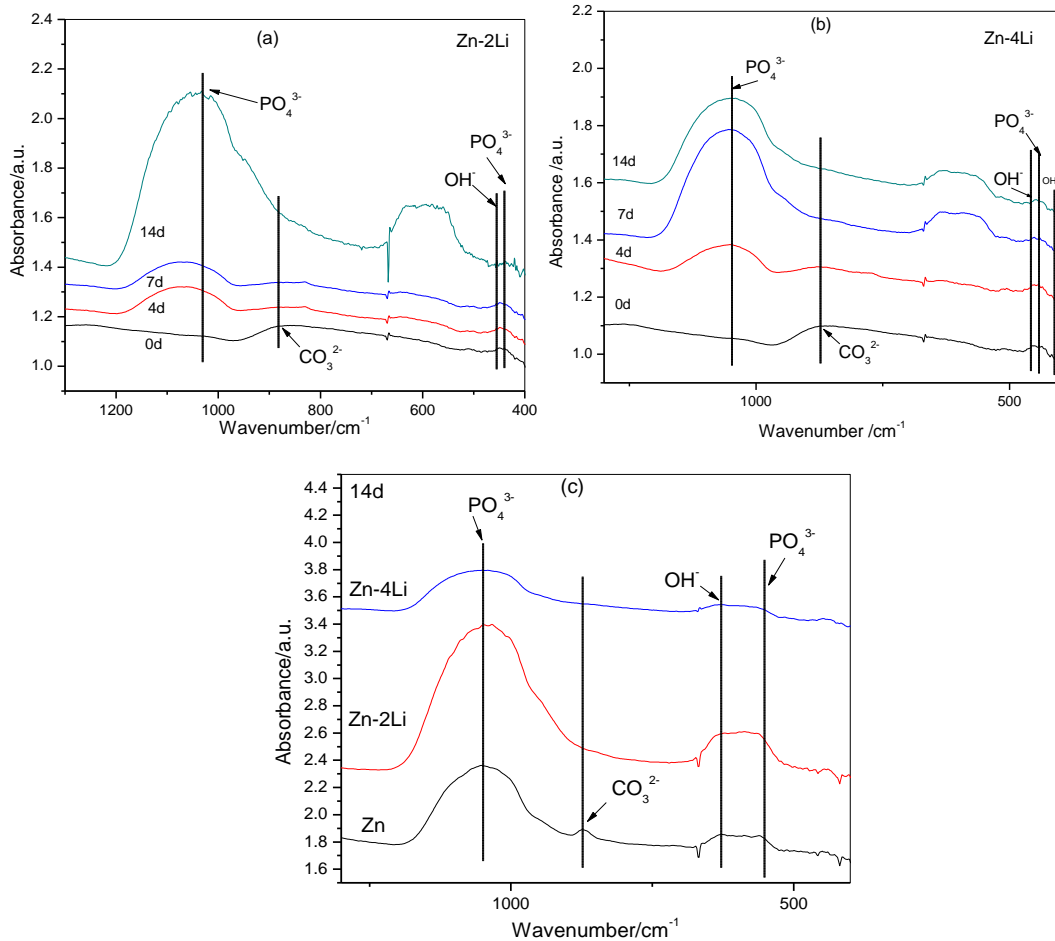
Fig. 3.11. FTIR spectra after 14 days immersion in SBF for Zn, Zn-2Li, and Zn-4Li

To determine the phase composition and functional groups among the different alloys after immersion testing, FTIR analysis was employed. In the FTIR spectrum (Fig.3.11), the PO_4^{3-} group band is observed at 570 cm^{-1}, which is related to asymmetric deformation modes of v4 group; the absorption band in the range of 1040-1090 cm^{-1} is characteristic of the asymmetrical stretching mode of v3 group. The locations of absorption bands for PO_4^{3-} group and OH$^-$ at 631 cm^{-1}, combined with the decrease of Ca^{2+} in SBF medium confirmed

through ICP-OES testing, explicitly indicates the formation of hydrated apatite phases in the corroded alloys. Absorption intensity of PO_4^{3-} group and OH^- group (Fig.3.11a, b) increases with prolonged immersion time, which may indicate improvement of apatite properties making this phase more stable. Presence of CO_3^{2-} bands in pure Zn after 14 days' immersion (Fig.3.11c) is identified at 875 cm^{-1}, corresponding to v2 stretching mode of CO_3^{2-}. This indicates the possible formation of a calcite phase after immersion, while this peak is missing from both Zn-Li alloys.

3.4 Conclusions

By using a vacuum induction melting technique, a new class of Zn-Li alloys has been cast, hot rolled, and analyzed for biomedical-focused application. XRD results indicate the formation of LiZn$_4$ through the emergence of diffraction peaks corresponding to (001) and (004) for this phase when deformed by hot rolling, which increased hardness significantly in all cases. Mechanical testing showed that alloying Zn with Li increases the tensile strength to 360 MPa with a nominal addition of 2 at.% and 560 MPa with 6 at.% Li following hot rolling. Addition of Li above the eutectic composition caused a severe decrease in elongation to failure making the 6% Li alloy unsuitable for cardiovascular stent application.

Our *in vitro* study with the newly formulated Zn-2Li and Zn-4Li alloys demonstrates that the corrosion rates and products in modified SBF solution closely resemble that of pure Zn observed *in vivo*, in plasma, and in whole blood from previous studies. The Zn-4Li alloy exhibited higher resistance to corrosion compared to Zn-2Li suggesting a positive effect of Li content on protective characteristics of the corrosion layer.

References

[1] Farb A. Morphological Predictors of Restenosis After Coronary Stenting in Humans. Circulation 2002;105:2974-80.

[2] Cook S, Wenaweser P, Togni M, Billinger M, Morger C, Seiler C, et al. Incomplete stent apposition and very late stent thrombosis after drug-eluting stent implantation. Circulation 2007;115:2426-34.

[3] Colombo A, Karvouni E. Bio-degradable stents : "fulfilling the mission and stepping away". Circulation 2000;102:371-3.

[4] Erne P, Schier M, Resink TJ. The road to bio-degradable stents: reaching clinical reality? Cadiovasc Intervent Radiol 2006;29:11-6.

[5] Peuster M, Wohlsein P, Brugmann M, Ehlerding M, Seidler K, Fink C, et al. A novel approach to temporary stenting: degradable cardiovascular stents produced from corrodible metal-results 6-18 months after implantation into New Zealand white rabbits. Heart 2001;86:563-9.

[6] Waksman R, Pakala R, Baffour R, Seabron R, Hellinga D, Tio FO. Short-term effects of biocorrodible iron stents in porcine coronary arteries. J Interv Cardiol 2008;21:15-20.

[7] Bowen PK, Shearier ER, Zhao S, Guillory Ii RJ, Zhao F, Goldman J, et al. Bio-degradable Metals for Cardiovascular Stents: from Clinical Concerns to recent Zn-Alloys. Adv Healthc Mater 2016;03 1-20.

[8] Nishio S, Kosuga K, Igaki K, Okada M, Kyo E, Tsuji T, et al. Long-Term (>10 Years) clinical outcomes of first-in-human bio-degradable poly-l-lactic acid coronary stents: Igaki-Tamai stents. Circulation 2012;125:2343-53.

[9] Moravej M, Prima F, Fiset M, Mantovani D. Electroformed iron as new biomaterial for degradable stents: Development process and structure–properties relationship. Acta Biomater 2010;6:1726-35.

[10] H. Hermawan MM, D. Dubé, M. Fiset, D. Mantovani. Degradation Behaviour of Metallic Biomaterials for Degradable Stents. Adv Mater Res 2006;15-17:113-8.

[11] Yang L, Zhang E. Biocorrosion behavior of magnesium alloy in different simulated fluids for biomedical application. Mater Sci Eng C 2009;29:1691-6.

[12] Waksman R, Pakala R, Kuchulakanti PK, Baffour R, Hellinga D, Seabron R, et al. Safety and efficacy of bio-degradable magnesium alloy stents in porcine coronary arteries. Catheter Cardiovasc Interv 2006;68:607-17.

[13] Tapiero H, Tew KD. Trace elements in human physiology and pathology: zinc and metallothioneins. Biomed Pharmacother 2003;57:399-411.

[14] Bowen PK, Drelich J, Goldman J. Zinc exhibits ideal physiological corrosion behavior for bio-degradable stents. Adv Mater 2013;25:2577-82.

[15] Werkhoven RJ, Sillekens WH, van Lieshout JBJM. Processing Aspects of Magnesium Alloy Stent Tube. Magnesium Technology: John Wiley & Sons, Inc.; 2011. p. 419-24.

[16] Vojtech D, Kubasek J, Serak J, Novak P. Mechanical and corrosion properties of newly developed bio-degradable Zn-based alloys for bone fixation. Acta Biomater 2011;7:3515-22.

[17] Bowen PK, Shearier ER, Zhao S, Guillory RJ, Zhao F, Goldman J, et al. Bio-degradable Metals for Cardiovascular Stents: from Clinical Concerns to Recent Zn-Alloys. Adv Healthc Mater 2016.

[18] Zhang X, Yuan G, Wang Z. Mechanical properties and biocorrosion resistance of Mg-Nd-Zn-Zr alloy improved by cyclic extrusion and compression Mater Lett 2012;74:128-31

[19] Kang F, Liu JQ, Wang JT, Zhao X. Equal Channel Angular Pressing of a Mg–3Al–1Zn Alloy with Back Pressure. Adv Eng Mater 2010;12:730-4.

[20] Pelton AD. The Li-Zn (Lithium-Zinc) phase diagram. J Phase Equilib 1991;12:42-5.

[21] Schrauzer GN. Lithium: occurrence, dietary intakes, nutritional essentiality. J Am Coll Nutr 2002;21:14-21.

[22] Micronutrients IoMUPo. Dietary Reference Intakes for Vitamin A, Vitamin K, Arsenic, Boron, Chromium, Copper, Iodine, Iron, Manganese, Molybdenum, Nickel, Silicon, Vanadium, and Zinc. Dietary Reference Intakes for Vitamin A, Vitamin K, Arsenic, Boron, Chromium, Copper, Iodine, Iron, Manganese, Molybdenum, Nickel, Silicon, Vanadium, and Zinc. Washington (DC): National Academy Press; 2001. p. 480-81.

[23] Xu LP, Yu GN, Zhang E, Pan F, Yang K. In vivo corrosion behavior of Mg-Mn-Zn alloy for bone implant application. J Biomed Mater Res, Part A 2007;83A:703-11.

[24] Witte F, Abeln I, Switzer E, Kaese V, Meyer-Lindenberg A, Windhagen H. Evaluation of the skin sensitizing potential of bio-degradable magnesium alloys. J Biomed Mater Res, Part A 2008;86:1041-7.

[25] Thomann M, Krause C, Bormann D, von der Höh N, Windhagen H, Meyer-Lindenberg A. Comparison of the resorbable magnesium . alloys LAE442 und MgCa0.8 concerning their mechanical properties, their progress of degradation and the bone-implant-contact after 12 months implantation duration in a rabbit model. Mat-wiss u Werkstofftech 2009;40:82-7.

[26] Witte F, Fischer J, Nellesen J, Vogt C, Vogt J, Donath T, et al. In vivo corrosion and corrosion protection of magnesium alloy LAE442. Acta Biomater 2010;6:1792-9.

[27] Krause A, Von der Höh N, Bormann D, Krause C, Bach FM, Windhagen H, et al. Degradation behaviour and mechanical properties of magnesium implants in rabbit tibiae. J Mater Sci 2010;45:624-32.

[28] Pavlyuk V, Chumak I, Akselrud L, Lidin S, Ehrenberg H. LiZn(4-x) (x=0.825) as a (3+1)-dimensional modulated derivative of hexagonal close packing. Acta Crystallogr B Struct Sci Cryst Eng Mater 2014;70(Pt 2):212-7.

[29] Wang JQ, King P, Huggins RA. Investigations of binary lithium-zinc, lithium-cadmium and lithium-lead alloys as negative electrodes in organic solvent-based electrolyte. Solid State Ionics 1986;20:185-9.

[30] Bichat MP, Pascal JL, Gillot F, Favier F. Electrochemical Lithium Insertion in Zn_3P_2 Zinc Phosphide. Chem Mater 2005;17:6761-71.

[31] Zintl E, Schneider A. Metals and alloys. XV. X-ray analysis of lithium-zinc alloys. Z Elektrochem Angew Phys Chem 1935;41:764-7

[32] Schönemann H, Schuster H-U. Rev Chim Miner 1976;13:32-40.

[33] Pavlyuk V, Chumak I, Ehrenberg H. Polymorphism of Li_2Zn_3. Acta Crystallogr Sect B 2012;68:34-9.

[34] Kokubo T, Kushitani H, Sakka S, Kitsugi T, Yamamuro T. Solutions able to reproduce in vivo surface-structure changes in bioactive glass-ceramic A-W. J Biomed Mater Res 1990;24:721-34.

[35] ASTM G31-72 SPfLICToM. West Conshohocken, PA: ASTM International; 2004.

[36] Wang Q, Tan LL, Xu WL, Zhang BC, Yang K. Dynamic behaviors of a Ca-P coated AZ31B magnesium alloy during in vitro and in vivo degradations. Mater Sci Eng B 2011;176:1718-26.

[37] Witte F, Fischer J, Nellesen J, Crostack HA, Kaese V, Pisch A, et al. In vitro and in vivo corrosion measurements of magnesium alloys. Biomaterials 2006;27:1013-8.

[38] Yang L, Zhang EL. Biocorrosion behavior of magnesium alloy in different simulated fluids for biomedical application. Mater Sci Eng C 2009;29:1691-6.

[39] Helson JA, Breme HJ. Metals as Biomaterials. 4th ed. ed: New York Wiley; 1998. p. 101-51.

[40] Khan MA, Williams RL, Williams DF. The corrosion behaviour of Ti-6Al-4V, Ti-6Al-7Nb and Ti-13Nb-13Zr in protein solutions. Biomaterials 1999;20:631-7.

[41] Jones DA. Principles and prevention of corrosion, 2nd ed. New York, NY: Macmillan Publishing Co.; 1996. p. 142-7.

[42] Bowen PK, Drelich J, Goldman J. Magnesium in the murine artery: probing the products of corrosion. Acta Biomater 2014;10:1475-83.

Chapter 4 Results and Discussions: Zn-Li Alloy after Extrusion and Drawing: Structural, Mechanical Characterization, and Biodegradation in Abdominal Aorta of Rat*

Abstract

Zinc shows great promise as a bio-degradable metal. The implantation of pure Zn into the abdominal aorta of Sprague-Dawley rats exhibited an optimal corrosion rate and biocompatibility for endovascular applications. However, the low tensile strength of zinc remains a major concern.

A cast billet of the Zn-Li alloy was produced in a vacuum induction caster under argon atmosphere, followed by a wire drawing process. Two phases of the binary alloy identified by x-ray diffraction include the zinc phase and intermetallic $LiZn_4$ phase. Mechanical testing proved that incorporating 0.1 wt.% of Li into Zn increased its ultimate tensile strength from 116 ± 13 MPa (pure Zn) to 274 ± 61 MPa while the ductility was held at $17 \pm 7\%$.

Implantation of 10 mm Zn-Li wire segments into abdominal aorta of rats revealed an excellent biocompatibility of this material in the arterial environment. The biodegradation rate for Zn-Li was found to be about 0.008 mm/yr and 0.045 mm/yr at 2 and 12 months, respectively.

4.1 Introduction

Followed by decades of developing strategies to minimize the corrosion of metallic biomaterials, there is now an increasing trend to use absorbable metals in medical applications [1]. The concept of absorbable metals stents (AMS) was envisaged to treat the disease of artery occlusions and then disappear harmlessly when they are no longer needed as mechanical scaffolding. Since the major effect of stent implantation is provided by its scaffolding, it is required to be retained for 6-12 months during which time arterial remodeling and healing is completed [2]. After this period, the stent is preferred to be broken down and excreted by the body, leaving behind a natural functioning artery. The advances of AMS for vascular scaffolding may allow for circumventing the long term risks of permanent stents, such as chronic inflammation, late stage thrombosis (clotting) and stent strut disruption (fracture) [3]. In pediatric intervention, which involves arteries that have not completed their growth cycle, the disappearance of the stent would enable natural vessel growth and avoid the need for recatheterization and serial stent balloon dilatation

until adulthood [4]. Thus, the development of bio-degradable stents, which can fulfill the mission and step away, is the next logical progression for the industry [5-7].

Mg-based and Fe-based materials have been widely investigated as potential base materials in recent years due to their biocompatible elements and mechanical characteristics [2, 8-10]. However, previous corrosion studies with bare Mg- and Fe-based metals demonstrated that the *in vivo* degradation performance cannot satisfy the requirement for the coronary stent yet. Tremendous work on improvement has been focused on: (1) pure Mg and pure Fe and their alloying with essential elements (Ca, Sr, Zn, Co, C and Si) or low contents of toxic elements (Mn, Sn and Zr), and the rare earth elements (Y and Gd) [11-17]; (2) novel structured bio-degradable metals (porous, ultrafine, nanocrystalline and glassy structures) [18-20]; (3) surface modifications by mechanical, chemical and electrochemical treatment [21, 22]. Presently, with the exception of the limus-eluting bio-degradable magnesium scaffold introduced in 2016 by Biotronic, these modifications have not resulted in a bio-degradable metallic stent with clinical success.

With the purpose of searching for suitable alloying elements, zinc as one of the most abundant nutritionally essential elements in the human body [23] began to be studied as an alloying element or bio-degradable base material [24]. In 2011, Vojtech et al. [25] prepared binary Zn-Mg alloys containing Mg content up to 3 wt.%, and found that the binary Zn-Mg alloys exhibited corrosion rates ($\approx$ 0.018 mm/yr) close to pure Zn, which were significantly lower than those of Mg and AZ91HP alloys. As a breakthrough, Bowen et al. [26, 27] examined the corrosion behavior of pure Zn for the first time and found that 1) Zn exhibited excellent biocompatibility after resided in the arterial lumen of

89

Sprague-Dawley rats for 6.5 months; 2) the corrosion products are not potentially hazardous like those of iron; 3) the corrosion rate in the first 2-3 months is very close to the ideal degradation rate for medical implants (0.02 mm/y) [28] and followed by an acceleration in 3-6 months; 4) a uniform corrosion is detected in earlier months so that the corrosion is more or less uniformly distributed over the entire exposed surface and the corrosion proceeds at approximately the same rate over the exposed metal surface [29]. All these corrosion characteristics of pure Zn suggest that Zn arterial corrosion behavior may be superior to other explored materials in the AMS field [24, 27]. The major concern for a pure Zn stent is that the tensile strength is relatively low (80 - 120 MPa). Stent materials used to prop open the lumen of arteries needs to have a tensile strength of at least 200 MPa, preferably close to 300 MPa [30]. Improvements in mechanical properties of Zn can be obtained through manipulation of its microstructure [31, 32] or alloying [25].

Zn-Li is one of a few potentially age-hardenable systems due to the significant solubility of lithium in zinc [33]. The *in vivo* studies of LAE442 (4 wt.% of lithium) confirmed suitability of this implant material for orthopedic use [34]. Additionally, lithium was approved by the U.S. Food and Drug Administration (FDA) as a drug in the early 1970s to treat manic depression [35]. It has also been reported to be beneficial in treatments of brain injury, stroke, Alzheimer's, Huntington's, and Parkinson's diseases, amyotrophic lateral sclerosis (ALS), spinal cord injury, and other conditions [35]. However, the drug's therapeutic window is very narrow and an overdose of lithium may induce tremors, frequent urination, thyroid problems, weight gain, and kidney failure [36]. Clinical experience with lithium suggests that its effective dose range is 0.6-1.0 mM serum level (500-1200 mg of lithium per day) while toxic levels occur at 1.2 mM or greater [35]. The

U.S. Environmental Protection Agency (EPA) in 1985 recommended the daily lithium intake of a 70 kg adult to range from 650 to 3100 µg [37]. Our previous estimates of the Zn-Li system indicated that [33]: 1) the overall quantities of lithium released from a zinc-lithium stent (with 0.7 wt.% of Li) is two orders of magnitude below the daily bodily consumption allowances; and 2) the incorporation of Li into Zn would increase the ultimate tensile strength (UTS) from < 120 MPa (pure Zn) to > 560 MPa (6 at.% Li).

However, an excessive content of Li lowers the ductility significantly due to the larger volume fractions of the $LiZn_4$ phase. To maintain applicable ductility and sufficient strength for the cardiovascular stent application, the addition of Li should remain below 4 at.% (0.4 wt.%).

Novel Zn-Li alloy wires (with 0.1 wt.% of Li) were prepared in this study. Metallurgical characterizations, *in vivo* biodegradation and *in vivo* biocompatibility analysis of the Zn-Li wire were carried out. The present body of work aimed at retaining corrosion behavior suitable for bio-degradable stent application, yet improving the mechanical and corrosion uniformity characteristics.

4.2 Materials and methods

4.2.1 Materials

Prior to casting, Zn shot (99.99+ wt.%, Alfa Aesar company, Ward Hill, MA), Zn foil (99.9 wt.%, Alfa Aesar company, Ward Hill, MA) and Li foil (99.9 wt.%, Alfa Aesar company, Ward Hill, MA) were weighed using a laboratory balance located in an inert-atmosphere glove box to avoid oxidation of Li. The total Zn shot and Zn foil weighed 1.0 kg, while the Li foil weighed 2.2 g. The Li foil was then wrapped tightly inside the Zn foil to form a

charge. The combined material was then sealed inside a sequence of three plastic specimen bags before being removed from the glove box. The Zn-Li foil charge and the Zn shots were immediately loaded into a graphite crucible. A custom vacuum induction melting setup at Michigan Tech was used to fabricate the Zn-Li alloys. They were cast by induction melting with a power of ≈ 3 kW under a 0.9 atm argon atmosphere. The temperature was set to be slightly above the melting point of Zn, 419.5 ºC for a few minutes. The ultimate vacuum level was 2×10^{-4} torr. A stepper motor controlled by a custom LabView (National Instruments, Austin, TX) script tilt-poured the melt into a 25 mm diameter stainless steel mold. 4N Zn wire (99.99+ wt.%, Goodfellow Corporation, Oakdale, Pennsylvania) was utilized as control samples.

4.2.2 Manufacture of Zn-Li wires

The Zn-Li alloy was further processed following a hot extrusion process employing a 10 MN extruder (SMS MEER GmbH). Prior to the extrusion, the Zn-Li billets possessing a diameter of 25 mm were heated to a temperature of 200 °C and the extruder's recipient was heated to 210 °C. In order to reduce the extrusion ratio, a die with four 0.5 mm in diameter openings was used for extrusion. Extrusion of the billets was carried out with a ram velocity of 0.1 mm/s ($F_{max} = 4.1$ MN) resulting in four Zn-Li rods, each with a diameter of 0.5 mm. The extrusion ratio is 625 due to the four openings in the die. Cooling of the rods was allowed at RT.

Subsequent wire drawing was carried out at a temperature of 180 °C by means of a self-constructed drawing machine at Leibniz Universität Hannover. Multiple drawing passes were used to reduce the wires' diameters to 0.25 mm. The drawing dies opening diameters

used for the drawing sequence were: 0.477 mm, 0.435 mm, 0.362 mm, 0.330 mm, 0.274 mm and 0.250 mm. Annealing or other heat treatment procedures were not required between the particular drawing passes.

4.2.3 Material characterizations

Inductively Coupled Plasma Optical Emission Spectrometry (ICP-OES) (PerkinElmer Optima 7000DV, Waltham, MA) was utilized in detecting the compositions of Zn alloy wire after drawing. To produce a solution suitable for ICP-OES analysis, 80 mg of alloy wire was dissolved in 12 ml of 6M HCl, which was diluted for analysis.

The Zn-Li sections were positioned in epoxy in order to obtain both the longitudinal (parallel to the extrusion or rolling direction) and transverse (perpendicular to the extrusion or rolling direction) view of each material. Mounted wires were ground with 600-grit, 800-grit, and 1200-grit silicon carbide. Final polishing steps were performed using 6 μm, 1 μm and 0.1 μm diamond cloth and 0.05 μm alumina slurry on microfiber. Microstructure of alloys were recorded using a Leica EC3 (Leica Microsystems; Buffalo Grove, Illinois) digital camera on an Olympus PMG-3 metallograph (Olympus, Shinjuku, Tokyo, Japan).

The polished wire sections were also carbon-coated and imaged with a JSM 6400 scanning electron microscope (SEM) (JEOL, Peabody, MA). The accelerating voltage and working distance used for SEM were 15 kV and 39 mm. Elemental contrast from the alloy surface was assessed from the collected backscattering electrons.

X-ray diffraction (XRD) was performed on an XDS2000 θ/θ X-ray diffractometer (Scintag Inc., Cupertino, CA) with CuKα radiation ($\lambda = 1.540562$ Å). The scans were performed continuously from 35° to 45° in 2θ at a speed of 0.2°/min with a step size of 0.02°.

Uniaxial tensile tests were performed using a Bose ELF 3200 mechanical tester (Bose Inc., MN, US). Prior to the test, wires were mounted on two polycarbonate (PC) holders using Loctite General Purpose epoxy (Henkel Corporation; Westlake, OH). The gauge length was set to be 10 mm. A small load cell (max. load: 22.2 N) was used, and the relative displacement and the strain rate were 12mm and 0.01 mm/sec. Yield stress, tensile stress, elongation to failure were calculated from the stress-strain curves. Standard deviation was estimated from eight 4N Zn and five Zn-Li wires. The ductility in % area reduction was also estimated by measuring the area reduction at the fracture based on four different wires. Vickers microhardness (HV) was measured using an M-400-G1 digital hardness tester (LECO, St Joseph, MI) at a load of 200 g for 5 s and 18 indentations per sample. Standard deviation was estimated from eighteen different points from the longitudinal section of a 4N Zn and a Zn-Li wire.

Area fraction and average particle size of the intermetallic phase were determined using the ImageJ software. The volume fraction of precipitation phase was calculated as the sum of areas of all black particles divided by the total area of the image. The average area of precipitates was calculated as the sum of the area of precipitates divided by number of particles. The average particle size was calculated from this average area assuming spherical geometry.

4.2.4 Arterial implantation

The primary method of this *in vivo* evaluation was based on a Sprague Dawley rat (Harlan Labs) model [38]. All animal tests have been approved by the animal care and use committee (IACUC) of Michigan Technological University. 4N Zn and Zn-Li alloy wire

samples with diameter of 0.25 mm and length of 2 cm were punched into the abdominal

aorta and then directed into the lumen for 10 mm before exteriorization. In this case, wires

were immersed in the flowing blood to mimic the environment of a stent strut. After 2-12

months, rats were euthanized and rat aortas containing the wire implants were harvested.

The wires had not become dislocated from their implant location at the time of collection.

To preserve the corrosion layer, explanted wires were preserved in 200 proof ethanol.

4.2.5 Biodegradation analysis

Part of the corroded wires were mounted in epoxy and cut transversely to expose the cross

section. Wire mounts were ground with 800 grit SiC, 1200 grit SiC, 6 μm diamond and 1

μm alumina and then cut into slices with thickness of 1 mm to fit into an aluminum mount

with carbon tape. The wire cross section was coated with thin layer of carbon before

imaging with the scanning electron microscope. Imaging of the wires was conducted at 15

kV accelerating voltage with a reduced working distance of 12 mm using a backscattered

detector. Cross sectional area (CSA) analysis of the backscattered image were conducted

using ImageJ software (Fig.4.5a) [39]. The penetration rate was determined according to

the following equation:

$$\text{Penetration rate (μm/yr)} = \frac{\sqrt{\frac{Nominal\ CSA}{\pi}} - \sqrt{\frac{Metallic\ CSA}{\pi}}}{\frac{Corrosion\ Time}{360}} \qquad \text{Eq. 4.1}$$

Elemental mappings of Ca, P, C, Cl, Zn, O from cross sections were captured to signify

the corrosions using an environmental scanning microscope (FEI Philips XL 40). The

accelerating voltage and working distance were 15 kV and 10 mm.

FT-IR was conducted in diffuse reflectance mode with a Jasco FTIR-4200 spectrophotometer. A series of 64 scans were performed at 4 cm^{-1} resolutions from 800 to 2000 cm^{-1}.

4.2.6 Histological evaluation

The leftover wires with aortas were snap-frozen in liquid nitrogen and cryo-sectioned for histological analysis [38]. Before staining, samples were preserved in a -80 $^{\circ}$C freezer. Cross sections were ethanol fixed and then stained with hematoxylin and eosin (H&E), mounted in Permount solution and imaged using an Olympus BX51, DP70 bright-field microscope.

The neointimal tissue with smooth muscle cells and inflammatory cells were inspected around the implants; variations of cell densities in the artery wall, lumen interface and biocorrosion area were measured.

4.2.7 Statistical analysis

All quoted errors and error bars correspond to the sample standard error.

4.3 Results

4.3.1 Material characterizations

Experimental composition of Zn-Li and purity of 4N Zn are given in Table 4.1. For this Zn-Li alloy, the experimental composition for Li is 0.1 wt.%. Cu, Mg, Fe and Pb were detected as trace impurities from Zn; and Cd, Al and Ni remained below the detection limit.

Table 4.1. ICP-OES compositional analysis of Zn-Li wires (wt.%)

Sample	Li	Cu	Mg	Fe	Pb	Cd	Al	Ni	Zn
4N Zn	<0.001	<0.003	<0.002	<0.002	<0.001	<0.001	<0.001	<0.001	Bal.
Zn-Li	0.103	0.003	0.002	0.002	0.001	<0.001	<0.001	<0.001	Bal.
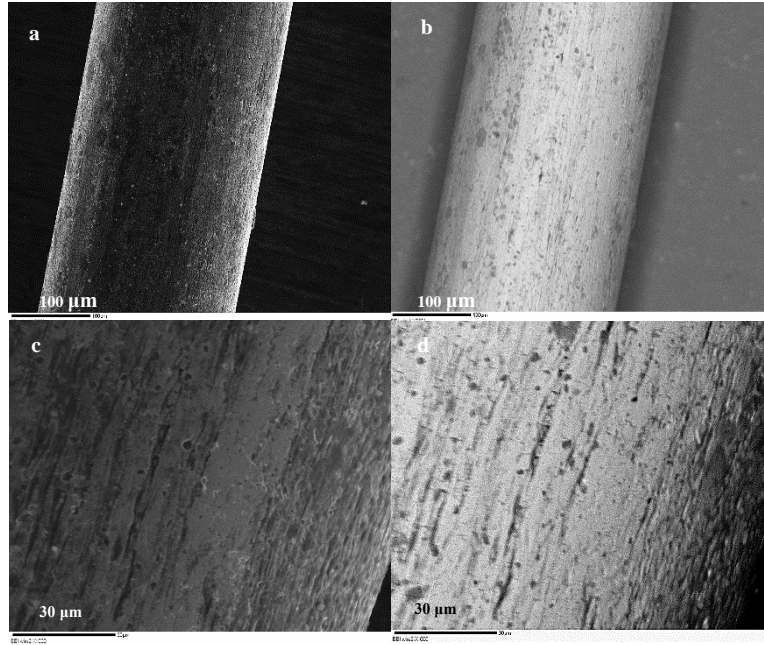
Fig. 4.1. SEM secondary electron (a, c) and backscattered electron images (b, d) for the surfaces of as-received Zn-Li wires

Surface images in Fig.4.1(a, c) exhibited severe rolling texture and precipitates. The darkest phase (representing the lowest atomic number) from the BEI images in Fig.4.1(b, d) indicate the occurrence of spherical and ribbon-like precipitates. This could be the Li-rich phase.
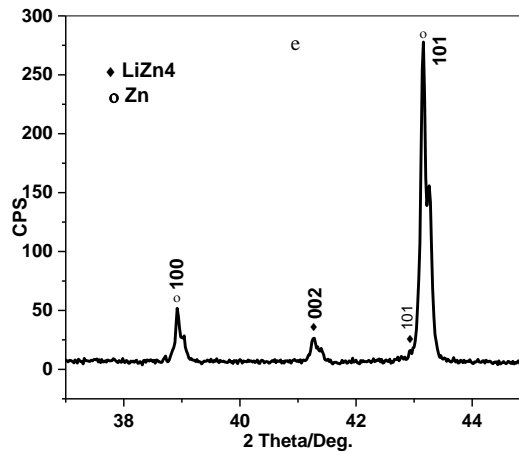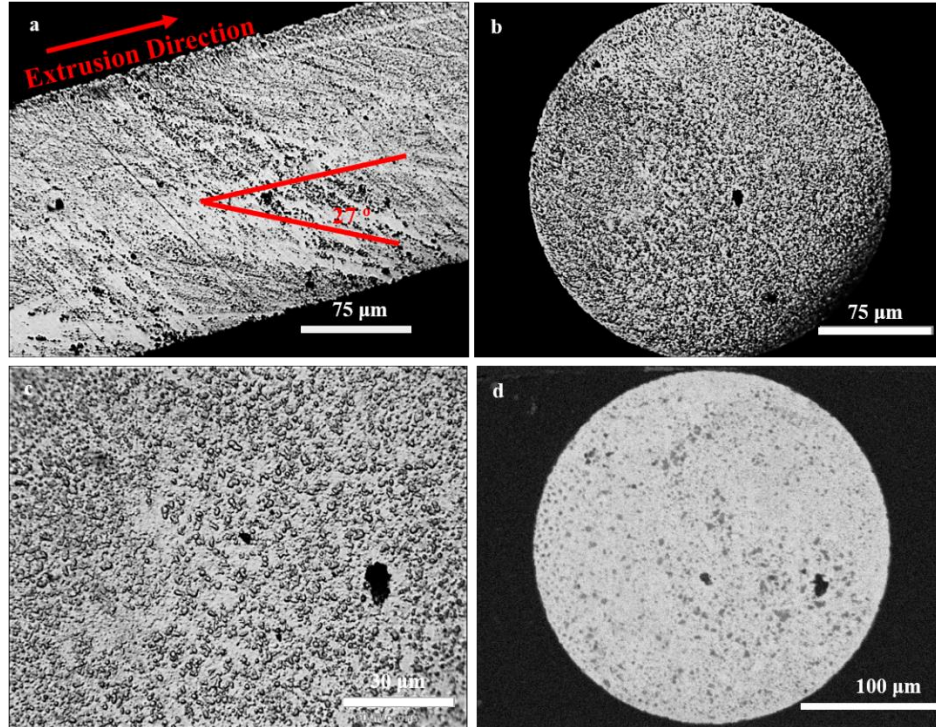
Fig. 4.2. Optical microscopy images of the Zn-Li wire (Ø = 0.25 mm) from longitudinal (a), transverse cross sections (b, c), backscattered electron image (d) and X-ray pattern for Zn-Li (e).

Fig.4.2 illustrates the optical microstructure, back-scattering electron imaging and XRD result for the extruded Zn-Li wires. The longitudinal sections of the Zn-Li alloy after drawing attained a preferential orientation at an angle of 27° with the extrusion direction. As both LiZn4 and Zn possess hcp structure, so this 27° orientation may come from the

formation of non-basal <c+a> slip system based on a junction between glissile <a> and sessile c dislocations from the prism plane into a pyramidal plane, which is energetically favorable for all hcp metals [40]. The transverse sections exhibited two main phases. The bright phase is the Zn rich matrix and the dark phase corresponds to Li rich precipitates, formed in the eutectic reaction. This is consistent with the BEI images in Fig.4.2(d). The darkest precipitate phase (Li-rich phase) possessed the lowest average atomic number. The area fraction and average particle size determined from the ImageJ software was 10±3 % and 3.0 ± 0.5 μm, respectively. This is a slightly larger value than the phase fraction of 6 % calculated from the Zn-Li phase diagram at 200°C.

The XRD result in Fig.4.2(e) indicates that the two phases from the micrographs are the zinc phase (43.24° and 39.02°) and the minor phase is $LiZn_4$ (41.20° and 42.96°). For the intermetallic $LiZn_4$ phase (P63/mmc (No. 194), a=2.7702(8), c=4.3785(9)) [41], the highest relative intensities of peaks came from the crystallographic plane sets of {002}. According to Pearson's Crystal powder pattern for $LiZn_4$ (No. 1321631), the strongest peak should be (101). This inconsistency could be due to the preferred orientation along (002) exerted from the extruding process.

Table 4.2 summarizes the mechanical properties of Zn-Li wires compared with the 4N Zn wire

Table 4.2. Mechanical properties of 4N Zn and Zn-Li wires

Sample	Yield strength (MPa)	Tensile strength (MPa)	Ductility %elongation	Ductility %area reduction	Hardness (Vickers)
4N Zn	86 ± 14	116 ± 13	50 ± 5	97 ± 2	42 ± 3
Zn-Li	238 ± 60	274 ± 61	17 ± 7	74 ± 5	97 ± 2

It should be noted that Zn-Li exhibited higher yield strength, tensile strength, hardness and lower ductility than 4N Zn.
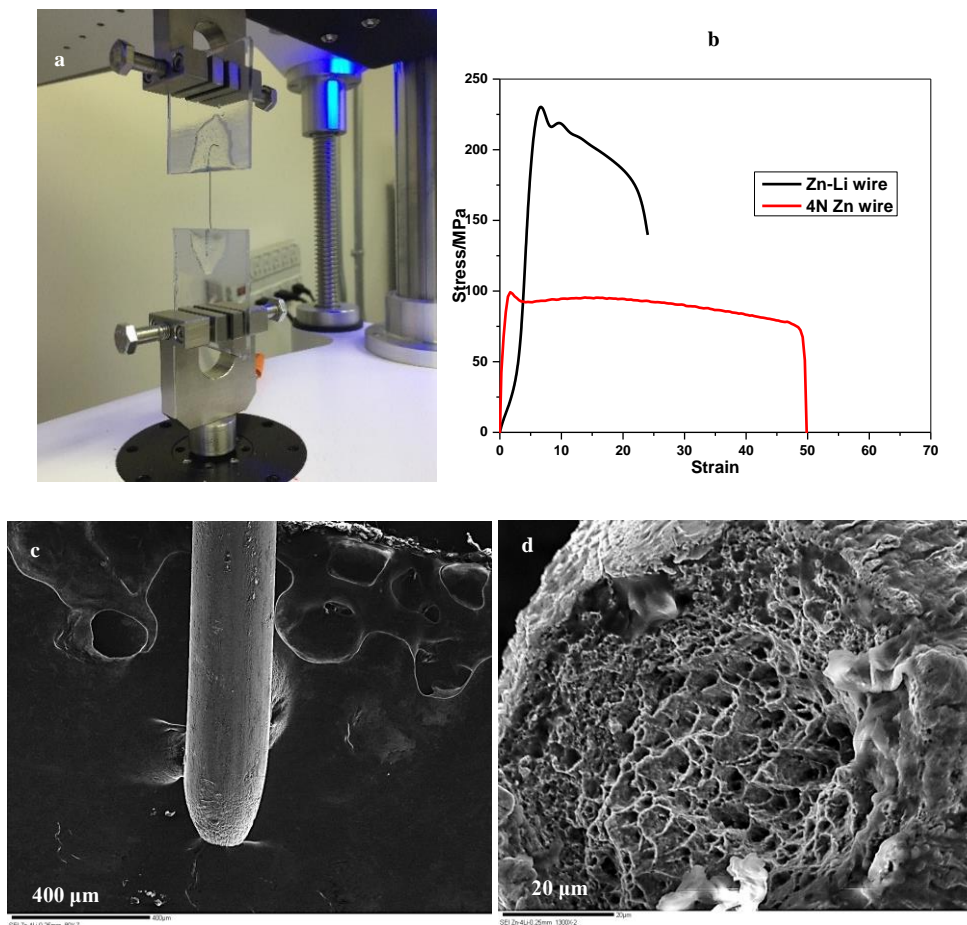

Fig.4.3. Set-up for the tensile test (a), representative tensile stress-strain curve of 4N Zn and Zn-Li (b) and fracture images of Zn-Li (c,d).

The representative tensile stress curve (Fig.4.3b) shows that the zinc alloy endured a significant plastic deformation and necking before fracture occurred. The curve indicates an ultimate tensile stress of 220 MPa and an elongation to failure of 24%. The average strength values from the five Zn-Li wires increased by over 100% relative to 4N Zn and

the ductility in percent of elongation was also retained at 17%, reaching the minimum mechanical requirement for a stent [30]. The increase in strength could be due to the large volume fractions of the $LiZn_4$ phase for the alloy wires. SEM examination of the fracture surface (Fig. 4.3c, d) revealed a clear necking shrinkage and dimpled surface, indicating a moderately ductile behavior for the Zn alloy. The spherical "dimples" corresponding to microvoids are believed to initiate the crack formation.

4.3.2 *In vivo* corrosion analysis

(b)

$PO_4^{3-}(v_3)$

$PO_4^{3-}(v_1)$

$CO_3^{2-}(v_3)$

Wavenumber/cm^{-1}
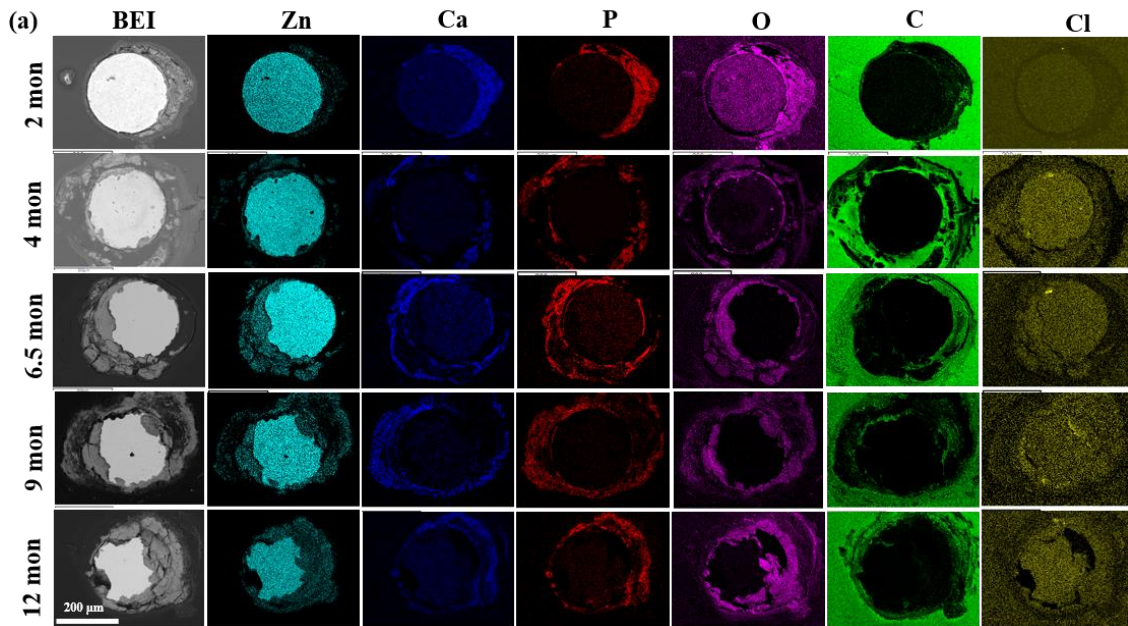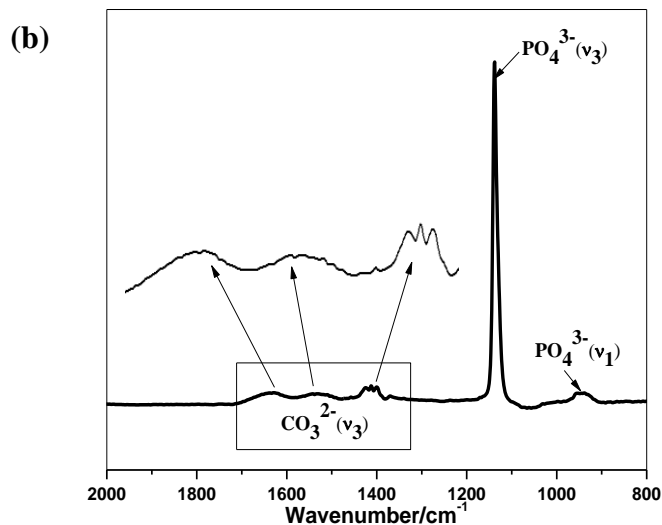
Fig. 4.4. (a) Backscattered electron images and elemental maps (EDS) of Zn-Li wire sections after residing in the rat arterial for 2 to 12 months; (b) FTIR spectrum of Zn-Li wire for 13.5-month residence.

From the backscattered electron images (BEI), both the remaining metallic sections (shown as the lighter phase) and the mixture of corrosion products, the epoxy and tissue (shown as the darker phase) were detected. Dark areas inside the boundaries of explant cross sections indicated a lower atomic number corrosion product made of zinc oxide, as will be demonstrated later by x-ray maps. BEI images recorded after different periods of the alloy wire explants (Fig.4.4a) indicated the loss of the circular wire integrity after 2 months of *in vivo* degradation. It progressed further until 12 months.

Elemental maps of the same series of cross sections revealed the presence of the following major elements: Zn, Ca, P, O, C and Cl (Fig.4.4a). At 2 months, a Ca and P-containing exterior layer was detected adjacent to the inner layer containing Zn, C and O. A variation in distribution of the corrosion products containing those elements is apparent from elemental maps in Fig.4.4a. The outermost layer consists mainly of Ca and P, and the thin layer adjacent to the metallic leftover is enriched with Cl, O and Zn, followed by a tiny

102

content of C in particular regions. The distributions of Ca and P are almost identical, indicating the presence of a more uniform layer of CaP at 2 months. This is in a disparity to what was reported for the Mg wire [42], where Ca was incorporated in a more outer layer than P. At 4 months, apart from the more evident loss of the metallic area, wire cross sections are surrounded by ceramic layer composed of Ca and P elements, which thickness appears to be more uniform around perimeter. The higher content of C at 4 months is believed to be related to the penetration of epoxy into the oxide corrosion product, and not result of the corrosion. This conclusion is in agreement with the contrast for the BEI image.

As shown in Fig.4.4, the distribution of Cl is similar to Zn. The high intensity Cl spot is aligned with O, indicating the possible corrosion product of Zn-O-Cl. At 6.5 months, both the CaP layer and the Zn-O layer thickened and the C signals started to appear in some inner regions adjacent to O and Zn. This suggests the onset of the formation of Zn-O-C at 6.5 months. At 9 months, the coverage and distribution of all elements of interest around metallic implant suggest increased amount of corrosion products, especially Zn-O-C. Approximately 1/5 of the inner Zn area was lost at 12 months. The corrosion layer of Zn-O segregated in the locations where most corrosion occurred. The layers of CaP and Zn-O-C did not increase significantly as compared to the previous stage. The nearly identical distribution of the Cl and Zn elements and the overlap between O and Cl in the enlarged island area provide evidence for formation of Zn-O-Cl product(s) at 12 months.

FT-TR (infrared spectroscopy) was used to substantiate the surface products present on explanted Zn alloy wires. In the FT-IR spectrum (Fig.4.4b), a narrow and high intensity PO_4^{3-} band is observed at 1050-1180 cm^{-1}, which is related to the asymmetric stretching of

the v3 group [42,43]. The absorption band in the range of 920-1000 cm^{-1} is characteristic of the symmetrical stretching of the v1 group [44]. The CO_3^{2-} bands from the v3 apatitic substitution were detected at 1390-1500 and 1540-1620 cm^{-1} [45,46].

Based on the signature of Zn, O, Ca, P, C from elemental map and the presence of PO_4^{3-} and CO_3^{2-} from FT-IR, it is assumed that the compact degradation product of Zn-Li consisted of an inner Zn-O layer, followed by Zn-Cl-O, zinc carbonate ($ZnCO_3$) and a calcium phosphate (CaP) layer. Another possible corrosion product, $Zn_3(PO_4)_2 \cdot 2H_2O$, which is a more thermodynamically stable mineral at physiological pH [47] were absent based on the lack of spatial overlapping between the elements Zn and P. This may either indicate that the formation of $Zn_3(PO_4)_2 \cdot 2H_2O$ in this system needs longer time or that the local pH had increased to above the physiological state due to the corrosion reaction: $Zn+O_2+H_2O = Zn^{2+}+4OH^-$.
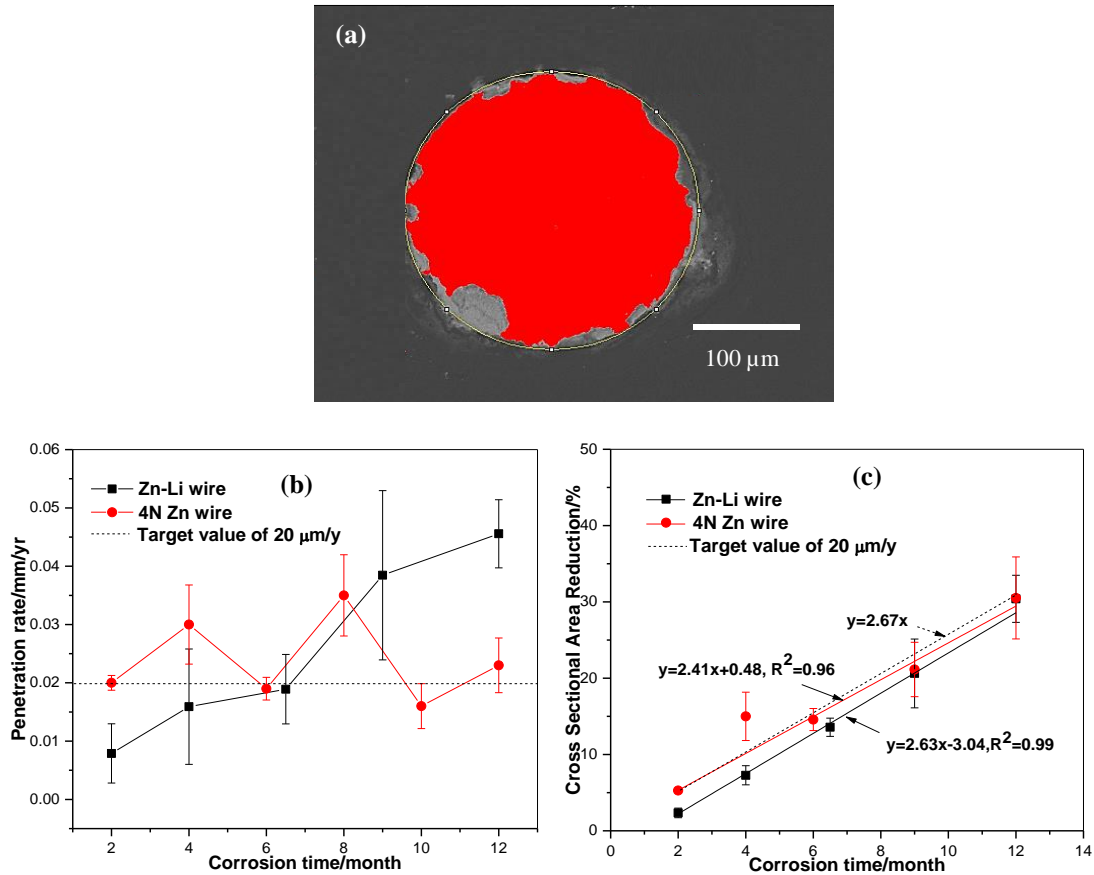
Fig. 4.5.(a) Typical ImageJ screenshot used for cross sectional analysis. The original local cross-sectional area (yellow) is approximated by an ellipse. The red area selected by thresholding is to represent the remaining Zn-Li alloy. (b) Penetration rates calculated from reduction of cross sectional areas. (c) Cross sectional area reduction of alloy wires after explanation.

Cross-sectional analysis showed an incremental increase of the degradation rate for Zn-Li alloy during the implantation from 2 to 12 months. A moderate low degradation rate of 0.08 to 0.016 mm/yr was observed at 2 to 4 months. The earlier degradation for the alloy wire was a little slower than that of 4N Zn and the benchmark for the ideal degradation (0.02 mm/y) of medical implants [28]. However, the degradation of Zn-Li alloy accelerated to 0.019 mm/yr at 9 months and 0.046 mm/yr at 12 months, which is twice as high as that

of the 4N Zn sample (Fig.4.5b). This acceleration in later stage is preferred since the stent would dissolve quickly in the body after the supporting function has ceased. Fig.4.5c demonstrates the percent of cross sectional area reduction for 4N Zn and the Zn-Li alloy over implantation time. The dashed line corresponds to the targeted cross area reduction of 20 μm/yr reported earlier [28]. The corroded area for Zn-Li was a little less than for 4N Zn before 9 months and increased thereafter, which is consistent with the penetration rate results shown in Fig.4.5b. Both 4N Zn and Zn-Li followed almost the same trend with the targeted value and retained about 70% of the original area after 12 months *in vivo*. The identical loss of area for 4N Zn and Zn-Li over 12 months indicates the very similar average corrosion rate for the two materials. Surprisingly, the Zn-Li curve displayed a near-liner relationship ($R^2 = 0.99$) between the percent of area reduction and time, and the slope of the curve ($k = 2.63$) was much closer to the target value ($k = 2.67$). This suggests a near ideal uniform gradual acceleration of biodegradation for this alloy.

4.3.3 *In vivo* biocompatibility analysis
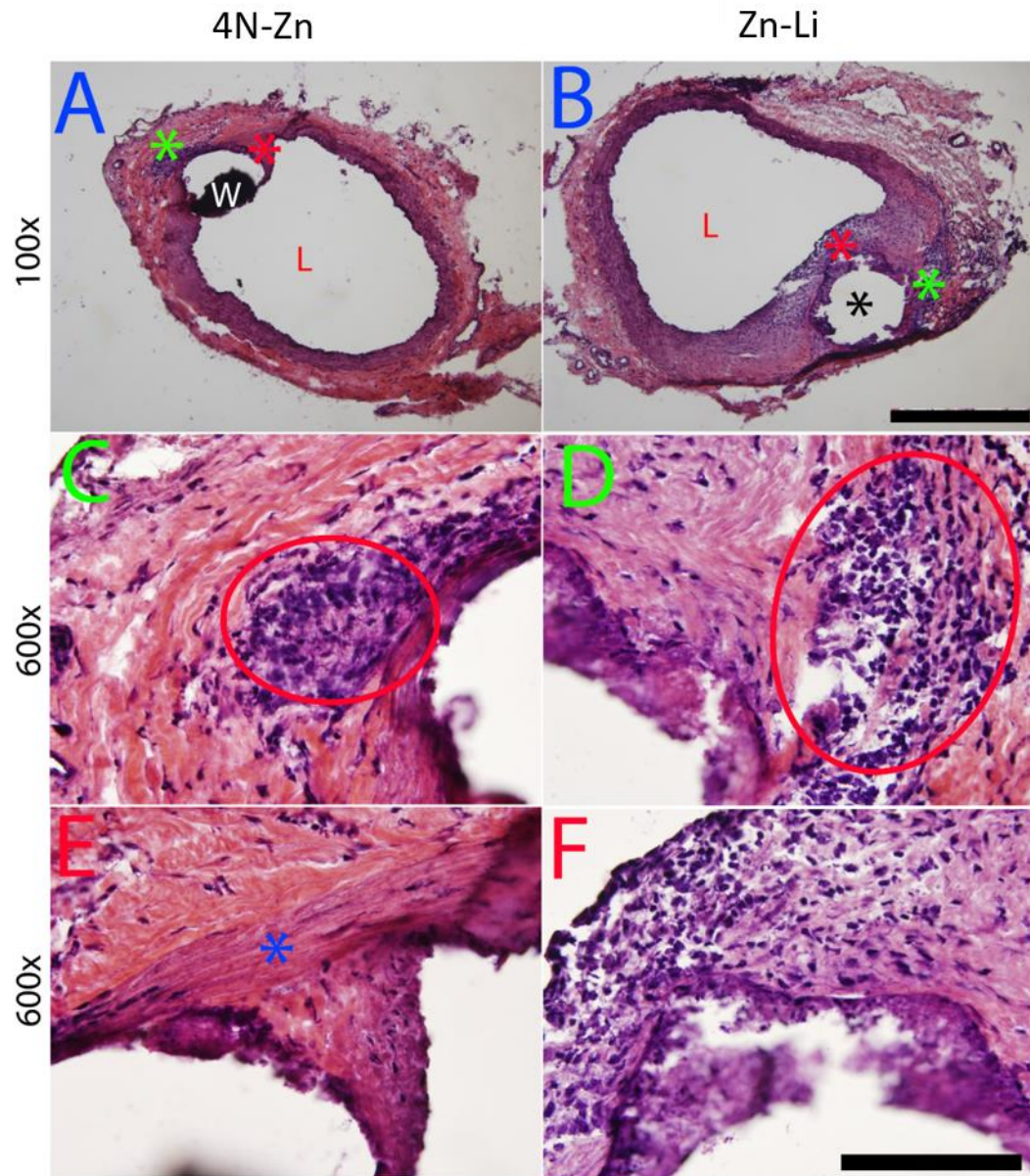
Fig. 4.6. Arterial explants stained with H&E at 11 months. Low magnification images show two subsequent areas selected for high magnification. "L" is the luminal opening of the artery. Scale bars are 500 µm and 100 µm for 100x and 600x, respectively.

Fig.4.6 also shows two areas of interest at higher magnification for the 11 month luminal explants. Panels C and D demonstrate regions of chronic inflammation within the red circle that correspond to the green asterisks on panels A and B.

In panel E, the blue asterisk identifies a media layer largely devoid of smooth muscle cells, while panel F identifies a neo-intima largely populated with cells. These areas corresponded to the red asterisks on panels A and B. It should be noted that the media layer for the Zn-Li specimen appears largely deteriorated closer to the implant. Wide open arterial lumens and low neointimal growth around the implant is evident from the images and indicates excellent biocompatibility for Zn-Li, although inflammation and neointima thickness appear to be slightly higher for Zn-Li relative to 4N Zn.

4.4 Discussion

4.4.1 The role of Li in the corrosion rate of Zn

It is known that alloying a second element into a metallic structure may not only change the mechanical properties but also modify the corrosion behavior. In the Zn-Li alloys, based on the optical micrographs and XRD results, it is assumed that element Li existed partly in solid solution but also precipitated in the form of $LiZn_4$ as part of a eutectic structure.
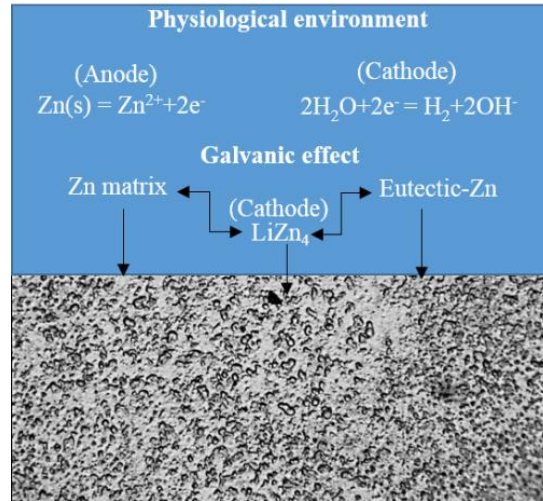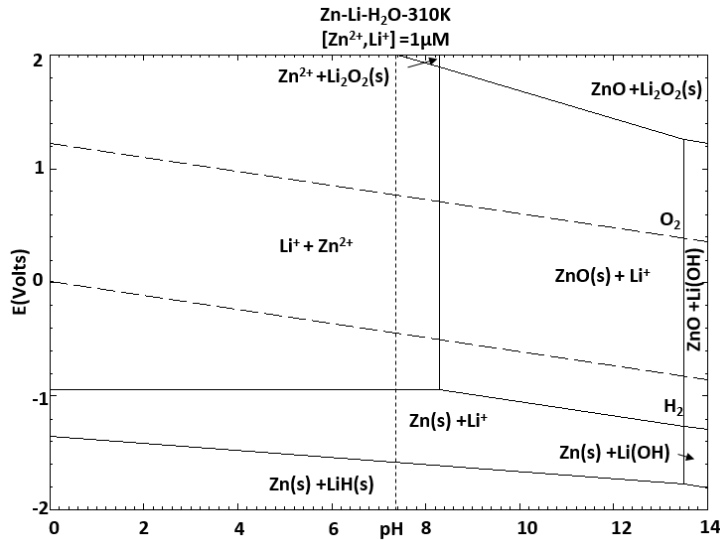
Fig. 4.7. Illustration of the galvanic effect between the Zn matrix and secondary phase in physiological environment.
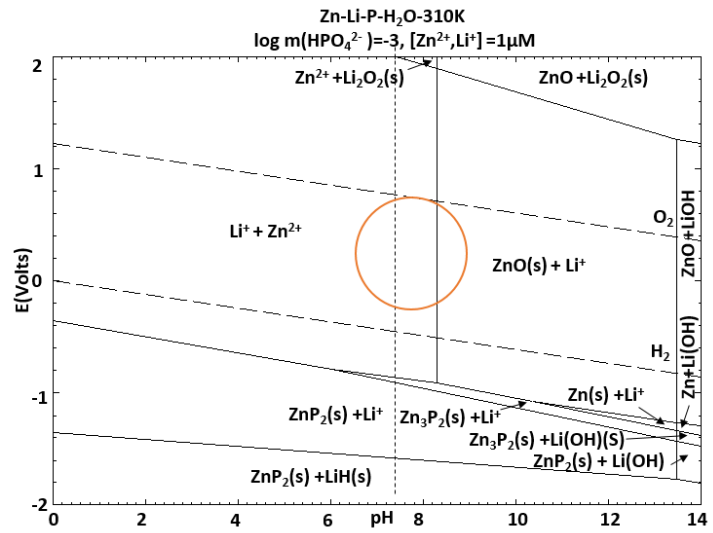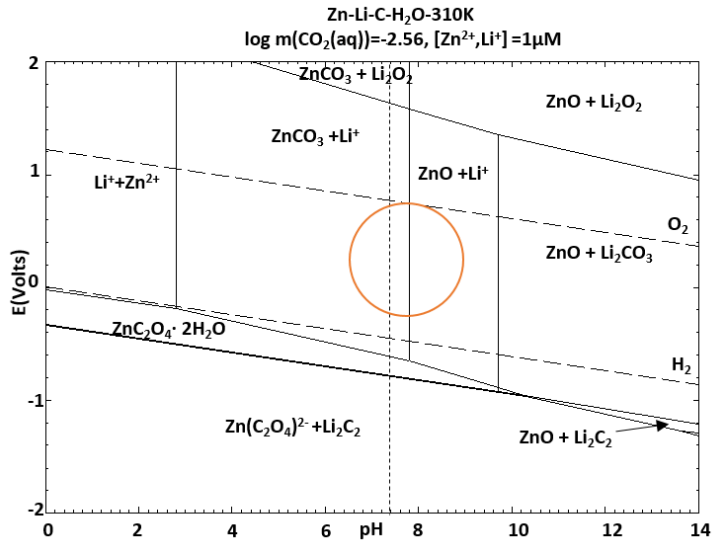
As shown schematically in Fig.4.7, there are two sources of galvanic corrosion in this system: one is between the Zn-matrix and $LiZn_4$ and the other is between the eutectic-Zn and $LiZn_4$. Due to the potential difference of the two, the precipitated secondary phase $LiZn_4$, which is nobler than Zn, can accelerate the corrosion of the matrix due to micro-galvanic corrosion. However, the comparison of the penetration rates in Fig.4.5(b) showed that the Zn-Li alloy corrodes slower than 4N Zn in the early stage. This can be explained as follows: the area fraction of the $LiZn_4$ phases as determined using the ImageJ software is up to $10 \pm 3\%$. During the corrosion processes these large amounts of precipitates could act as an anodic barrier and an enrichment of the corrosion product (which consists of inner Zn-O layer, Zn-Cl-O, $ZnCO_3$ and CaP layer) to inhibit the overall corrosion rate of the alloy. Therefore, the formation of the $LiZn_4$ phase in this alloy contributes to a slower corrosion of the Zn-Li alloy. The decrease of the susceptibility to atmospheric corrosion resulting from alloying with Li was also detected in Mg-12 at.% Li [48]. Moreover, the

molar ratio of LiZn$_4$ to the adjacent eutectic-Zn for Zn-Li was 40% (calculated from the Zn-Li phase diagram) and this may also influence the galvanic cells. Apart from the high volume fraction effect, the aggregates of the corrosion layers from the uncorroded intermetallic LiZn$_4$ phase, together with other corrosion coatings consisting of zinc oxide, perchlorate, carbonate and calcium phosphate layers also retarded the corrosions. However, this decrease of the susceptibility to atmospheric corrosion from large volume fractions of LiZn$_4$ can be undermined with the progression of corrosion, as evidenced by the drastic increase of the corrosion rate for the alloy wire after 9 months. This can be due to the dissolution of the passive film and the incorporation of dissolved oxygen, ions or other proteins and cells. In this way, the structure of the passive film will loosen and the previous initiated pits may spread, which promotes a rapid attack of the bulk metal [49].
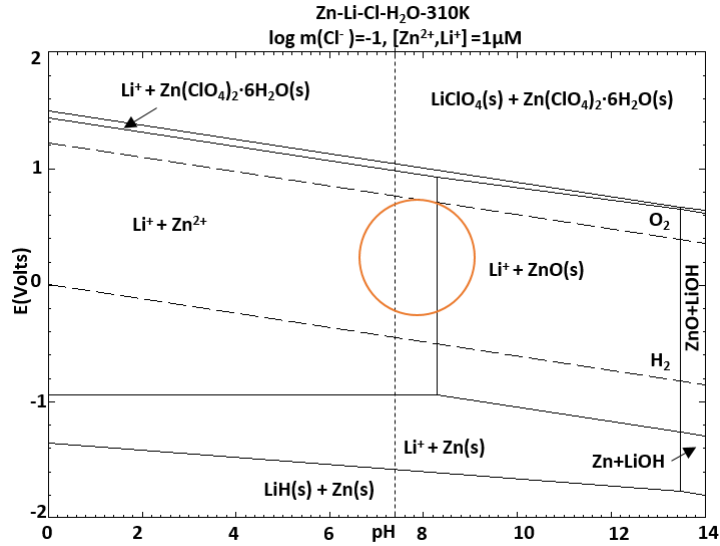
4.4.2 Corrosion mechanism

The production of the corrosion products in this system were estimated based on the Pourbaix diagram of Zn-Li-H$_2$O at 37°C (calculated using FactSage 7.0 software).
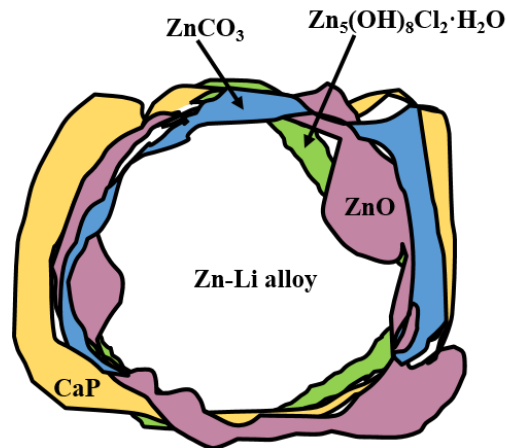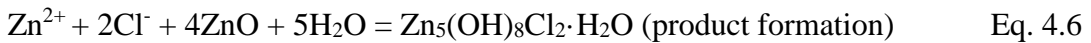

110

Zn-Li-C-H$_2$O-310K
log m(CO$_2$(aq))=-2.56, [Zn^{2+},Li$^+$] =1μM

Top figure labels:
- ZnCO$_3$ + Li$_2$O$_2$
- ZnO + Li$_2$O$_2$
- ZnCO$_3$ +Li$^+$
- ZnO +Li$^+$
- Li$^+$+Zn^{2+}
- O$_2$
- ZnO + Li$_2$CO$_3$
- ZnC$_2$O$_4$· 2H$_2$O
- H$_2$
- Zn(C$_2$O$_4$)$^{2-}$ +Li$_2$C$_2$
- ZnO + Li$_2$C$_2$

Axes: E(Volts) vertical, pH horizontal (0 to 14)

Zn-Li-P-H$_2$O-310K
log m(HPO$_4{}^{2-}$)=-3, [Zn^{2+},Li$^+$] =1μM

Bottom figure labels:
- Zn^{2+} +Li$_2$O$_2$(s)
- ZnO +Li$_2$O$_2$(s)
- Li$^+$ + Zn^{2+}
- O$_2$
- ZnO(s) + Li$^+$
- ZnO +LiOH
- H$_2$
- Zn +Li(OH)
- Zn(s) +Li$^+$
- ZnP$_2$(s) +Li$^+$
- Zn$_3$P$_2$(s) +Li$^+$
- Zn$_3$P$_2$(s) +Li(OH)(S)
- ZnP$_2$(s) + Li(OH)
- ZnP$_2$(s) +LiH(s)

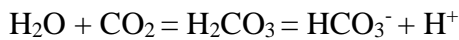Axes: E(Volts) vertical, pH horizontal (0 to 14)

111

Fig. 4.8. Zn-Li-H$_2$O and Zn-Li-H$_2$O-X Pourbaix diagrams for physiological concentrations of X = {C, Cl, P } at 37 °C. Physiological pH of 7.4 is shown by the dotted lines and physiological potential for tissue fluid is marked by the circles.

All of the thermodynamic equilibrium equations of Zn and Li with the physiological ions present in H$_2$O are shown in Fig.4.8. Zn-Li-H$_2$O and Zn-Li-X-H$_2$O diagrams are shown for X = {C, P, Cl} and [Zn^{2+}, Li$^+$]={10^{-6}}. To mimic the *in vivo* corrosion environment, concentrations for Cl$^-$, HPO$_4$$^{2-}$ and HCO$_3$$^-$(CO$_2$(aq)) in this diagram were set to be identical to the values in human blood plasma (0.1 mol/L for Cl$^-$, 0.001 mol/L for HPO$_4$$^{2-}$, and 0.027 mol/L for CO$_2$(aq)) [50]. In the Zn-Li-H$_2$O system, at low potentials of $E < $ -1.4 V, both Zn and Li are in the immunity region and thus stable in their metallic form. As Li possesses higher activity than Zn, with potential increases, Li would be oxidized first. If surface potential E is over -0.8 V, and at pH < 8.3, both Zn and Li would go into solution. The Pourbaix diagram also shows that both the Zn^{2+} and Li$^+$ are stable at low pH; the oxide, ZnO, at intermediate pH; and the ZnO and LiOH at very high pH.

112

The Pourbaix diagram is assumed to represent the thermodynamic equilibrium conditions. On a contrary, in a real corrosion situation, the local pH values in the cathodic and anodic areas are always higher and smaller, respectively, than at equilibrium. Therefore, the red circles marked on the Pourbaix diagrams in Fig.4.8 which stand for physiological conditions with tissue fluid (pH ≈ 7.4 and $E ≈ 0.78$ V) [51]. At pH ≈ 7.4, the Zn-Li-C-H_2O system reaches the equilibrium with $ZnCO_3$ and ZnO as the corrosion product. In the diagram of Zn-Li-P-H_2O, it is believed that Zn_3P_2 only exists if the potential is in the range of -0.7 V $< E <$ -0.6V. At physiological potential, Zn_3P_2 dissolves and ZnO becomes the only solid product. No $Zn_3(PO_4)_2·2H_2O$ was detected under all conditions. From the elemental mapping in Fig.4.4a, there was still a signal for a Zn-Cl-O mineral. However, in the Zn-Li-Cl-H_2O system, no solid Zn-Cl-O products were suggested around the potential of the tissue fluid. It is possible that the as-formed chloride product was not stable at pH = 7.4. $Zn_5(OH)_8Cl_2·H_2O$, which can be formed due to the reaction of $ZnCl_2$ with ZnO only exists at a pH of 6.9. Furthermore, after implantation, apart from the contact with Cl^-, HCO_3^-, HPO_4^{2-}, the Zn-Li alloy implants were also exposed to an environment rich in blood, protein, cations (Na^+, K^+, Ca^{2+}, Mg^{2+}, etc.), organic substances of low-molecular-weight species, polymeric components of high molecular-weight, as well as dissolved oxygen [52]. This physiological environment makes the corrosive medium extremely complex, which can alter the properties of corrosion products and corrosion rates [51].

Based on the Pourbaix diagram, the following degradation sequence of the Zn-Li alloy in a physiological environment is assumed: when Zn-Li is exposed to the aqueous solutions, it shows some hydrogen gas evolution (Eq. 2), which is balanced by dissolution of Zn (Eq. 3). As dissolution progresses, the pH increases with the formation of OH^- from the cathodic

113

reaction, which promotes the production of ZnO according to the Pourbaix diagram. Along with the deposition of a passive ZnO layer (Eq. 4), the existence of HCO_3^- (Eq. 5), Cl^-(Eq. 6) and HPO_4^{2-} (biomineralization from the introduction of calcium) in the body fluid also favors thermodynamically the formation of new phases. The passive film would thus be reconstructed into layers of zinc oxide, zinc chloride hydroxide, zinc carbonate and calcium phosphate layer, as illustrated in schematic phase map in Fig. 4.9.

$2H_2O + 2e^- = H_2 + 2OH^-$ (cathodic reaction)   Eq. 4.2

$Zn(s) = Zn^{2+}(aq) + 2e^-$ (anodic reaction)   Eq. 4.3

$Zn^{2+} + 2OH^- = Zn(OH)_2 = ZnO + H_2O$ (product formation)   Eq. 4.4

$H_2O + CO_2 = H_2CO_3 = HCO_3^- + H^+$

$Zn^{2+} + 2HCO_3^- = ZnCO_3 + H_2$ (product formation)Equation   Eq.4.5

$Zn^{2+} + 2Cl^- + 4ZnO + 5H_2O = Zn_5(OH)_8Cl_2 \cdot H_2O$ (product formation)   Eq. 4.6

Fig. 4.9. Schematic phase map for 9-month residence.

Based on histological observations, inflammation for the Li bearing metal consistently appeared to be higher than for the 4N Zn wire. This increased inflammation did not detrimentally affect the ability of the artery to propagate blood flow. The greater inflammatory response exhibited by Zn-Li over the 12 month evaluation period can be explained by the increased variety of chemical species displayed to immune cells during the course of the corrosion process, such as the $LiZn_4$ intermetallic.

4.5 Conclusions

A new Zn-Li alloy has been cast, extruded and analyzed for biomedical-focused applications. XRD results indicated the formation of $LiZn_4$ through the emergence of diffraction peaks corresponding to (002) and (101) for this phase. Mechanical testing showed that alloying of Zn with 0.1 wt.% of Li increased the tensile strength from 116 ± 13 MPa (pure Zn) to 274 ± 61 MPa while the ductility was still being held at $17 \pm 7\%$.

The elemental mapping and FT-IR analysis jointly confirmed that the corrosion products are calcium phosphate, zinc oxide, zinc chloride hydroxide and zinc carbonate. The quantitative corrosion analysis showed a moderate low degradation rate of 0.019 mm/yr at 6.5 months that increased to 0.046 mm/yr at 12 months. This later stage acceleration is beneficial in that the stent would dissolve quickly in the body after the scaffolding function ceased around 6 months. The corroded volume for Zn-Li was only slightly smaller than that of 4N Zn at 6 months but both of them retained about 70% of their original dimensions after 12 months *in vivo*. The nearly identical oxidation progression for 4N Zn and Zn-Li indicates a very similar corrosion rate for the two materials. Moreover, the cross sectional area reduction curve for Zn-Li displayed a near-liner relationship between the percent of

area reduction and time. This suggests a near ideal uniform gradual acceleration of biodegradation for this alloy. Biocompatibility results for the Zn-Li alloy at 11 months *in vivo* indicated a moderate inflammation with a non-obstructive neointima.

All the preliminary results obtained from implantation in rat abdominal arteries demonstrated that this new Zn-Li alloy is another promising bio-degradable coronary stent material based on its improved mechanical properties and the outstanding corrosion behavior as compared to pure Zn.

References

[1] Y.F. Zheng, X.N. Gu, F. Witte, Biodegradable metals, Mater. Sci. Eng. Reports, 77 (2014) 1-34.

[2] M. Moravej, D. Mantovani, Biodegradable metals for cardiovascular stent application: interests and new opportunities, Int. J. Mol. Sci., 12 (2011) 4250-4270.

[3] B. Heublein, R. Rohde, V. Kaese, M. Niemeyer, W. Hartung, A. Haverich, Biocorrosion of magnesium alloys: a new principle in cardiovascular implant technology?, Heart, 89 (2003) 651-656.

[4] S. Hascoët, A. Baruteau, Z. Jalal, L. Mauri, P. Acar, M. Elbaz, Y. Boudjemline, A. Fraisse, Stents in paediatric and adult congenital interventional cardiac catheterization, Arch. Cardiovasc. Dis., 107 (2014) 462-475.

[5] A. Colombo, E. Karvouni, Biodegradable stents : "fulfilling the mission and stepping away", Circulation, 102 (2000) 371-373.

[6] P. Erne, M. Schier, T.J. Resink, The road to bioabsorbable stents: reaching clinical reality?, Cadiovasc. Intervent. Radiol., 29 (2006) 11-16.

[7] S. Saito, New horizon of bioabsorbable stent, Catheter. Cardiovasc. Interv., 66 (2005) 595-596.

[8] N.E. Saris, E. Mervaala, H. Karppanen, J.A. Khawaja, A. Lewenstam, Magnesium: An update on physiological, clinical and analytical aspects, Clin. Chim. Acta, 294 (2000) 1-26.

[9] J. Cheng, Y.F. Zheng, In vitro study on newly designed biodegradable Fe-X composites (X = W, CNT) prepared by spark plasma sintering, J. Biomed. Mater. Res., Part B, 101 (2013) 485-497.

[10] J.M. Seitz, A. Lucas, M. Kirschner, Magnesium-based compression screws: a novelty in the clinical use of implants, JOM, 68 (2016) 1177-1182.

[11] N.T. Kirkland, J. Lespagnol, N. Birbilis, M.P. Staiger, A survey of bio-corrosion rates of magnesium alloys, Corros. Sci., 52 (2010) 287-291.

[12] W.D. Mueller, M.L. Nascimento, M.F. Lorenzo de Mele, Critical discussion of the results from different corrosion studies of Mg and Mg alloys for biomaterial applications, Acta Biomater., 6 (2010) 1749-1755.

[13] E. Zhang, L. Yang, Microstructure, mechanical properties and bio-corrosion properties of Mg–Zn–Mn–Ca alloy for biomedical application, Mater. Sci. Eng. A, 497 (2008) 111-118.

[14] N. Hort, Y. Huang, D. Fechner, M. Störmer, C. Blawert, F. Witte, C. Vogt, H. Drücker, R. Willumeit, K.U. Kainer, F. Feyerabend, Magnesium alloys as implant materials-Principles of property design for Mg-RE alloys, Acta Biomater., 6 (2010) 1714-1725.

[15] Q. Peng, Y. Huang, L. Zhou, N. Hort, K.U. Kainer, Preparation and properties of high purity Mg–Y biomaterials, Biomaterials, 31 (2010) 398-403.

[16] B. Liu, Y.F. Zheng, Effects of alloying elements (Mn, Co, Al, W, Sn, B, C and S) on biodegradability and in vitro biocompatibility of pure iron, Acta Biomater., 7 (2011) 1407-1420.

[17] B. Liu, Y.F. Zheng, L.Q. Ruan, In vitro investigation of $Fe_{30}Mn_6Si$ shape memory alloy as potential biodegradable metallic material, Mater. Lett., 65 (2011) 540-543.

[18] A.H. Yusop, A.A. Bakir, N.A. Shaharom, M.R. Abdul Kadir, H. Hermawan, Porous biodegradable metals for hard tissue scaffolds: a review, Int. J. Biomater., 2012 (2012) 1-10.

[19] Q. Ge, D. Dellasega, A.G. Demir, M. Vedani, The processing of ultrafine-grained Mg tubes for biodegradable stents, Acta Biomater. , 9 (2013).

[20] H. Li, Y. Zheng, L. Qin, Progress of biodegradable metals, Prog. Nat. Sci.: Mater. Int., 24 (2014) 414-422.

[21] T.S.N. Sankara Narayanan, I.S. Park, M.H. Lee, Surface modification of magnesium and its alloys for biomedical applications: Opportunities and challenges, in: T.S.N. Sankara Narayanan, I.S. Park, M.H. Lee (Eds.) Surface Modification of Magnesium and its Alloys for Biomedical Applications, Woodhead Publishing, Oxford, 2015, pp. 29-87.

[22] P.K. Chu, G.S. Wu, Surface design of biodegradable magnesium alloys for biomedical applications, in: T.S.N. Sankara Narayanan, I.S. Park, M.H. Lee (Eds.) Surface Modification of Magnesium and its Alloys for Biomedical Applications, Woodhead Publishing, Oxford, 2015, pp. 89-119.

[23] H. Tapiero, K.D. Tew, Trace elements in human physiology and pathology: zinc and metallothioneins, Biomed. Pharmacother., 57 (2003) 399-411.

[24] P.K. Bowen, E.R. Shearier, S. Zhao, R.J. Guillory Ii, F. Zhao, J. Goldman, J. Drelich, Biodegradable metals for cardiovascular stents: from clinical concerns to recent Zn-Alloys, Adv. Healthc. Mater., 03 (2016) 1-20.

[25] D. Vojtech, J. Kubasek, J. Serak, P. Novak, Mechanical and corrosion properties of newly developed biodegradable Zn-based alloys for bone fixation, Acta Biomater., 7 (2011) 3515-3522.

[26] P.K. Bowen, J. Drelich, J. Goldman, Zinc exhibits ideal physiological corrosion behavior for bioabsorbable stents, Adv. Mater., 25 (2013) 2577-2582.

[27] P.K. Bowen, R.J. Guillory Ii, E.R. Shearier, J.-M. Seitz, J. Drelich, M. Bocks, F. Zhao, J. Goldman, Metallic zinc exhibits optimal biocompatibility for bioabsorbable endovascular stents, Mater. Sci. Eng., C, 56 (2015) 467-472.

[28] M.L. A. Atrens, N. I. Zainal Abidin, G. L. Song, Corrosion of magnesium (Mg) alloys and metallurgical influence, in: G.L. Song (Ed.) Corrosion of Magnesium Alloys, Woodhead Publishing, Cambridge, 2011, pp. 153.

[29] D.A. Jones, Principles and Prevention of Corrosion, 2nd ed., Macmillan Publishing Co., New York, NY, 1996, pp. 142-147.

[30] R.J. Werkhoven, W.H. Sillekens, J.B.J.M. Van Lieshout, Processing aspects of magnesium alloy stent tube, in: W.H. Sillekens, S.R. Agnew, N.R. Neelameggham, S.N. Mathaudhu (Eds.) Magnesium Technology, John Wiley & Sons, Inc.2011, pp. 419-424.

[31] X. Zhang, G. Yuan, Z. Wang, Mechanical properties and biocorrosion resistance of Mg-Nd-Zn-Zr alloy improved by cyclic extrusion and compression, Mater. Lett., 74 (2012) 128-131

[32] F. Kang, J.Q. Liu, J.T. Wang, X. Zhao, Equal channel angular pressing of a Mg–3Al–1Zn alloy with back pressure, Adv. Eng. Mater., 12 (2010) 730-734.

[33] S. Zhao, C.T. McNamara, P.K. Bowen, N. Verhun, J.P. Braykovich, J. Goldman, J.W. Drelich, Structural characteristics and in vitro biodegradation of a novel Zn-Li alloy prepared by induction melting and hot rolling, Metall. Mater. Trans. A, DOI 10.1007/s11661-016-3901-0(2017).

[34] A. Krause, N. Von der Höh, D. Bormann, C. Krause, F.M. Bach, H. Windhagen, A. Meyer-Lindenberg, Degradation behaviour and mechanical properties of magnesium implants in rabbit tibiae, J. Mater. Sci., 45 (2010) 624-632.

[35] W. Young, Review of lithium effects on brain and blood, Cell Transplant., 18 (2009) 951-975.

[36] B. Halford, Limits of lithium, Chemical & Engineering News, American Chemical Society, 2013, pp. 15-20.

[37] G.N. Schrauzer, Lithium: occurrence, dietary intakes, nutritional essentiality, J. Am. Coll. Nutr. , 21 (2002) 14-21.

[38] D. Pierson, J. Edick, A. Tauscher, E. Pokorney, P. Bowen, J. Gelbaugh, J. Stinson, H. Getty, C.H. Lee, J. Drelich, J. Goldman, A simplified in vivo approach for evaluating the bioabsorbable behavior of candidate stent materials, J. Biomed. Mater. Res., Part B, 100B (2012) 58-67.

[39] M.D. Abramoff, P.J. Magalhaes, S.J. Ram, Image processing with ImageJ, Biophotonics Intern., 11 (2004) 36-42.

[40] M.H. Yoo, S.R. Agnew, J.R. Morris, K.M. Ho, Non-basal slip systems in HCP metals and alloys: source mechanisms, Mater. Sci. Eng. A, 319-321 (2001) 87-92.

[41] M.P. Bichat, J.L. Pascal, F. Gillot, F. Favier, Electrochemical lithium insertion in Zn_3P_2 Zinc phosphide, Chem. Mater., 17 (2005) 6761-6771.

[42] P.K. Bowen, J. Drelich, J. Goldman, Magnesium in the murine artery: Probing the products of corrosion, Acta Biomater., 10 (2014) 1475-1483.

[43] R.L. Frost, W. Martens, P.A. Williams, J.T. Kloprogge, Raman and infrared spectroscopic study of the vivianite-group phosphates vivianite, baricite and bobierrite, Mineral. Mag., 66 (2002) 1063-1073.

[44] C. Holt, M.J.J.M. van Kemenade, J.E. Harries, L.S. Nelson, R.T. Bailey, D.W.L. Hukins, S.S. Hasnain, P.L. De Bruyn, Preparation of amorphous calcium-magnesium phosphates at pH 7 and characterization by x-ray absorption and fourier transform infrared spectroscopy, J. Cryst. Growth, 92 (1988) 239-252.

[45] I.R. Gibson, W. Bonfield, Preparation and characterization of magnesium/carbonate co-substituted hydroxyapatites, J. Mater. Sci. Mater. Med., 13 (2002) 685-697.

[46] S. Meejoo, W. Maneeprakorn, P. Winotai, Phase and thermal stability of nanocrystalline hydroxyapatite prepared via microwave heating, Thermochim. Acta, 447 (2006) 115-120.

[47] B. Zberg, P.J. Uggowitzer, J.F. Loffler, MgZnCa glasses without clinically observable hydrogen evolution for biodegradable implants, Nat. Mater., 8 (2009) 887-891.

[48] A. Białobrzeski, K. Saja, M. Żmudzińska, Corrosion behaviour of binary Mg-Li alloys for plastic forming, Arch. Foundry Eng., 11 (2011) 15-20.

[49] A.J. Drelich, P.K. Bowen, L. LaLonde, J. Goldman, J. Drelich, Importance of oxide film in endovascular biodegradable zinc stents, Surf. Innovations, 4 (2016) 133-140.

[50] T. Kokubo, H. Takadama, How useful is SBF in predicting in vivo bone bioactivity?, Biomaterials, 27 (2006) 2907-2915.

[51] F.Z. Cui, Q.L. Feng, Biomaterials Science (Chinese Edition), Tsinghua University Press 2004.

[52] Y. Ding, C. Wen, P. Hodgson, Y. Li, Effects of alloying elements on the corrosion behavior and biocompatibility of biodegradable magnesium alloys: a review, J. Mater. Chem. B, 2 (2014) 1912-1933.

Chapter 5 Summary

In this dissertation, a new class of Zn-xLi alloys (with x=2, 4, 6 at.%) was prepared by induction melting in an argon atmosphere and processed through hot rolling for biomedical-focused applications. XRD results indicate the formation of $LiZn_4$ through the emergence of diffraction peaks corresponding to (001) and (004) for this phase when deformed by hot rolling, which increased hardness significantly in all cases. Mechanical testing showed that alloying Zn with Li increases the tensile strength to 360 MPa with a nominal addition of 2 at.% and 560 MPa with 6 at.% Li following hot rolling. Addition of Li above the eutectic composition caused a severe decrease in elongation to failure making the 6% Li alloy unsuitable for cardiovascular stent application.

In vitro corrosion behavior was evaluated by immersion tests in simulated body fluid. The *in vitro* study with the newly formulated Zn-2Li and Zn-4Li alloys also demonstrates that the corrosion rates and products in modified SBF solution closely resemble that of pure Zn observed *in vivo*, in plasma, and in whole blood from previous studies. The Zn-4Li alloy exhibited higher resistance to corrosion compared to Zn-2Li suggesting a positive effect of Li content on protective characteristics of the corrosion layer. The findings herein encourage further exploration of Zn-Li systems for structural use in biomedical vascular support applications with the ultimate goal of simplifying stent procedures thereby reducing stent related complications.

For the *in vivo* corrosion studies, a new Zn-Li alloy wire has been cast, extruded and analyzed for biomedical-focused applications. XRD results indicated the formation of

LiZn$_4$ through the emergence of diffraction peaks corresponding to (002) and (101) for this phase. Mechanical testing showed that alloying of Zn with 0.1 wt.% of Li increased the tensile strength from 116 ± 13 MPa (pure Zn) to 274 ± 61 MPa while the ductility was still being held at $17 \pm 7\%$.

The elemental mapping and FT-IR analysis jointly confirmed that the corrosion products are calcium phosphate, zinc oxide, zinc chloride hydroxide and zinc carbonate. The quantitative corrosion analysis showed a moderate low degradation rate of 0.019 mm/yr at 6.5 months that increased to 0.046 mm/yr at 12 months. This later stage acceleration is beneficial in that the stent would dissolve quickly in the body after the scaffolding function ceased around 6 months. The corroded volume for Zn-Li was only slightly smaller than that of 4N Zn at 6 months but both of them retained about 70% of their original dimensions after 12 months *in vivo*. The nearly identical oxidation progression for 4N Zn and Zn-Li indicates a very similar corrosion rate for the two materials. Moreover, the cross sectional area reduction curve for Zn-Li displayed a near-liner relationship between the percent of area reduction and time. This suggests a near ideal uniform gradual acceleration of biodegradation for this alloy. Biocompatibility results for the Zn-Li alloy at 11 months *in vivo* indicated a moderate inflammation with a non-obstructive neointima.

All the preliminary results obtained from implantation in rat abdominal arteries demonstrated that this new Zn-Li alloy is another promising bio-degradable coronary stent material based on its improved mechanical properties and the outstanding corrosion behavior as compared to pure Zn.

Appendix A Copyright Permission of Fig. 2.2 and Fig. 3.1.

Fig. 2.2 and Fig. 3.1. used in Chapter 2 and 3 of this dissertation was originally published in ASM Phase Diagram Center. Permission to reuse material from the published work was obtained with kind permission from ASM International. A copy of the granting permission for reproduction is shown below.

![ASM International logo]

COPYRIGHT PERMISSION REQUEST

Please complete all contact information:

Name: Shan Zhao   Title: PhD Candidate

Company/Organization: Michgan Technological University

Address: 1400 Townsend Drive

City/State/Zip/Country: Houghton,MI 49931-1295

Phone: 906-370-3368   Email: shanzhao@mtu.edu

I am preparing an article/chapter for publication in the following formats (*check as applicable*):
Print Only ☐   Internet Only ☐   Print and Electronic Media ☑

The information will be used for (*check as applicable*):
Journal article ☐   Conference presentation ☐   Internal company records ☐
Dissertation ☑   Student course material ☐   Commercial publication* ☐

Please complete the following:
The article/chapter title will be: Chapter 2 Objectives and Hypotheses; Chapter 3 Results and Discussions: Structural characteristic

The publication title will be: STRUCTURAL CHARACTERISTICS AND CORROSION BEHAVIOR OF BIODEGRADABLE ZN-LI ALI

Publisher: ProQuest/UMI

Planned date of publication: May 2017

I hereby request permission for non-exclusive world rights for the above publication and all subsequent editions, revisions, and derivative works in English and foreign translations, in the formats indicated above from the following copyrighted content by **ASM International**:

Book ISBN: Copyright date: 2006
Book/Publication title: ASM Alloy Phase Diagram Database
Author name(s): Pelton A.D
Article title: Li-Zn (Lithium-Zinc)
Text page numbers: p 2479-2480
Figure numbers (with page numbers): 1-Diagram No:901532
Table numbers (with page numbers):

Signature: Shan Zhao   [digital signature]   Date: 12/6/16

FOR ASM INTERNATIONAL USE ONLY:
I (we) grant permission requested above. Please ensure that ASM International receives proper credit as publisher by citing the above ASM publication as a reference and including the following: Reprinted with permission of ASM International. All rights reserved. www.asminternational.org

ASM International Representative: Sue Sellers   [digital signature]   Date: 12-07-2016

*For Commercial Publications, a copyright permission fee of $50 per figure will be assessed.
Exceptions can be made for reuse of content by its original authors.

ASM International, Permissions, 9639 Kinsman Road, Materials Park, Ohio 44073-0002   SUBMIT
permissions@asminternational.org, Phone: 440-338-5151 x5465, Fax: 440-338-8542

Appendix B Copyright Permission of Chapter 1 section 1.2.3

Chapter 1 section 1.2.3 of this dissertation was originally published in "Bio-degradable metals for cardiovascular stents: From clinical concerns to recent Zn-alloys", *2016 Advanced Healthcare Materials 5 (10), 1121-1140*. Permission to reuse material from the published work was obtained with kind permission from John Wiley and Sons. A copy of the granting permission for reproduction is shown below.

Appendix C Copyright Permission of Chapter 3

Chapter 3 of this dissertation was originally published in "Structural characteristics and in vitro biodegradation of a novel Zn-Li alloy prepared by induction melting and hot rolling", *2017 Metallurgical and Materials Transactions A, 48(3), 1204-1215*. Permission to reuse material from the published work was obtained with kind permission from Springer. A copy of the granting permission for reproduction is shown below.

126

Appendix D Copyright Permission of Chapter 4

Chapter 4 of this dissertation was originally published in "Zn-Li alloy wire after extrusion and drawing: Structural, mechanical characterization, and biodegradation in abdominal aorta of rat", *2017 Materials Science and Engineering: C, 76, 301-312*. Permission to reuse material from the published work was obtained with kind permission from Elsevier. A copy of the granting permission for reproduction is shown below.

ELSEVIER LICENSE
TERMS AND CONDITIONS

Mar 31, 2017

This Agreement between Shan Zhao ("You") and Elsevier ("Elsevier") consists of your license details and the terms and conditions provided by Elsevier and Copyright Clearance Center.

License Number	4079470619236
License date	
Licensed Content Publisher	Elsevier
Licensed Content Publication	Materials Science and Engineering: C
Licensed Content Title	Zn-Li alloy after extrusion and drawing: Structural, mechanical characterization, and biodegradation in abdominal aorta of rat
Licensed Content Author	Shan Zhao,Jan-M. Seitz,Rainer Eifler,Hans J. Maier,Roger J. Guillory,Elisha J. Earley,Adam Drelich,Jeremy Goldman,Jaroslaw W. Drelich
Licensed Content Date	1 July 2017
Licensed Content Volume	76
Licensed Content Issue	n/a
Licensed Content Pages	12
Start Page	301
End Page	312
Type of Use	reuse in a thesis/dissertation
Intended publisher of new work	other
Portion	full article
Format	both print and electronic
Are you the author of this Elsevier article?	Yes
Will you be translating?	No
Order reference number	
Title of your thesis/dissertation	STRUCTURAL CHARACTERISTICS AND CORROSION BEHAVIOR OF BIODEGRADABLE ZN-LI ALLOYS IN STENT APPLICATION
Expected completion date	Apr 2017
Estimated size (number of pages)	119
Elsevier VAT number	GB 494 6272 12
Requestor Location	Shan Zhao 1830D Woodmar Dr